Technical Report

TR-08-02

# Validation of coastal oceanography at Laxemar-Simpevarp

## Site descriptive modelling SDM-Site Laxemar

Anders Engqvist, Royal Institute of Technology (KTH)

Oleg Andrejev, Finnish Institute of Marine Research

December 2008

**Svensk Kärnbränslehantering AB**
Swedish Nuclear Fuel
and Waste Management Co
Box 250, SE-101 24 Stockholm
Tel +46 8 459 84 00

# Validation of coastal oceanography at Laxemar-Simpevarp

## Site descriptive modelling SDM-Site Laxemar

Anders Engqvist, Royal Institute of Technology (KTH)

Oleg Andrejev, Finnish Institute of Marine Research

December 2008

*Keywords:* Numerical model, 3D, Oceanographic measurement, Validation, Current velocity, Salinity, Temperature, Northern entrance of Kalmar Strait, Baltic Sea.

# Abstract

The Swedish Nuclear Fuel and Waste Management Company (SKB) is undertaking site characterization at two different locations, the Forsmark and the Laxemar-Simpevarp areas, with the objective of siting a geological repository for spent nuclear fuel. The characterization work is divided into an initial site investigation phase and a complete site investigation phase /SKB 2001/. In this context, the water exchange of the coastal zone is one link of the chain of possible nuclide transport mechanisms that must be assessed in the site description of potential repository areas /Lindborg et al. 2006/.

For the purpose of validating the pair of nested 3D-models and the coupled discrete basin (CDB-) model employed to simulate the water exchange in the near-shore coastal zone in the Laxemar-Simpevarp area, an encompassing measurement program entailing data from six stations (of which two are close) has been performed. The design of this program was to first assess to what degree the forcing of the fine resolution (FR-) model of the Laxemar-Simpevarp study area at its interfacial boundary to the coarse resolution (CR-) model of the entire Baltic was reproduced. In addition to this, it is of particular interest how the time-varying density-determining properties, salinity and temperature, at the borders are propagated into the FR-domain and further influence the water exchange with the interior, more secluded, basins. An important part of the validation process has been to carefully evaluate which measurement data that can be considered reliable. The result was that some periods of foremost near-surface salinity data had to be discarded due to growth of algae on the conductivity sensors. Interference with ship traffic and lack of absolute calibration of the salinity meters necessitated dismissal of measurement data too. In this study so-called Mesan data have been consistently used for the meteorological forcing of the 3D-models.

Relative the assessed data that can be accepted as adequate, the outcome of the validation can be summarized in three points: (*i*) The Baltic CR-model reproduces the measured salinity and the temperature profiles of the three peripheral stations acceptably well, while the correlation levels of the velocities are on an acceptable level for only one component, the other being close to zero; (*ii*) For the interior station Si24, the FR-model reproduces the salinity and the temperature profiles with a yet improved level of correlation compared with the CR-model; (*iii*) The bottom current velocity measured at Djupesund corresponds to an internal strait within the CDB-model and yields a correlation level of nearly 50% for salinity and about 95% for temperature.

The conclusion is that the present validation of *velocity* components of the peripheral stations between the CR- and FR-domains has mainly confirmed what was found in the corresponding validation study of the Forsmark area /Engqvist and Andrejev 2008/, namely that this represents a challenge that demands considerably more measuring effort than has been possible to muster presently in order to average out sub-grid eddies that the model cannot resolve. This applies even though the levels of the correlation analysis are considerably higher than was found for the parallel study of the waters off the Forsmark coast. This together with supporting current velocity transects in the vicinity of the measurement stations can be explained by a more horizontally homogeneous flow field. For the inner station (Si24) that was computed by the FR-model, the correlation levels are considerably improved. Also for the station (Si25) pertaining to the CDB-model good correlation levels are reproduced. All temperature profiles are also acceptably well captured by the models, but this is judged to be more an effect of the seasonal variation than an expression of the virtue of the actual models. As for the Forsmark validation program, the salinity dynamics of the interior FR-domain is the strong point of the model, but in the present study high levels of salinity correlations also extend to the peripheral measurement stations computed with the CR-model. Taken together this means that the overall earlier modeled water exchange of the Laxemar-Simpevarp caostal area can continue to be invested with due confidence.

# Sammanfattning

Svensk Kärnbränslehantering AB genomför platsundersökningar vid två olika platser: Forsmarks- och Laxemar-Simpevarpsområdet. Syftet är att lokalisera en långsiktig förvaringsplats för utbränt kärnbränsle. Karaktäriseringsarbetet är uppdelat i två faser varav den första är en initial platsundersökning och den andra en komplett sådan /SKB 2001/. I detta sammanhang utgör vattenutbytet genom kustzonen en länk i en lång transportkedja av möjligt utläckande radionuklider /Lindborg m fl 2006/.

Ett omfattande mätprogram har genomförts i syfte att validera det par av två sammankopplade 3D-modeller som har använts för att simulera vattenutbytet i den strandnära kustzonen i Forsmarksområdet. Modellansatsen består av en grövre upplöst (GU-) modell över hela Östersjön och en finare upplöst (FU-) modell samt en kopplad diskret bassäng (KDB-) modell över det studerade kustområdet i Forsmark. Utformningen av detta program syftade i första hand till att utröna i vilken omfattning drivningen över gränssnittet mellan dessa två modeller bestämmer vattenutbytet i det inre högupplösta området. Utöver denna granskning, omfattande sex mätstationer, har det varit av speciellt intresse att se hur densitetsbestämmande egenskaperna salinitet (S) och temperatur (T) vid dessa modellränder propagerar in till de inre delarna av FU-domänen. En viktig del av valideringsprocessen har varit att noggrannt utvärdera vilka mätdata som kan betraktas som tillförlitliga. Resultatet blev att några företrädesvis ytnära salinitetsdata måste förkastas på grund av algpåväxt som inverkar menligt på konduktivitetssensorerna. Brister avseende absolutkalibrering av salinitetsinstrumenten har också medfört att vissa sammanhörande data måst utelämnas från den fortsatta statistiska analysen av uppenbara skäl. För den meteorologiska drivningen av 3D-modellerna har Mesandata använts genomgående.

I förhållande till de insamlade data som kan accepteras såsom rättvisande, kan resultatet av denna validering summeras i tre punkter: (*i*) GU-modellen över Östersjön simulerar de uppmätta salinitets- och temperaturprofilerna för de perifera mätstationerna på ett acceptabelt väl sätt. Motsvarande korrelationer för strömhastigheterna är tillfredsställande endast för en av de två vinkelräta komponenterna, medan den andra är nära noll. (*ii*) För den inre mätstationen Si24 vars värden beräknats med FU-modellen uppkommer korrelationsnivåer för salinitet och temperatur som överträffar de som erhållits med GU-modellen. (*iii*) Bottenströmhastigheten som uppmätts i Djupesund som motsvaras av ett internt sund inom KDB-modellen ger en korrelationsnivå nära 50 % för salinitet och omkring 95 % för temperatur.

Sammanfattningsvis har valideringen av *hastighets*komponenterna i stort bekräftat vad som har visats i många tidigare studier, nämligen att detta utgör en krävande utmaning som fordrar väsentligt större mätansträngning än vad som varit möjligt att mobilisera i denna studie för att kunna medelvärdesbilda över tids- och rumsskalor som modellerna inte upplöser. Detta gäller även om korrelationsnivåerna är avsevärt högre än vad som befanns för den parallella studien rörande Forsmarks kustvatten /Engqvist and Andrejev 2008/, vilket tillsammans med stöd av utförda strömhastighetstransekter kring de perifera mätstationerna, kan förklaras med ett mer sammanhållet homogent strömningsfält i horisontell led. Även om temperaturvariationerna har modellerats acceptabelt väl, hör detta också samman med den uttalade säsongsdynamiken. Salinitetsdynamiken utgör dessa modellers starka sida. Dess variationer reproduceras övertygande väl av denna modellansats inte enbart för den inre stationen (Si24) beräknad med HU-modellen, utan också för de som beräknats med GU-modellen. Detta gäller även för den station (Si25) som modellerats med KDB-modellen. Sammantaget betyder det att tidigare modellerat övergripande vattenutbyte för Laxemar-Simpevarpsområdet med tillförsikt även fortsättningsvis kan betraktas som trovärdigt.

# Contents

# 1 Introduction

## 1.1 The cascaded 3D-model approach

The Baltic model (AS3D) employed in this study /Andrejev and Sokolov 1989, 1990/ has been developed for the main purpose of providing insight into the circulation of the central Baltic. Its present horizontal resolution is set to 2′×2′ (nautical miles) based on the Warnemünde hypsographic data, see Figure 1-1. This is conveniently referred to as the coarse-resolution (CR) model. In spherical coordinates the model spans the area defined by the southwest corner (53° 48' N, 9° 27' E) and the northeast (65° 52' N, 30° 27' E). The horizontal diffusivity is nominally set to 30 [$m^2$/s], consistent with assuming the grid cells to be well mixed. This model is presently involved in several ongoing Baltic hydrographic studies /e.g. Andrejev et al. 2004ab/. A thorough testing of this model in comparison to measured data /Engqvist and Andrejev 2003/ revealed that along an interface to a model area comprising the Stockholm archipelago, the measured salinity and temperature profiles were acceptably well reproduced, with the main difference being an offset in salinity approximately evenly distributed over the depth range. This evaluation thus increased confidence in the realism of the AS3D model. The heat exchange with the atmosphere is mainly determined by the air temperature; likewise the ice formation and melting processes are formulated in a simple but straightforward manner. This would be a liability if the main concern were to correctly predict the ice situation /e.g. Omstedt 1999/. The ice dynamics is not a concern for the part of the Baltic coast that is situated offshore of the Laxemar-Simpevarp area, however. For projection into a distant future, climate scenarios could more likely supply a forecast of shifting air temperatures, while other factors determining the heat exchange (insolation, relative humidity and nebulosity) would probably be more inaccessible.

The grid of the local fine-resolution (FR) 3D-model has been computed from a Digital Elevation Model (DEM) based on national digitized charts, complemented with shoreline information from economical maps. The grid has been specified in spherical coordinates WGS84 (sweref 99 long lat ellh) with the constraint that to be considered as a wet grid cell at least 50% of the covered area must consist of water. The numerical scheme is identical to the Baltic (CR) model but the horizontal diffusivity is nominally set to 20 [$m^{-2}s^{-1}$] compared to 30 [$m^{-2}s^{-1}$] for the Baltic model. The Laxemar-Simpevarp coastal area was resolved horizontally into grid cells with a side length of 0.1 × 0.1 nautical mile (Figure 1-2) defined by the SW corner with spherical coordinates (57° 20' N; 16° 31' E) and the NE corner (57° 32' N; 17° 03' E). The final choice of the actual model area includes a small section of the major island Öland in the SE corner. The inner more secluded embayments, e.g. those that surround the Äspö island, do not become sufficiently resolved with this resolution and their water exchange with the Baltic coast must therefore be computed using another model approach in the form of a coupled discrete basin model that will be referred to as the CDB-model. In fact, when using the objective gridding criterion that at least 50% of area must consist of water meant that these interior waters were disconnected in the FR-grid at a few locations. In order to attach these to the main computational domain, manual corrections were performed.

The CDB-model has been developed in stages since it was first applied to the basins adjacent to the Äspö island /Engqvist 1997/. Its present enhanced features have been described in /Engqvist and Stenström 2004/ and it has been successfully validated in the Himmerfjärden area about 40 km south of Stockholm /Engqvist and Stenström 2008/. This model will be presented in more detail in section 3.6 below that deals with the measurement validation of station Si25.

The overall objective has been to evaluate these three nested numerical models with differing resolution (CR, FR and CDB) regarded as an operational entity and to investigate their combined capacity to simulate the measured oceanographic data.

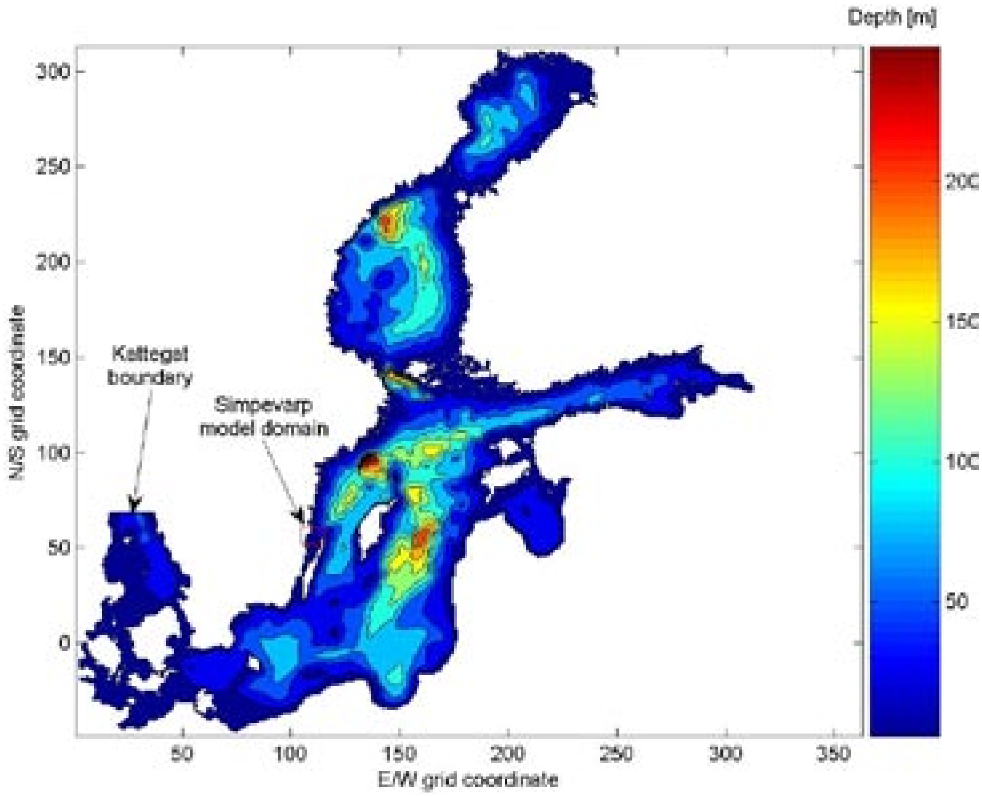


*Figure 1-1. Baltic model bathymetry resolved into a grid with 2×2 nautical mile side length The fine-resolution model of the Laxemar-Simpevarp area and its approximate location relative the Baltic model is indicated with a red rectangle. The open boundary of Baltic model falls where Kattegat borders to the Skagerrak.*

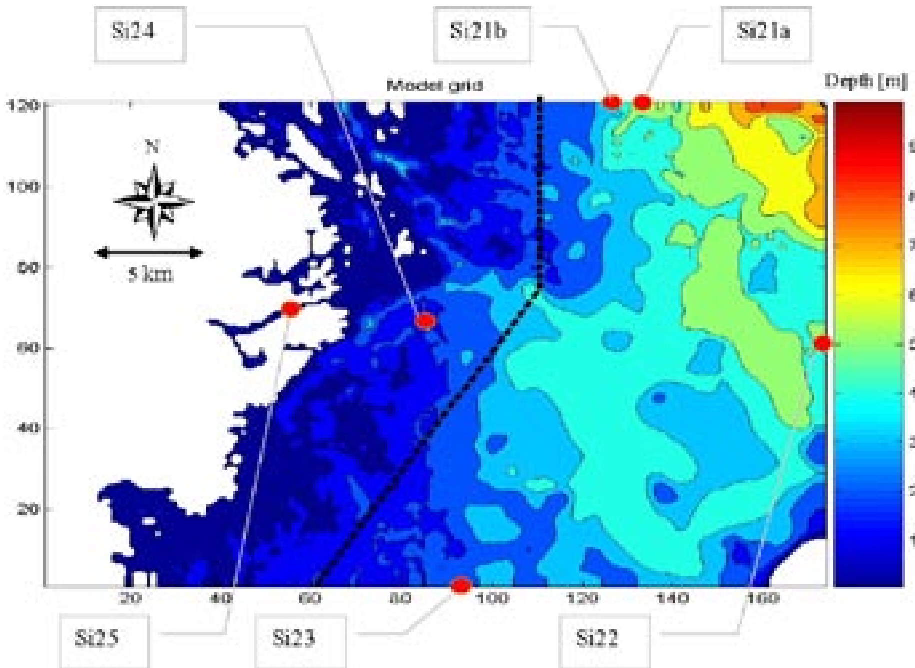


*Figure 1-2. Local fine-resolved model domain with red dots indicating the measurement stations where the oceanographic instruments were deployed during the validation year cycle starting in spring 2004. The labels denote the reference naming of these stations used in the text. The axes are graded in grid cell number with a horizontal resolution of 0.1 nautical mile i.e. 185.2 m.*

## 1.2 Design of the field program

The general design idea of the field program was primarily to assess the oceanographic state parameters at some locations distributed as evenly as possible on the boundaries of the local model (FR-) grid which coincide with the interfaces to the nested (CR-) grid of the Baltic model. These stations are listed in Table 1-1 (their positions are shown in Figure 1-2) and are meant to represent the forcing of the large-scale events onto the fine-resolved local model domain. The oceanographic measurements consist of both vector entities, i.e. current velocities, and the scalar properties temperature and salinity.

Temperature is measured directly by use of thermistors but salinity is indirectly inferred from measured conductivity. All salinities in the following are presented dimensionless in the psu-scale. These two scalar properties determine (together with pressure) the density of the sea water. Assessment of these entities at the periphery together with the atmospheric heat exchange and freshwater discharge makes it possible to model their propagation into the center of the domain where an evaluation relative other measurement sites can be performed. The measurement procedures of oceanographical parameters have been specified by / Johansson and Morosini 2002/.

Based on experience from other similar validation endeavors, it was anticipated that for the scalar data, it should be straightforward to make a direct and fair evaluation, while vector comparisons would be considerably more difficult. In negotiations with the contracted executioner of the field program, Swedish Meteorological and Hydrological Institute (SMHI), bottom-placed ADCP-instruments were recommended over RCM-instruments that also normally can be equipped to measure salinity and temperature. The argument was partly that bottom-placed instruments are less vulnerable to interfering with other maritime activities and partly that they are less expensive to deploy and operate.

In order to secure data, the one-year measurement period was subdivided into four sections with approximately equal duration but open to allowances due to poor weather conditions and other incidents that are difficult to apprehend. This plan was specified in detail in the Activity plan AP PS 400-04-10 with Karin Aquilonius as the contemporary SKB representative.

**Table 1-1. Overview of the naming and locations of the measurement stations. The RT90 coordinates differ from corresponding positions stated in /Lindow 2005/. For the measured entities C denotes conductivity, T temperature and D direction. U and V denote current speed components.**

| Location name | Measured entity | Station ID SKB | Station ID SMHI | Position Northing (RT90 2.5 gon V (0:-1 | Position Easting | Position lat (WGS 84 Sweref 99) | Position long | Depth desired [m] | Depth realized [m] |
|---|---|---|---|---|---|---|---|---|---|
| | | | | RT90 data from P-05- | | | | | |
| North boundary E | 4xC/T | PSM6927 | Si21a | 6377920 | 1566900 | 57° 32.0'N | 16° 55.5'E | ~40 | 66 |
| North boundary W | U,V | PSM6928 | Si21b | 6379016 | 1565837 | 57° 32.0'N | 16° 54.5'E | ~40 | 42 |
| East boundary | C/T/U/D | PSM6929 | Si22 | 6368104 | 157496 | 57° 26.0'N | 17° 03.0'E | ~50 | 50 |
| South boundary | U,V | PSM6930 | Si23 | 6356926 | 1559731 | 57° 20.0'N | 16° 48.0'E | 24 | 26 |
| Inner station | 3xCT | PSM6931 | Si24 | 6368855 | 1558314 | 57° 26.5'N | 16° 46.8'E | 20 | 28 |
| Inner station (non-icecover time) | 11xT | PSM6931 | Si24T | 6368855 | 1558314 | 57° 26.5'N | 16° 46.8'E | ~20 | 28 |
| Djupesund | C/T/U/D | PSM6932 | Si25 | 6369500 | 1552493 | 57° 27.0'N | 16° 41.0'E | ~6 | 4.2 |

## 1.3 Overview of the measurement program

The measurement program was originally planned to start on January 1, 2004, but due to various reasons, e.g. the ice situation on the parallel program of Forsmark, this was delayed until mid-April the same year. In Table 1-2 the field program is specified in detail regarding the measured parameters and their deployment with regard to depth. This table also gives a first rough presentation of the data yield and also lists the names of the resulting 83 data files.

It seems safe to state that the actual handling and deployment of the instruments has been conducted professionally and with due care. The handling and communication of data has, on the other hand, left more to be desired. Initially there was a complete abandonment of the specified protocol, and even in the same file (e.g. time denoting), the data format could be changed several times. No inspection of the presumed validity of data was performed by SMHI, but the chore of quality inspection was passed over to be performed by SKB. It is also fair to state that by the end of the validation year, the accumulated criticism also led to a noticeable improvement in SMHI's performance in this regard.

The report on the assessment of oceanographic data conducted by SMHI /Lindow 2005/ admits most of the shortcomings, but not all. In Table 1-3 some of the additional sources of consternation have been commented upon.

## 1.4 Validation strategy

The overall validation plan is straightforward and consists of first inspecting the measurement data to dismiss the sections that for various reasons cannot be trusted. Then follows an investigation of the spectral appearance of the remaining data in order to determine an appropriate sampling frequency for the ensuing comparison with matching simulated data. Finally the actual comparisons are performed, which in most cases result in cross-correlation analysis. The five measurement locations, Si21 through Si25, are treated in order.

**Table 1-2. Overview of the naming of the data files and what measured entity they denote. Gray fields indicate data problems, see Figure 2-1 for an explanation.**

| period | | | Depth | | | File number | SMHI file name | Systematic name | SICADA_06_104_2 |
|---|---|---|---|---|---|---|---|---|---|
| 1st | Si21a | PSM6927 | 2 m | CTD | T,C | 1 | SBE37 Si21_2m.xls | Si21_1st4_N1_TC_02m.csv | |
| 1st | | PSM6927 | 10 m | CTD | T,C | 2 | SBE37 Si21_10m.xls | Si21_1st4_N1_TC_10m.csv | |
| 1st | | PSM6927 | 17 m | CTD | T,C | | missing | | |
| 1st | | PSM6927 | 30 m | CTD | T,C | 3 | SBE37 Si21_30m.xls | Si21_1st4_N1_30m_TC.csv | |
| 2nd | | PSM6927 | 2 m | CTD | T,C | 4 | SBE37 Si21_2m.xls | Si21_2nd4_N1_TC_02m.csv | |
| 2nd | | PSM6927 | 10 m | CTD | T,C | 5 | SBE37 Si21_10m.xls | Si21_2nd4_N1_TC_10m.csv | |
| 2nd | | PSM6927 | 17 m | CTD | T,C | 6 | SBE37 Si21_17m.xls | Si21_2nd4_N1_TC_17m.csv | |
| 2nd | | PSM6927 | 30 m | CTD | T,C | 7 | SBE37 Si21_30m.xls | Si21_2nd4_N1_TC_30m.csv | |
| 3rd | | PSM6927 | 2 m | CTD | T,C & D | 8 | Si21_2m.xls | Si21_3rd4_N1_TC_02m.csv | |
| 3rd | | PSM6927 | 10 m | CTD | T,C | 9 | Si21_10m.xls | Si21_3rd4_N1_TC_10m.csv | |
| 3rd | | PSM6927 | 17 m | CTD | T,C | 10 | Si21_17m.xls | Si21_3rd4_N1_TC_17m.csv | |
| 3rd | | PSM6927 | 30 m | CTD | T,C | 11 | Si21_30m.xls | Si21_3rd4_N1_TC_30m.csv | |
| 4th | | PSM6927 | 5 m | CTD | T,C & D | 12 | Si21-4_SBE37-130_5m.xls | Si21_4th4_N1_TC_05m.csv | |
| 4th | | PSM6927 | 10 m | CTD | T,C | 13 | Si21-4_SBE37-129_10m.xls | Si21_4th4_N1_TC_10m.csv | |
| 4th | | PSM6927 | 17 m | CTD | T,C | 14 | Si21-4_SBE37-124_17.5m | Si21_4th4_N1_TC_17m.csv | |
| 4th | | PSM6927 | 30 m | CTD | T,C | 15 | Si21-4_SBE37-126_30m.xls | Si21_4th4_N1_TC_30m.csv | |
| | Si21b | PSM6928 | 3:2:39 m | ADCP | 15xU | 16 | Si21_101_V1_korr.xls | Si21_1st4_N1_U_hr.csv | OC140\current_east_aquadop.csv |
| 1st | | PSM6928 | 3:2:39 m | ADCP | 15xV | 17 | Si21_101_V2_korr.xls | Si21_1st4_N1_V.csv | OC140\current_north_aquadop.csv |
| 1st | | PSM6928 | 3:2:39 m | ADCP | 15xW | 18 | Si21_101_V3_korr.xls | Si21_1st4_N1_W.csv | |
| 1st | | PSM6928 | | | 3 P,T | | missing | | |
| | | PSM6928 | 3:2:39 m | ADCP | 15xU | 19 | Si21-201_v1.xls | Si21_2nd4_N1_U.csv | OC140\current_east_aquadop.csv |
| 2nd | | PSM6928 | 3:2:39 m | ADCP | 15xV | 20 | Si21-201_v2.xls | Si21_2nd4_N1_V.csv | OC140\current_north_aquadop.csv |
| 2nd | | PSM6928 | 3:2:39 m | ADCP | 15xW | 21 | Si21-201_v3.xls | Si21_2nd4_N1_W.csv | OC140\current_up_aquadop.csv |
| 2nd | | PSM6928 | 3:2:39 m | ADCP | 15xU | 22 | Si21-301_v1.xls | Si21_2nd4_N2_U.csv | OC140\current_east_aquadop.csv |
| 2nd | | PSM6928 | 3:2:39 m | ADCP | 15xV | 22 | Si21-301_v2.xls | Si21_2nd4_N2_V.csv | OC140\current_north_aquadop.csv |
| 2nd | | PSM6928 | 3:2:39 m | ADCP | 15xW | 23 | Si21-301_v3.xls | Si21_2nd4_N2_W.csv | OC140\current_up_aquadop.csv |
| 2nd | | PSM6928 | | | P,T | 24 | Si21_201_sen.xls | Si21_2nd4_N1_PT.csv | |
| 2nd | | PSM6928 | | | P,T | 25 | Si21_301_sen.xls | Si21_2nd4_N2_PT.csv | |
| | | PSM6928 | 3:2:40 m | ADCP | 20xU | 26 | Si21-401_v1.xls | Si21_3rd4_N1_U.csv | OC140\current_east_aquadop.csv |
| 3rd | | PSM6928 | 3:2:40 m | ADCP | 20xV | 27 | Si21-401_v2.xls | Si21_3rd4_N1_V.csv | OC140\current_north_aquadop.csv |
| 3rd | | PSM6928 | 3:2:40 m | ADCP | 20xW | 28 | Si21-401_v3.xls | Si21_3rd4_N1_W.csv | OC140\current_up_aquadop.csv |
| 3rd | | PSM6928 | | | 14 P,T | 29 | Si21_401_sen.xls | Si21_3rd4_N1_PT.csv | |
| | | PSM6928 | 3:2:37 m | ADCP | 18xU | 30 | Si21-4_AQD1358_v1.xls | Si21_4th4_N1_U.csv | OC140\current_east_aquadop.csv |
| 4th | | PSM6928 | 3:2:37 m | ADCP | 18xV | 31 | Si21-4_AQD1358_v2.xls | Si21_4th4_N1_V.csv | OC140\current_north_aquadop.csv |
| 4th | | PSM6928 | 3:2:37 m | ADCP | 18xW | 32 | Si21-4_AQD1358_v3.xls | Si21_4th4_N1_W.csv | OC140\current_up_aquadop.csv |
| 4th | | PSM6928 | | | P,T | 33 | Si21_AQD1358_sen.xls | Si21_4th4_N1_PT.csv | |
| 1st | Si22 | PSM6929 | | RCM+ | U,D,C,T,S | | missing | | |
| 2nd | | PSM6929 | | | 8 U,D,C,T,S | | missing | | |
| 3rd | | PSM6929 | | RCM+ | U,D,T,C,S | 34 | Si22-3-4_Aa93009.xls | Si22_3rd4_E1_UDTC_49m.csv | |
| 4th | | PSM6929 | 49 m | RCM | U,D,T | 35 | Si22-4_Aa93036-49m.xls | Si22_4th4_E1_UDT-_49m.csv | |
| 1st | Si23 | PSM6930 | 3:2:24 m | ADCP | 12xU | 36 | Si23_101_V1.xls | Si23_1st4_S1_U.csv | OC140\current_east_awac.csv |
| 1st | | PSM6930 | 3:2:24 m | ADCP | 12xV | 37 | Si23_101_V2.xls | Si23_1st4_S1_V.csv | OC140\current_northing.csv |
| 1st | | PSM6930 | 3:2:24 m | ADCP | 12xW | 38 | Si23_101_V3.xls | Si23_1st4_S1_W.csv | OC140\currents_up.csv |
| 1st | | PSM6930 | | | P,T | | missing | | |
| 2nd | | PSM6930 | 2:2:24 m | ADCP | 12xU | 39 | Si23-201_v1.xls | Si23_2nd4_S1_U.csv | OC140\current_east_awac.csv |
| 2nd | | PSM6930 | 2:2:24 m | ADCP | 12xV | 40 | Si23-201_v2.xls | Si23_2nd4_S1_V.csv | OC140\current_northing.csv |
| 2nd | | PSM6930 | 2:2:24 m | ADCP | 12xW | 41 | Si23-201_v3.xls | Si23_2nd4_S1_W.csv | OC140\currents_up.csv |
| 2nd | | PSM6930 | 2:2:24 m | ADCP | 12xU | 42 | Si23-301_v1.xls | Si23_2nd4_S2_U.csv | OC140\current_east_awac.csv |
| 2nd | | PSM6930 | 2:2:24 m | ADCP | 12xV | 43 | Si23-301_v2.xls | Si23_2nd4_S2_V.csv | OC140\current_northing.csv |
| 2nd | | PSM6930 | 2:2:24 m | ADCP | 12xW | 44 | Si23-301_v3.xls | Si23_2nd4_S2_W.csv | OC140\currents_up.csv |
| 2nd | | PSM6930 | 2:2:24 m | ADCP | 12xU | 45 | Si23-401_v1.xls | Si23_2nd4_S3_U.csv | OC140\current_east_awac.csv |
| 2nd | | PSM6930 | 2:2:24 m | ADCP | 12xV | 46 | Si23-401_v2.xls | Si23_2nd4_S3_V.csv | OC140\current_northing.csv |
| 2nd | | PSM6930 | 2:2:24 m | ADCP | 12xW | 47 | Si23-401_v3.xls | Si23_2nd4_S3_W.csv | OC140\currents_up.csv |
| 2nd | | PSM6930 | | | P,T | 48 | Si23-201_sen.xls | Si23_2nd4_S1_PT.csv | |
| 2nd | | PSM6930 | | | P,T | 49 | Si23-301_sen.xls | Si23_2nd4_S2_PT.csv | |
| 2nd | | PSM6930 | | | P,T & C | 50 | Si23-401_sen.xls | Si23_2nd4_S3_PT.csv | |
| 3rd | | PSM6930 | 2:2:28 m | ADCP | 14xU | 51 | Si23-302_v1.xls | Si23_3rd4_S1_U.csv | OC140\current_east_awac.csv |
| 3rd | | PSM6930 | 2:2:28 m | ADCP | 14xV | 52 | Si23-302_v2.xls | Si23_3rd4_S1_V.csv | OC140\current_northing.csv |
| 3rd | | PSM6930 | 2:2:28 m | ADCP | 14xW | 53 | Si23-302_v3.xls | Si23_3rd4_S1_W.csv | OC140\currents_up.csv |
| 3rd | | PSM6930 | | | P,T & C | 54 | Si23-301_sen.xls | Si23_3rd4_S1_PT.csv | |
| 4th | | PSM6930 | 2:2:26 m | ADCP | 13xU | 55 | Si23-4_AWAC_v1.xls | Si23_4th4_S1_U.csv | OC140\current_east_awac.csv |
| 4th | | PSM6930 | 2:2:26 m | ADCP | 13xV | 56 | Si23-4_AWAC_v2.xls | Si23_4th4_S1_V.csv | OC140\current_northing.csv |
| 4th | | PSM6930 | 2:2:26 m | ADCP | 13xW | 57 | Si23-4_AWAC_v3.xls | Si23_4th4_S1_W.csv | OC140\currents_up.csv |
| 4th | | PSM6930 | 28 m | | P,T & C | 58 | Si23-4_AWAC_sen.xls | Si23_4th4_S1_PT.csv | |
| 1st | Si24 | PSM6931 | 2 m | CTD | T,C | 59 | SBE37_Si24_2m.xls | Si24_1st4_I1_TC_02m.csv | |
| 1st | | PSM6931 | 10 m | CTD | T,C | 60 | SBE37_Si24_10m.xls | Si24_1st4_I1_TC_10m.csv | |
| 1st | | PSM6931 | 17 m | CTD | T,C | 61 | Si24_17m.xls | Si24_1st4_I1_TC_17m.csv | |
| 2nd | | PSM6931 | 2 m | CTD | T,C | 62 | Si24 2m.xls | Si24_2nd4_I1_02m_TC.csv | |
| 2nd | | PSM6931 | 10 m | CTD | T,C | 63 | Si24 10m.xls | Si24_2nd4_I1_10m_TC.csv | |
| 2nd | | PSM6931 | 17 m | CTD | T,C | 65 | Si24 17.5m.xls | Si24_2nd4_I1_17m_TC.csv | |
| 3rd | | PSM6931 | 2 m | CTD | T,C | 66 | Si24 2m.xls | Si24_3rd4_I1_TC_02m.csv | |
| 3rd | | PSM6931 | 10 m | CTD | T,C | 67 | Si24 10m.xls | Si24_3rd4_I1_TC_10m.csv | |
| 3rd | | PSM6931 | 17 m | CTD | T,C | 68 | Si24 17.5m.xls | Si24_3rd4_I1_TC_17m.csv | |
| 4th | | PSM6931 | 5 m | CTD | T,C | 69 | Si24-4_SBE37-127_5m.xls | Si24_4th4_I1_TC_05m.csv | |
| 4th | | PSM6931 | 10 m | CTD | T,C | 70 | Si24-4_SBE37-128_5m.xls | Si24_4th4_I1_TC_10m.csv | |
| 4th | | PSM6931 | 17 m | CTD | T,C | 71 | Si24-4_SBE37-125_17.5m | Si24_3rd4_I1_TC_17m.csv | |
| 1st | Si24T | PSM6931 | 1:2:21 m | TK | 11xT | 72 | Si24_T_1.xls | Si24_1st4_I1_TK.csv | |
| 2nd | | PSM6931 | 1:2:21 m | TK | 11xT | 73 | T3036 Si24juli-sept 2004.xls | Si24_2nd4_I1_TK.csv | |
| 3rd | | PSM6931 | 1:2:21 m | TK | 11xT | 74 | AaT3040 Si24T.xls | Si24_3rd4_I1_TK.csv | |
| 4th | | PSM6931 | | | | | | | |
| 1st | Si25 | PSM6932 | 4 m | RCM+ | U,D,C,T,S | 75 | s4_djupesund.xls | Si25_1st4_D1_UDCT.csv | |
| 2nd | | | 4 m | RCM+ | U,D,C,T | 76 | Si25_040928.xls | Si25_2nd4_D1_UDCT.csv | |
| 3rd | | PSM6932 | 4 m | RCM+ | U,D,C,T | 77 | Si25_3.xls | Si25_3rd4_D1_UDCT.csv | |
| 4th | | PSM6932 | 4 m | RCM+ | U,D,C,T | 78 | Si25-4_S4.xls | Si25_4th4_D1_UDCT.csv | |
| | Transects | | | | | | | | |
| 0th | | | | ADCP | | 79 | Simp040r.00 | | |
| 1st | | | | ADCP | | 80 | Simp070r.000 | | |
| 2nd | | | | ADCP | | 81 | Simp000r.000 | | |
| 3rd | | | | | | | | Dismissed due to weather conditions | |
| 4th | | | | ADCP | | 82 | simp006r.000 | | |
| | | | | ADCP | | 83 | simp007r.000 | | |

**Table 1-3. Overview of the temporal aspect of the data and ensuing remarks and responses of the executioner of the field program. Gray fields indicate data problems that are explained in the three last columns.**

| Station ID SMHI | SKB | period | Depth | | | start | kl | stop | kl | File number | Remarks | SMHI's response | SMHI reporting P-05-191 |
|---|---|---|---|---|---|---|---|---|---|---|---|---|---|
| SQ1 | PSM6927 | 1st | 2 m | CTD | T,C | 20040331 | 17 | 20040706 | 8 | 1 | Wrong conductivity unit | Corrected | |
| | PSM6927 | 1st | 10 m | CTD | T,C | 20040331 | 17 | 20040706 | 8 | 2 | | | |
| | PSM6927 | 1st | 17 m | CTD | T,C | | | | | | Missing | | Missing |
| | PSM6927 | 1st | 30 m | CTD | T,C | 20040331 | 16 | 20040706 | 7 | 3 | Unrealistic conductivity values | Instrument replaced | Not noted |
| | PSM6927 | 2nd | 2 m | CTD | T,C | 20040707 | 11 | 20040929 | 10 | 4 | | | |
| | PSM6927 | 2nd | 10 m | CTD | T,C | 20040707 | 11 | 20040929 | 10 | 5 | | | |
| | PSM6927 | 2nd | 17 m | CTD | T,C | 20040707 | 11 | 20040929 | 10 | 6 | | | |
| | PSM6927 | 2nd | 30 m | CTD | T,C | 20040707 | 11 | 20040723 | 2 | 7 | Unrealistic conductivity values | Acknowledged | |
| | PSM6927 | 3rd | 2 m | CTD | T,C & D | 20041001 | 11 | 20041107 | 1 | 8 | Dives to 26m 2004-11-07 01-02hrs | Hit by ship action | |
| | PSM6927 | 3rd | 10 m | CTD | T,C | 20041001 | 11 | 20041107 | 1 | 9 | Uncertain depth after 2004-11-07 | Dislocation accept. | |
| | PSM6927 | 3rd | 17 m | CTD | T,C | 20041001 | 11 | 20041107 | 1 | 10 | Uncertain depth after 2004-11-08 | Dislocation accept. | |
| | PSM6927 | 3rd | 30 m | CTD | T,C | 20041001 | 11 | 20050111 | 10 | 11 | | | |
| | PSM6927 | 4th | 5 m | CTD | T,C & D | 20050114 | 15 | 20050406 | 8 | 12 | Pressure unit in [m] | | Spikes in C; CTD of fi |
| | PSM6927 | 4th | 10 m | CTD | T,C | 20050114 | 16 | 20050406 | 8 | 13 | | | |
| | PSM6927 | 4th | 17 m | CTD | T,C | 20050114 | 16 | 20050406 | 8 | 14 | | | |
| | PSM6927 | 4th | 30 m | CTD | T,C | 20050114 | 15 | 20050406 | 8 | 15 | | | |
| SQ1 | PSM6928 | 1st | 3:2:39 m | ADCP | 15xU | 20040401 | 9 | 20040706 | 7 | 16 | | | |
| | PSM6928 | 1st | 3:2:39 m | ADCP | 15xV | 20040401 | 9 | 20040706 | 7 | 17 | | | |
| | PSM6928 | 1st | 3:2:39 m | ADCP | 15xW | 20040401 | 9 | 20040706 | 7 | 18 | File initially confused | File replaced | |
| | PSM6928 | 1st | | 3 | P,T | | | | | | | | Missing |
| | PSM6928 | 2nd | 3:2:39 m | ADCP | 15xU | 20040707 | 11 | 20040811 | 13 | 19 | | | |
| | PSM6928 | 2nd | 3:2:39 m | ADCP | 15xV | 20040707 | 11 | 20040811 | 13 | 20 | | | |
| | PSM6928 | 2nd | 3:2:39 m | ADCP | 15xW | 20040707 | 11 | 20040811 | 13 | 21 | | | |
| | PSM6928 | 2nd | 3:2:39 m | ADCP | 15xU | 20040819 | 6 | 20040912 | 19 | 22 | | | |
| | PSM6928 | 2nd | 3:2:39 m | ADCP | 15xV | 20040819 | 6 | 20040912 | 19 | 22 | | | |
| | PSM6928 | 2nd | 3:2:39 m | ADCP | 15xW | 20040819 | 6 | 20040912 | 19 | 23 | | | |
| | PSM6928 | 2nd | | | P,T | 20040707 | 12 | 20040811 | 14 | 24 | | | |
| | PSM6928 | 2nd | | | P,T | 20040819 | 6 | 20040912 | 20 | 25 | Missing data, no units stated | Instrument inspected | |
| | PSM6928 | 3rd | 3:2:43 m | ADCP | 20xU | 20041002 | 14 | 20050112 | 10 | 26 | | | |
| | PSM6928 | 3rd | 3:2:43 m | ADCP | 20xV | 20041002 | 14 | 20050112 | 10 | 27 | | | |
| | PSM6928 | 3rd | 3:2:43 m | ADCP | 20xW | 20041002 | 14 | 20050112 | 10 | 28 | | | |
| | PSM6928 | 3rd | | 14 | P,T | 20041002 | 14 | 20050111 | 11 | 29 | | | |
| | PSM6928 | 4th | 3:2:37 m | ADCP | 18xU | 20050114 | 14 | 20050413 | 12 | 30 | First measurement(s) implausible | | |
| | PSM6928 | 4th | 3:2:37 m | ADCP | 18xV | 20050114 | 14 | 20050413 | 12 | 31 | | | |
| | PSM6928 | 4th | 3:2:37 m | ADCP | 18xW | 20050114 | 14 | 20050413 | 14 | 32 | | | |
| | PSM6928 | 4th | | | P,T | 20050114 | 14 | 20050413 | 12 | 33 | Pressure unit in [m] | | |
| SQ2 | PSM6929 | 1st | | RCM+ | U,D,C,T,S | | | | | | | | water leak |
| | PSM6929 | 2nd | | 8 | U,D,C,T,S | | | | | | | | clock error |
| | PSM6929 | 3rd | 58 m | RCM+ | U,D,T,C,S | 20041020 | 9 | 20050427 | 9 | 34 | Believed lost for a period | | instrument replaced |
| | PSM6929 | 4th | 49 m | RCM | U,D,T | 20050304 | 14 | 20050309 | 21 | 35 | Works only 5 days – no salinity | | just 5 days due to ... |
| SQ3 | PSM6930 | 1st | 0:2:24 m | ADCP | 12xU | 20040331 | 17 | 20040706 | 11 | 36 | | | |
| | PSM6930 | 1st | 0:2:24 m | ADCP | 12xV | 20040331 | 17 | 20040706 | 11 | 37 | | | |
| | PSM6930 | 1st | 0:2:24 m | ADCP | 12xW | 20040331 | 17 | 20040706 | 11 | 38 | | | |
| | PSM6930 | 1st | | 4 | P,T | | | | | | | | Bad calibration |
| | PSM6930 | 2nd | 2:2:24 m | ADCP | 12xU | 20040707 | 16 | 20040811 | 10 | 39 | | | |
| | PSM6930 | 2nd | 2:2:24 m | ADCP | 12xV | 20040707 | 16 | 20040811 | 10 | 40 | | | |
| | PSM6930 | 2nd | 2:2:24 m | ADCP | 12xW | 20040707 | 16 | 20040811 | 10 | 41 | | | |
| | PSM6930 | 2nd | 2:2:24 m | ADCP | 12xU | 20040811 | 13 | 20040819 | 6 | 42 | | | |
| | PSM6930 | 2nd | 2:2:24 m | ADCP | 12xV | 20040811 | 13 | 20040819 | 6 | 43 | | | |
| | PSM6930 | 2nd | 2:2:24 m | ADCP | 12xW | 20040811 | 13 | 20040819 | 6 | 44 | | | |
| | PSM6930 | 2nd | 2:2:24 m | ADCP | 12xU | 20040819 | 9 | 20041001 | 13 | 45 | | | |
| | PSM6930 | 2nd | 2:2:24 m | ADCP | 12xV | 20040819 | 9 | 20041001 | 13 | 46 | | | |
| | PSM6930 | 2nd | 2:2:24 m | ADCP | 12xW | 20040819 | 9 | 20041001 | 13 | 47 | | | |
| | PSM6930 | 2nd | | | P,T | 20040707 | 16 | 20040811 | 11 | 48 | Vagont T/C sensor NG | Acknowledged | sensor out of order |
| | PSM6930 | 2nd | | | P,T | 20040811 | 13 | 20040819 | 6.5 | 49 | Vagont T/C sensor NG | Acknowledged | sensor reinstalled |
| | PSM6930 | 2nd | | | P,T & C | 20040819 | 9.5 | 20040929 | 13 | 50 | Two columns temp – no salinity | Acknowledged | no conductivity |
| | PSM6930 | 3rd | 2:2:28 m | ADCP | 14xU | 20041002 | 12 | 20050114 | 8 | 51 | | | |
| | PSM6930 | 3rd | 2:2:28 m | ADCP | 14xV | 20041002 | 12 | 20050114 | 8 | 52 | | | |
| | PSM6930 | 3rd | 2:2:28 m | ADCP | 14xW | 20041002 | 12 | 20050114 | 8 | 53 | | | |
| | PSM6930 | 3rd | | | P,T & C | 20041002 | 12 | 20050114 | 8 | 54 | Salinity not computed | | |
| | PSM6930 | 4th | 2:2:26 m | ADCP | 13xU | 20050114 | 9 | 20050414 | 7 | 55 | | | |
| | PSM6930 | 4th | 2:2:26 m | ADCP | 13xV | 20050114 | 9 | 20050414 | 7 | 56 | | | |
| | PSM6930 | 4th | 2:2:26 m | ADCP | 13xW | 20050114 | 9 | 20050414 | 7 | 57 | | | |
| | PSM6930 | 4th | 28 m | | P,T & C | 20050114 | 18 | 20050413 | 9 | 58 | Last 24h period exempted | | |
| SQ4 | PSM6931 | 1st | 2 m | CTD | T,C | 20040331 | 14 | 20040706 | 10 | 59 | Replaced by new file 2005-03-04 | Replacement | |
| | PSM6931 | 1st | 10 m | CTD | T,C | 20040331 | 14 | 20040706 | 10 | 60 | Replaced by new file 2005-03-05 | Replacement | |
| | PSM6931 | 1st | 17 m | CTD | T,C | 20040331 | 14 | 20040706 | 10 | 61 | Replaced by new file 2005-03-08 | Replacement | |
| | PSM6931 | 2nd | 2 m | CTD | T,C | 20040707 | 18 | 20040929 | 9 | 62 | | | |
| | PSM6931 | 2nd | 10 m | CTD | T,C | 20040707 | 18 | 20040929 | 9 | 63 | | | |
| | PSM6931 | 2nd | 17 m | CTD | T,C | 20040707 | 18 | 20040929 | 9 | 65 | | | |
| | PSM6931 | 3rd | 2 m | CTD | T,C | 20041001 | 7 | 20050111 | 9 | 66 | | | |
| | PSM6931 | 3rd | 10 m | CTD | T,C | | | | | 67 | End date is 2004-12-03 – not stated 2005-03-12 | | battery malfunct. |
| | PSM6931 | 3rd | 17 m | CTD | T,C | 20041001 | 7 | 20050111 | 8 | 68 | | | |
| | PSM6931 | 4th | 5 m | CTD | T,C | 20050112 | 11 | 20050406 | 7 | 69 | | | |
| | PSM6931 | 4th | 10 m | CTD | T,C | 20050112 | 11 | 20050406 | 7 | 70 | | | |
| | PSM6931 | 4th | 17 m | CTD | T,C | 20050112 | 11 | 20050406 | 7 | 71 | | | |
| SQ4T | PSM6931 | 1st | 1:2:21 m | TK | 11xT | 20040331 | 16 | 20040706 | 9 | 72 | | | |
| | PSM6931 | 2nd | 1:2:21 m | TK | 11xT | 20040707 | 11 | 20040929 | 9.5 | 73 | | | |
| | PSM6931 | 3rd | 1:2:21 m | TK | 11xT | 20040930 | 17 | 20050113 | 9 | 74 | | | |
| | PSM6931 | 4th | | 21 | | | | | | | Damaged according to plan | | |
| SQ5 | PSM6932 | 1st | 4 m | RCM+ | U,D,C,T,S | 20040401 | 12 | 20040705 | 14 | 75 | | | |
| | | 2nd | 4 m | RCM+ | U,D,C,T | 20040706 | 17 | 20040716 | 19 | 76 | Many errors. Worked only 10 d | Acknowledged | |
| | PSM6932 | 3rd | 4 m | RCM+ | U,D,C,T | 20040929 | 17 | 20050111 | 14 | 77 | T sensor OK until 2004-12-03 09:30 | | |
| | PSM6932 | 4th | 4 m | RCM+ | U,D,C,T | 20050111 | 15 | 20050329 | 9 | 78 | Depth not stated. Two missing data | | |
| Transects | | | | | | | | | | | | | |
| | | 0th | | ADCP | | 20040420 | | 20040420 | | 79 | Southern boundary | | |
| | | 1st | | ADCP | | 20040704 | | 20040704 | | 80 | Southern boundary | | |
| | | 2nd | | ADCP | | 20041020 | | 20041020 | | 81 | Northern boundary | | |
| | | 3rd | | | | | | | | | Purposely dismissed due to weather | | |
| | | 4th | | ADCP | | 20050413 | | 20050413 | | 82 | Northern boundary | | |
| | | 4th | | ADCP | | 20050413 | | 20050413 | | 83 | Eastern boundary | | |

# 2 Materials and methods

## 2.1 Model forcing data – temporal scales

The generic Baltic model (AS3D) employed in this study /Andrejev and Sokolov 1989, 1990/ together with its local variant modelling the Laxemar-Simpevarp area with a horizontal resolution of 0.1×0.1 nautical miles are both based on the primitive (*sensu* fundamental) Navier-Stokes equations formulated on a so-called C-grid /Arakawa 1966/ and is thus inherently similar to many other 3D-models. The numerical implementation has however several advanced features /Andrejev and Sokolov 1997/. The oceanographic state variables are condensed into files that can be inspected and graphically rendered with a specially designed tool named DAS (Data Assimilation System). In the Öregrundsgrepen area earlier development versions of this model have been applied a number of times /Engqvist and Andrejev 1999, 2000, 2008/ and also in special studies with focus on Average Age (*AvA*) and trajectory analysis /Engqvist et al. 2006/ as general measures of water exchange.

An important aspect in the general modelling context is the temporal resolution of the forcing given in Table 2-1. It is seen that the imposed forcing with the highest frequency pertains to the boundary data of salinity, temperature and sea level, which have been computed by the 3D-model of the Baltic. Of these data, the sea level subset is the one with the highest potential to induce rapid changes in the interior of the model domain since such changes are propagated with the speed of a long surface wave, while salinity and temperature fluctuations combine to form density variations which are propagated with the considerably slower speed of internal waves. For the long surface waves it would – under reasonable assumptions – take more than 20 minutes to travel the approximate 15 km from the boundaries to a mid-point of the model area. This in turn means that the shortest expected time-scale of the computed state variables would be of the order of an hour, so this has been the chosen frequency rate at which modelled data have been saved for the ensuing comparison with measurement data.

**Table 2-1. Overview of the forcing and other model data with regard to temporal resolution. ONP stands for Oskarshamn Nuclear Plants, DMI for Danish Meteorological Institute, and NLS denotes National Land Survey of Sweden. Gray fields denote that the data item applies to a particular time period.**

| | | | | Baltic model (BIS3D) | | | | | Local model (Sim3D) | | | | Remark |
|---|---|---|---|---|---|---|---|---|---|---|---|---|---|
| | | data | time re- | 2004 quarters | | | | 2005 | 2004 quarters | | | 2005 | |
| Forcing and other model data | | source | solution | 1st | 2nd | 3rd | 4th | 1st | 2nd | 3rd | 4th | 1st | |
| Grid of the 3D-modell | | NLS | - | | | | | | | | | | |
| Boundary forcing | | | | | | | | | | | | | |
| Göteborg | sea level | SMHI | 1h | | | | | | | | | | |
| Skager | sea level | DMI | 1h | | | | | | | | | | |
| Laxemar model domain | sea level + S&T | | 0.5h | | | | | | | | | | Data from the Baltic 3D-model |
| Meteorological data | misc. param. | SMHI | 3h | | | | | | | | | | Mesan data |
| Freshwater discharge | whole Baltic | SMHI | month | | | | | | | | | | HBV-model data. |
| | Laxemarsån | SMHI | w | | | | | | | | | | 2005 meas. delivered Mar'06 |
| | Gerseboån | SMHI | w | | | | | | | | | | |
| Cooling water | volume flow | ONP | month | | | | | | | | | | See Table 5 |
| | over temp. | ONP | - | | | | | | | | | | See Table 5 |
| | shut-down periods | ONP | 1d | | | | | | | | | | See Table 5 |
| Ice formation & breakup | | | 1d | | | | | | | | | | |
| Initialization S/T data | | ICES | - | | | | | | | | | | Climatic data + spin-up runs |
| Validation data: | | | | | | | | | | | | | |
| Salt- & Temp profiles | | SMHI | 1h | | | | | | | | | | |
| Current velocities | | SMHI | 1h | | | | | | | | | | |
| Sea level data | | SMHI | 1h | | | | | | | | | | |

The assessment of forcing data has not been without problems. The meteorological forcing data (so-called Mueller data set consisting of synoptical geostrophic wind) that have been used in earlier modeling studies /Engqvist and Andrejev 1999, 2000/ were stated by SMHI to be discontinued after 2001. To make up for this loss, so-called Mesan-data were offered to serve as a substitute. The first model runs of 2004 thus relied on the Mesan-data. Late in 2005 it was revealed that the Mueller data set for 2004 was available again and this extension eventually also included the first half year of 2005. A scatter diagram of these two data sets for July 2004 against measured wind speeds at Ölands Norra Udde is presented in Figure 2-1 and yields that the correlation coefficient for the Mesan-data is higher (0.84) than for the Mueller data (0.77), which is the reason for having chosen to use the former data consistently.

Freshwater discharge data with weekly resolution of the two major streams Laxemarsån and Gerseboån have been acquired from SMHI. Both of these streams display a marked seasonal variability, Figure 2-2.

The contemporary operation of the three reactors O1 through O3 requires cooling water which is withdrawn from the coast to the south of these reactors, and after fulfilling its cooling purpose is subsequently discharged with an average excess temperature of about 10°C. However, this cooling water is of no consequence for the advent of a possible leakage of nuclides from a future repository, since when this has been established, the reactors will be shut down according to plan. The cooling water is included in this study because of its factual but rather marginal influence on the water circulation and stratification during the study period April 2004 through April 2005, see Figure 2-3.

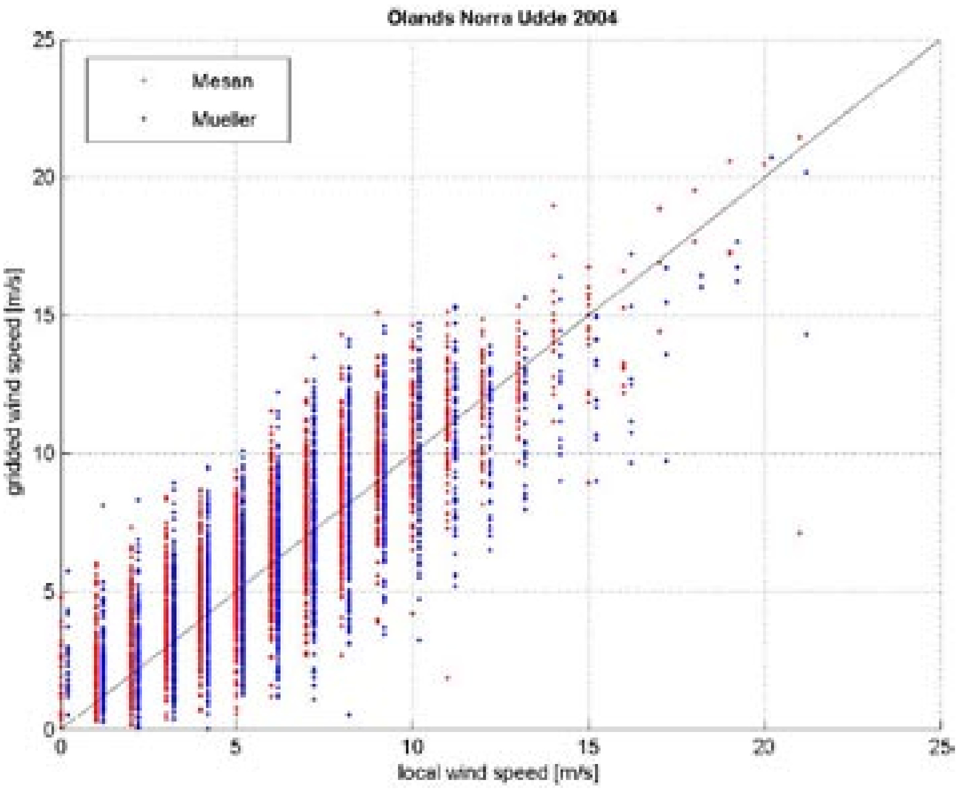


***Figure 2-1.*** *Comparison of Mueller and Mesan meteorological data relative measured local wind logged at Ölands Norra Udde. The geostrophical Mueller data have been projected to the standard height of 10 m above sea level and have been graphically shifted so that their points do not interfere with the Mesan data. The correlation coefficient of the Mesan data (ρ=0.84) is better than that for Mueller data (ρ=0.77), so the former data set has been used both for the Baltic and the fine-resoution local 3D-model.*

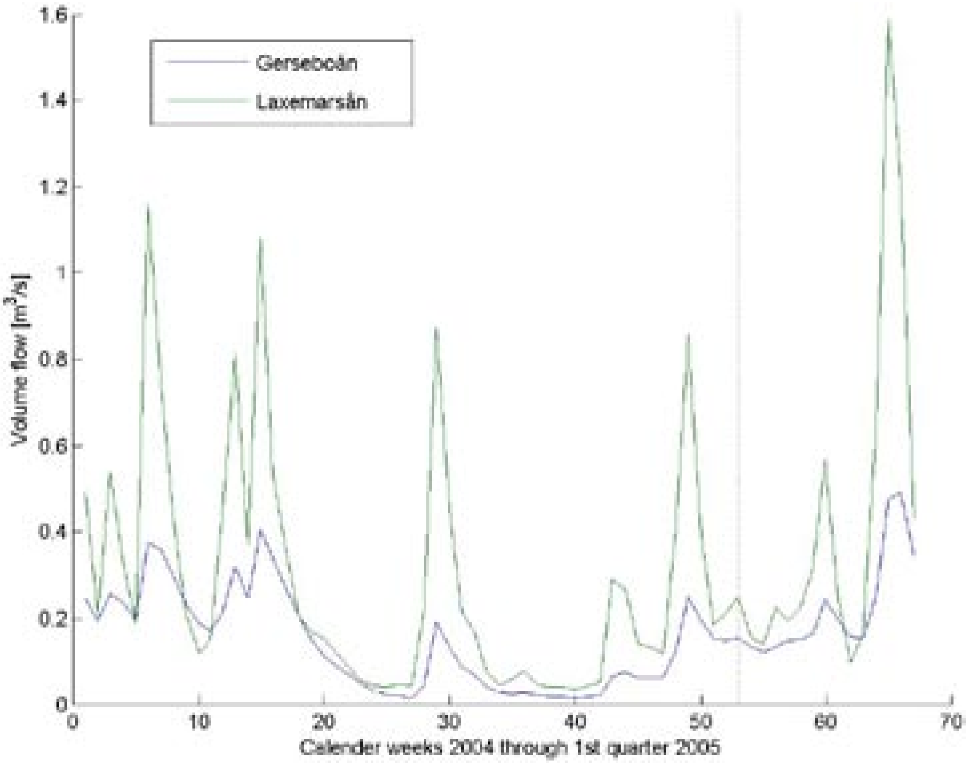


***Figure 2-2.*** *Freshwater discharge of the two major local streams that discharge into the interior of the local model area. The combined average discharge over the entire validation period amounts to about 0.5* $m^3s^{-1}$*. The transition between 2004/2005 is shown with a dotted line.*

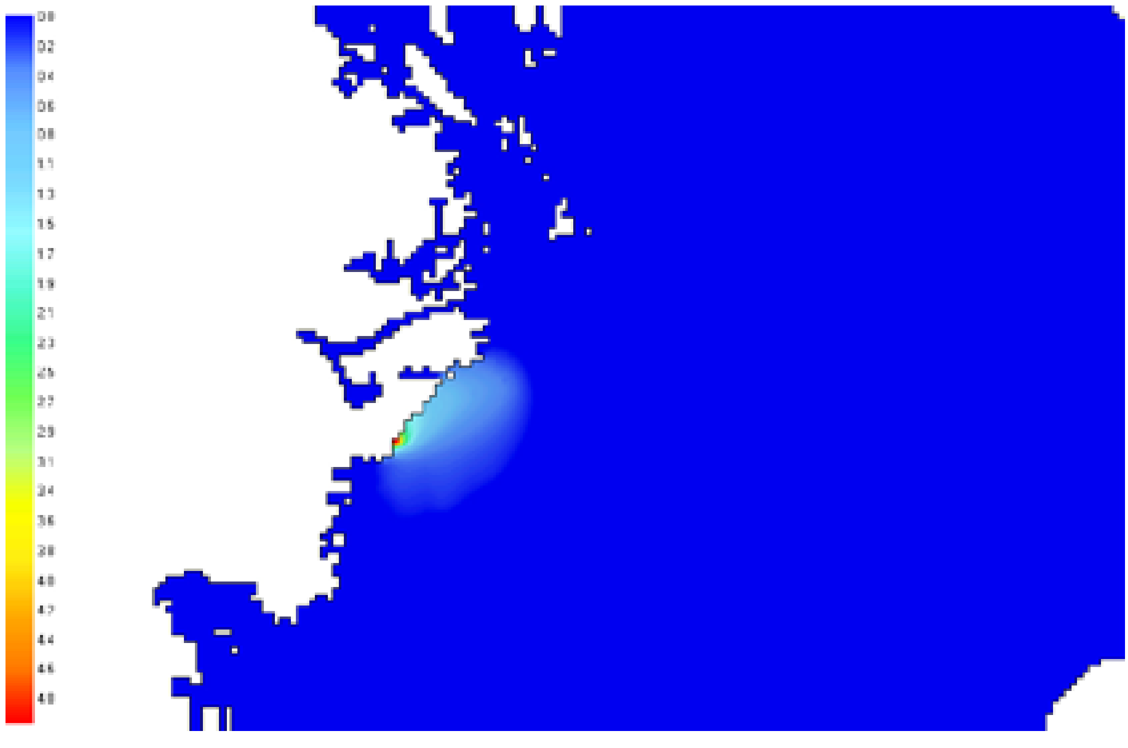

***Figure 2-3.*** *Snapshot of the surface temperature in winter conditions of the thermal plume discharge with an excess temperature between 10 and 11°C with a combined flow rate of about 90* $m^3s^{-1}$ *(Table 2-2). The three inlets are separately located south of the discharge point and on the shown occasion there is little evidence of recirculation.*

Cooling water data have been obtained from the operators of the three nuclear plants. During the model period (April 2004 through April 2005) the discharge of O1 and O2 has been 20 and 25 [$m^3/s$] respectively, while for O3 the flow rate amounts to 45 [$m^3/s$]. O1 was shut down during most of May 2004 and O2 during August same year, while the non-operational period of O3 mainly coincided with the month of July 2004, see Table 2-2. An indication of the outlet point of the cooling water can be seen in Figure 2-3.

It has not been possible to obtain any reliable ice observations for the coastal waters of the Laxemar-Simpevarp area most likely due to the fact that the comprised winter periods were mild and the coldest period with freezing air temperatures came late in the season (March 2004) and did not last more than a couple of weeks.

## 2.2 Extraction of model data

For the three stations located on the northern, eastern and southern boundary of the FR-model area encompassing both the data of the Baltic model CR-model code variant (BIS3D) and the local area FR-model (Sim3D) have been saved and made available. (The specific actual program versions are given in Table 2-3). For obvious reasons these data sets should not differ greatly since the latter is derived from interpolated data of the former, notwithstanding that the local FR-model boundary data are also to some degree modified by the interior dynamics of FR-model and the formulation of the boundary conditions. For these boundary stations the Baltic CR-model data have been used as a basis for comparison. For the other locations, that are interior in the FR-domain, the closest equivalent grid cell – both horizontally and vertically – has been chosen. The bulk of work has thus consisted of rearranging the output data of the models into appropriately formatted files suitable for statistical analysis.

**Table 2-2. Overview of nuclear reactor data and their implementation in the FR-model. The letters 'i' and 'j' denote E/W- and N/S-grid coordinates respectively in this local model.**

| | Volume flux | Over temp | Not in operation | Intake point: | | | Discharge point: | | | |
|---|---|---|---|---|---|---|---|---|---|---|
| Simpevarp 2004: | [m3/s] | [deg. C] | YYMMDD dates | i | j | depth | i | j | direction | depth |
| reactors | | | | | | | | | | |
| O1 | 20 | 10 | 040701-040815 | 47 | 46 | surface | 52 | 49 | E | surface |
| O2 | 25 | 11 | 040815-040916 | 49 | 46 | surface | 52 | 49 | E | surface |
| O3 | 45 | 11 | 040522-040612 | 51 | 45 | bottom | 52 | 49 | E | surface |

**Table 2-3. Correlation coefficients between measured and modelled data, averaged over all measurement periods with valid data taken together. Grey fields mean 'not applicable'. The actual program version of the CR(FR)-model is 'Bis3D1u4'('Sim3D4f3') and the CDB-model version is 'LaxBa25b'. Gray fields indicate 'not applicable'.**

| | | Salinity | | Temperature | | U-component | | V-component | | Model |
|---|---|---|---|---|---|---|---|---|---|---|
| Station | depth | corr coef | N= | corr coef | N= | corr coef | N= | corr coef | N= | type |
| Si21 | 2.0 m | 0.78 | 259 | 0.95 | 325 | 0.30 | 693 | 0.16 | 693 | CR |
| | 10 m | 0.77 | 259 | 0.93 | 325 | -0.08 | 693 | 0.44 | 693 | CR |
| | 17 m | 0.90 | 162 | 0.82 | 228 | 0.01 | 693 | 0.44 | 693 | CR |
| | 30 m | 0.73 | 196 | 0.60 | 257 | 0.27 | 693 | 0.21 | 693 | CR |
| Si22 | 58 m | 0.78 | 187 | 0.90 | 187 | 0.05 | 374 | -0.01 | 374 | CR |
| Si23 | 2-20 m | | | | | 0.10 | 684 | 0.01 | 685 | CR |
| Si24 | 2 & 5 m | 0.80 | 327 | 0.94 | 327 | | | | | FR |
| | 10 m | 0.69 | 269 | 0.92 | 327 | | | | | FR |
| | 17 m | 0.77 | 327 | 0.85 | 327 | | | | | FR |
| Si24T | 1-21 m | | | 0.84 | 266 | | | | | FR |
| Si25 | 4.5 m | 0.94 | 3202 | 0.97 | 3202 | 0.49 | 6510 | | | CDB |

## 2.3 Extraction of measurement data

Initially the extraction of the measurement data was hampered by the things that make data processing difficult: format changes, unmotivated change of units, data without specification, data with erroneous specification, varying depth ranges, transient data retained at the beginning and ending of a measurement period, etc. Most of these nuisances were mitigated for the data files that were submitted into the SICADA database from which the measurement data could be retrieved in a standard format. The naming of the files is given in Table 1-2, and the time of deployment and remarks in Table 1-3.

## 2.4 Spectral analysis and choice of comparison time frames

In order to find an appropriate sampling rate for making the comparison with simulated salinity and temperature data without missing relevant variations and thereby producing bias (so-called *alias* errors), the power spectra for representative months of the different seasons have been investigated using the Fast Fourier Transform (FFT) in the Matlab toolbox. The typical outcome of this encompassing analysis is presented in Figure 2-4 concerning temperature and Figure 2-5 for salinity, from which it is clear that the bulk of the contained variance concerning salinity and temperature measurements is located in the part of the spectra that lies below diurnal rates, i.e. once a day. Thus daily samples of measured and simulated salinity and temperature can be compared without loss of generality and introduction of spectral aliases.

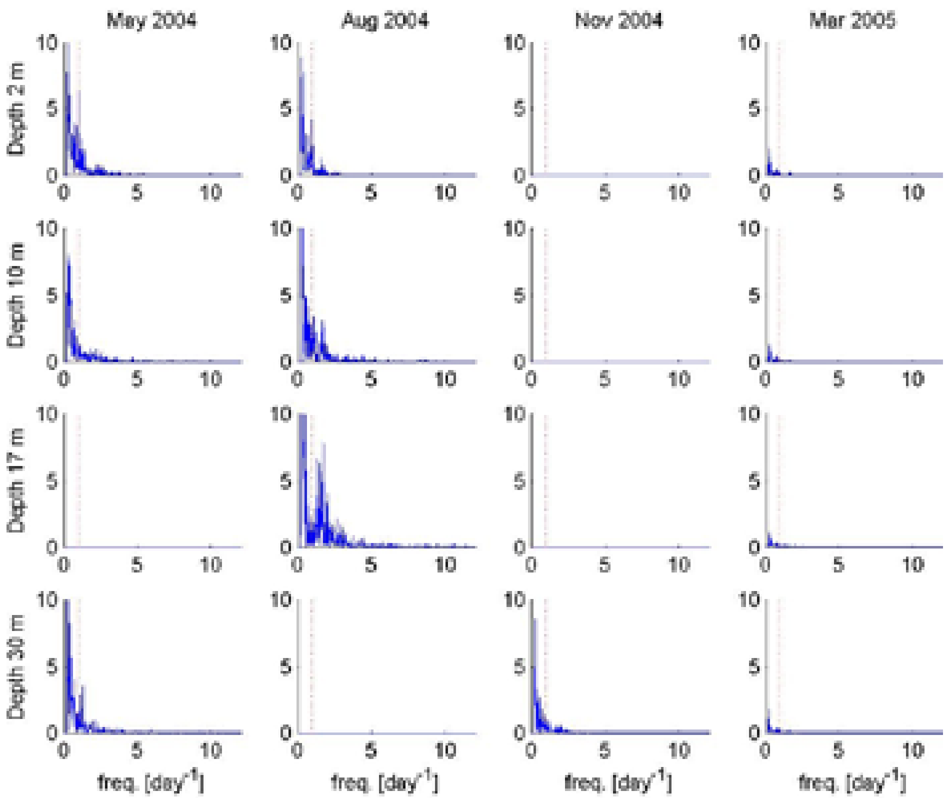


***Figure 2-4.*** *Temperature spectra of station Si21 with regard to depth and seasonality. Each of the 16 'subplots' is a so-called power spectrum and its y-axis thus denotes the variance distribution with regard to sampling frequency of the temperature measurements. Combinations with missing data are left empty. With the possible exception of August and 17-m depth, most variance is located at frequencies below 1 day$^{-1}$. This means that the comparisons to simulated data can be performed with daily samples, which frequency is indicated with a red dotted line.*

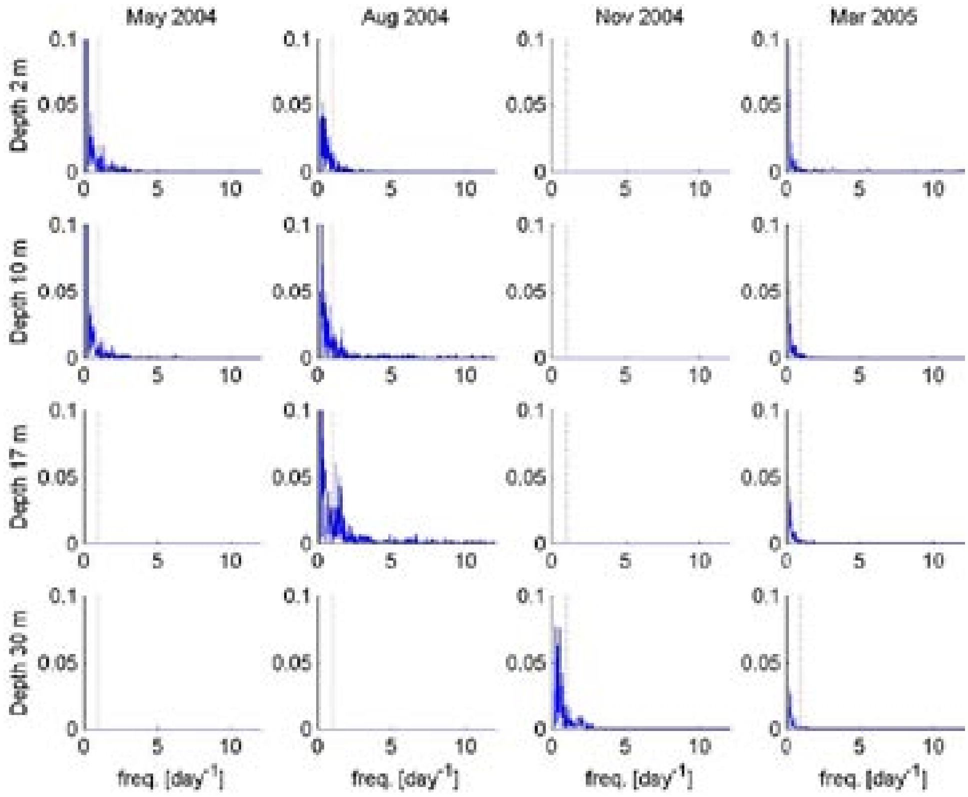


***Figure 2-5.*** *Salinity spectra of station Si21 with regard to depth and seasonality. Each of the 16 'subplots' is a so-called power spectrum and its y-axis thus denotes the variance distribution with regard to sampling frequency of the salinity measurements. Combinations with missing data are left empty. Without exception all variance is located on frequencies above 1 day$^{-1}$. This means that the comparisons to simulated data can be performed with daily samples, which frequency is indicated with a red dotted line.*

In Figure 2-6 the corresponding spectrum analysis is performed on the ADCP instrument placed at station Si21 where 19 layers of orthogonal current components are measured. Both panels pertain to period 1 and span the depth interval 3 m through 39 m. The east/west (U) current component displays more variance for frequencies higher than 2 day$^{-1}$ (i.e. twice a day), than the north/south (V) current component, but even for the bottom layers most of the variance is found below this frequency. This means that semidiurnal sampling suffices to give a fair comparison to simulated data. To be on the safe side all current comparisons have been conducted with a semidiurnal (12 h) sampling rate. This also applies to most of the current measurements at other locations.

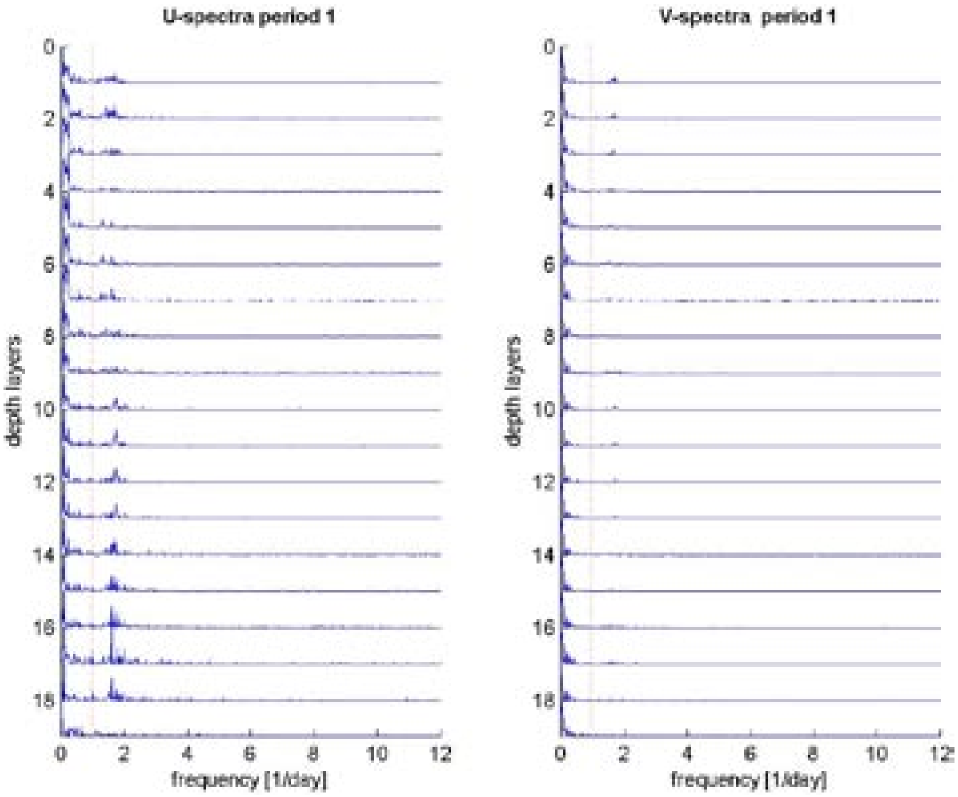


***Figure 2-6.*** *a (left panel). The spectra of the east/west(U)-velocity components. Each of these 19 'sub-plots' is a so-called power spectrum with its y-axis thus denoting the variance distribution with regard to the frequency of the measured velocity's U-component, which shows that most variance is located below the frequency 2 day$^{-1}$ i.e. twice a day. b (right panel). The spectra of the north/south(V)-velocity components. Each of these 19 'subplots' denotes the same the variance distribution as for figure a, but with regard to the frequency of  the measured velocity's V-component. Virtually all variance is located at frequencies below once a day or equivently with a diurnal periodicity. For all subplots in both panels this diurnal periodicity is indicated with a red dotted line.*

## 2.5 Statistical methods of comparison

The method of comparison is direct and straightforward. The corresponding data as to horizontal and vertical location are extracted with their FFT-determined appropriate sampling rates and are subsequently subjected to ocular and statistical comparison. The latter consists of invoking the cross-correlation function that is supplied in the Matlab toolbox together with graphically depicted regression lines. All computed correlation coefficients are summarized and accounted for in Table 2-3. It can be pointed out that concerning the regression lines, the slopes are often less than unity, which value corresponds to a hypothetical perfect match between the data set pairs. Inaccuracy in the measurements can be shown to significantly contribute to such less-than-ideal slopes (Anders Grimvall, pers comm).

# 3 Results

## 3.1 Overview and intercomparison of salinity and temperature measurements

First an overview of the scalar measurement entities salinity and temperature is given in Figure 3-1. The most striking feature is the noticeable fluctuation of salinity measured at station Si22 in the depth bracket around 50 m. Some tendencies towards unstable stratification (water with higher salinities on top of deeper layers at approximately the same temperature) can be observed, for example at Si24. This will be scrutinized more in detail when the data of the separate station are analyzed below. At station Si23 only velocity was measured. The inter-comparison of salinity and temperature measurements between the stations seems otherwise consistent within the allowance that the data gaps necessitate. The salinity and temperature levels are seemingly comparable between the stations. At station Si24 temperature was also measured with a thermistor chain with eleven levels giving an improved vertical resolution. This will be examined in detail below.

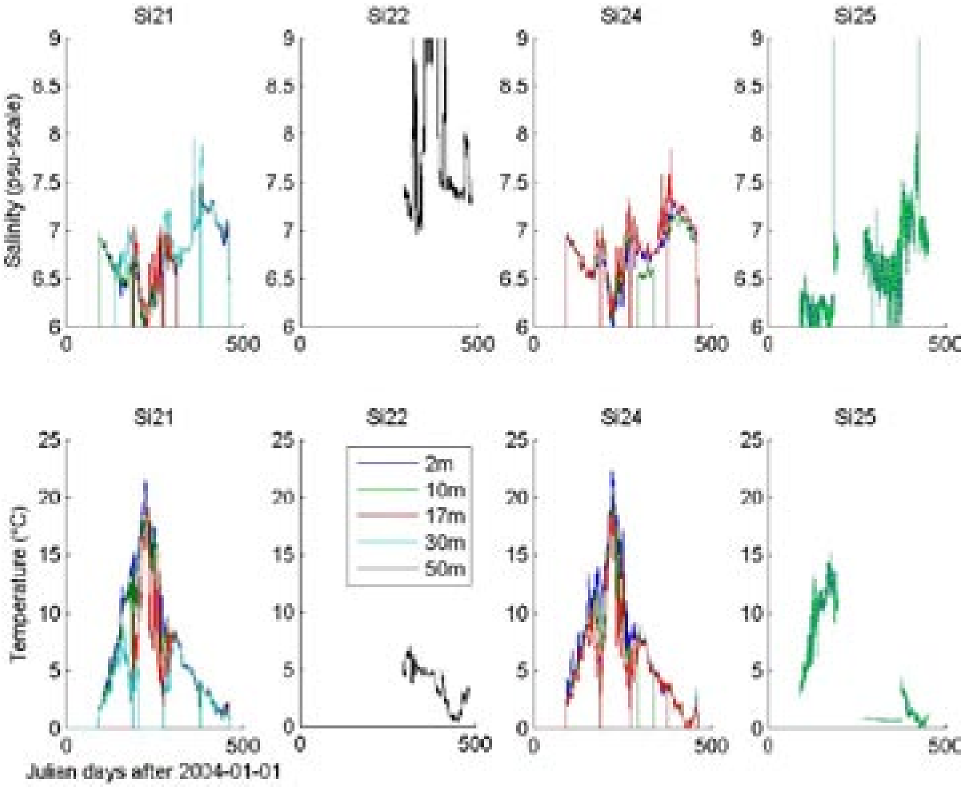


*Figure 3-1. Overview of the salinity and temperature measurements of all stations at which these scalar entities were measured. The overall signatures of different stations are strikingly similar with the exception of Si22 that is measured at a considerably deeper depths of about 50 m. This station displays a conspicuously extended leading data gap. Data gaps of other stations may not be as easily identified in this figure since curves may overlap. Obviously erroneous data can in spite of this be seen for Si25. At the station Si23 only velocities were measured and this station has thus been exempted from this overview.*

## 3.2 Station Si21

At the peripheral station Si21 positioned near the center of the northern boundary all four parameters (salinity, temperature and two orthogonal velocity components) were logged. A closer look at the salinity and temperature curves pertaining to Si21 in Figure 3-1 reveals that the salinity stratification (upper panel in Figure 3-2) is seemingly stable, while in autumn penetrative convection makes the salinity curves almost coincidental. The vertical line at the onset and termination of each measurement period help to identify the transitions between the four measurement periods. These endpoints have systematically been removed in the ensuing statistical analysis and this applies to the time series of all stations.

The temperature measurements (lower panel in Figure 3-2) made during the spring and summer heating period (before JD 225) are due to the formation of a thermocline, only occasionally interrupted by vertical mixing and possible up-/down-welling events that only affect the two surface-most measurement depths, e.g. near JD 160. The same consistency applies to the cooling period (after JD 300) when thermally well-mixed conditions mainly prevail from the 2- to 30-m depth. The noticeable continued cooling at the 30-m level during the first period is probably due to an onset of the same instrument malfunctioning that disqualified its data during the second period.

Such vertical mixing events represent an irreversible and thus lasting effect. A wind-induced down-welling, on the other hand, means a temporary vertical redistribution of water which should recoil quite soon after the wind subsides. This has little lasting effect on the internal vertical distribution of the salinity and temperature fields.

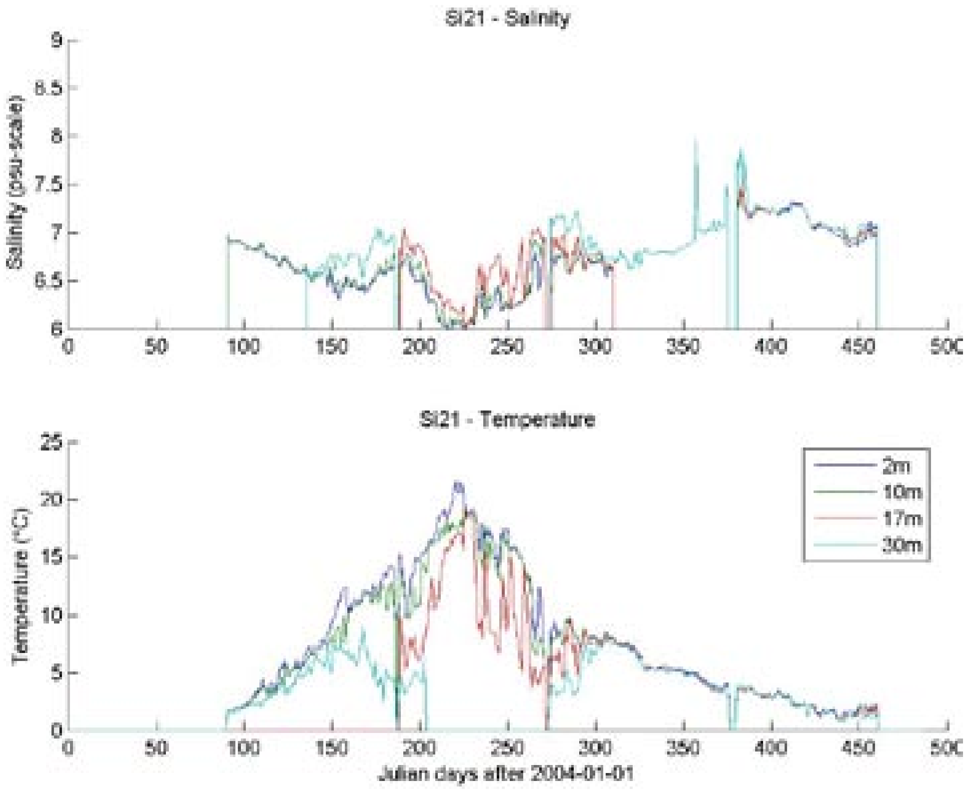


***Figure 3-2.*** *Overview of the salinity and temperature measurements at Si21. The salinity stratification is seemingly stable and the temperature curves are consistent with springtime formation of a thermocline, while in autumn penetrative convection makes both the salinity and the temperature curves almost coinciding. The vertical part on the onset and termination of each respective measurement period helps to identify the transitions between the four measurement periods.*

In Figure 3-3 the temperature development during the entire validation period is shown with measurements at the respective depth layers together with the corresponding simulated values. With the exception of the measurement at 30 m that was discontinued about JD 200, the transitions between the measurement periods are clearly visible. The surface-most measurements and simulated temperature curve match one another quite well. Also at the rapid cooling instance about JD 320–350 there is an almost exact match between observed and modeled temperatures at all four depths.

Simulated and observed salinities at station Si21 for the duration of the validation period are depicted in Figure 3-4. In addition to a general falling trend of the simulated salinity curves, there are both similarities and differences. In spite of the noticeable offset for the curve pairs for the depths between 2-m and 17-m until JD 300, these pairs are obviously strongly covariant, which is most clearly seen at the salinity depletion event occurring on JD 200 through 240. At the end of the entire simulation period all curves converge.

In Figure 3-5, the scatter diagram displays differences between measured and simulated temperatures at station Si21. The corresponding correlation coefficients are given in Table 2-3 and amounts to 0.95 for the surface layer but diminish to 0.60 at 30 m.

A scatter diagram between measured and simulated salinities of the station Si21 is displayed in Figure 3-6 with separate regression lines for the four depths. The corresponding correlation coefficients are given in Table 2-3 and are on the 0.80 level, which means that most of the measured salinity dynamics (64%) is captured by the model. The regression lines for the surface measurements are closer to the ideal diagonal line, and for all four depths the slope of the regression lines is close to the ideal 1:1 slope.

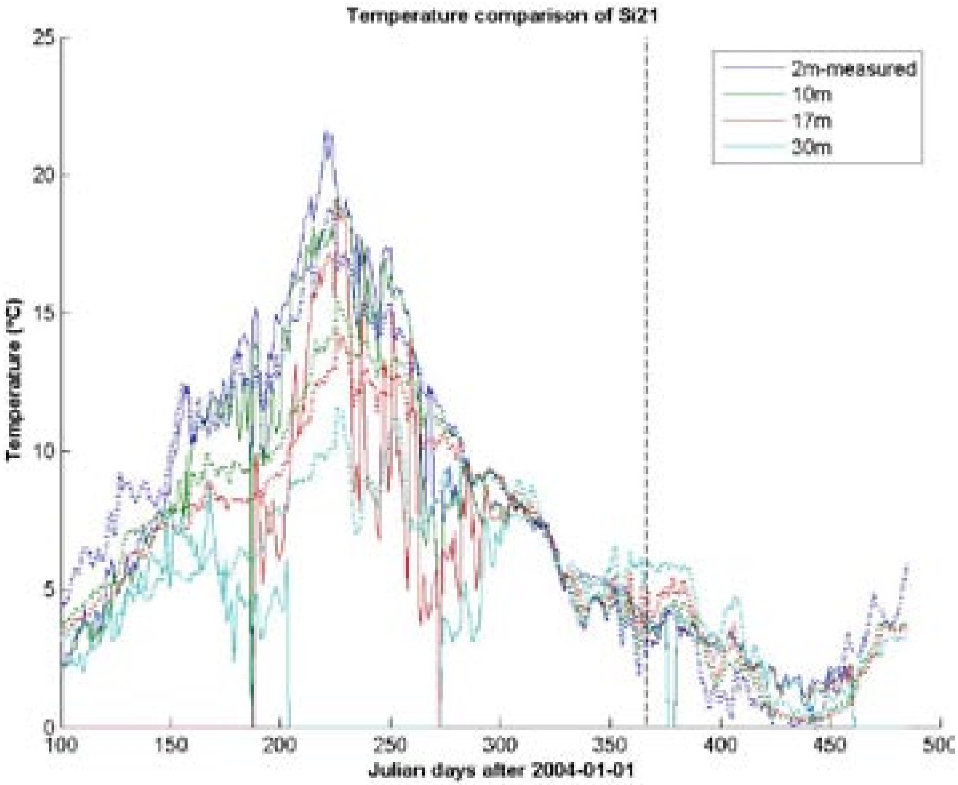


***Figure 3-3.*** *Comparison of simulated (dotted) and measured (solid) temperature data for different depths at station Si21. With the exception of the measurement at 30 m that was discontinued about JD 200, the transitions between the measurement periods are clearly visible. The surface-most measurements and simulated temperature curve match one another quite well. Also at the rapid cooling instance about JD 320 there is an almost exact match between all four pairs of curves.*

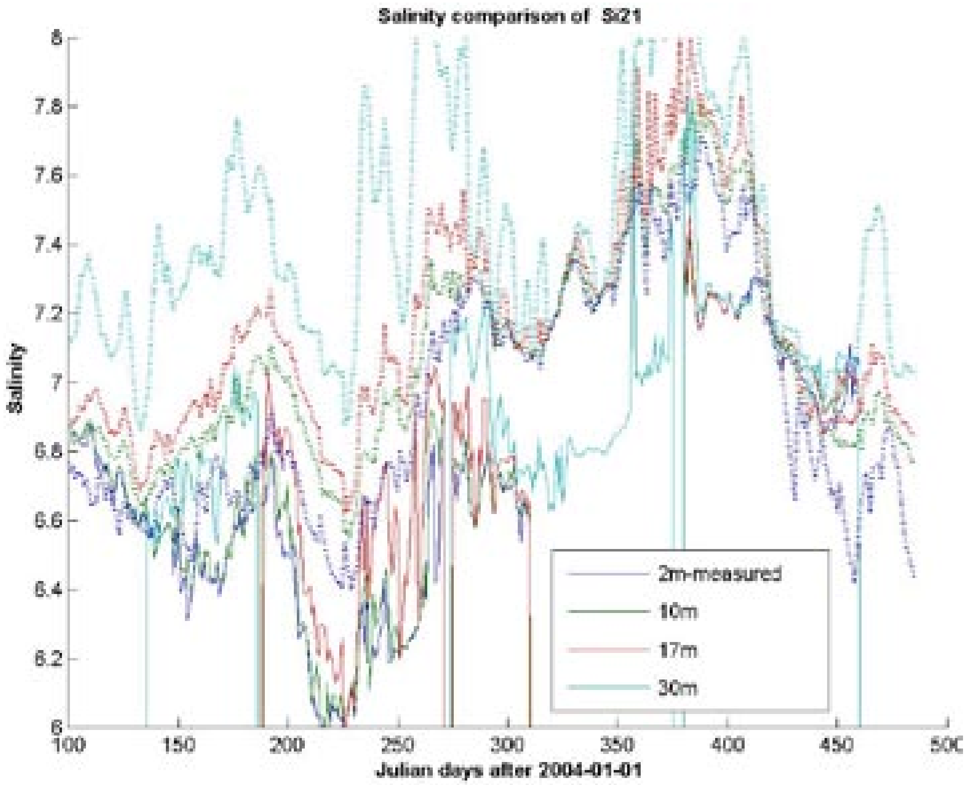


*Figure 3-4.* Comparison of simulated (dotted) and measured (solid) salinity data for different depths at station Si21. In spite of the noticeable offset between the measured and the simulated values until JD 300, these pairs are obviously strongly covariant, which is most clearly seen at the salinity depletion event occurring on JD 200 through 240. At the end of the entire simulation period all time series come closer together.

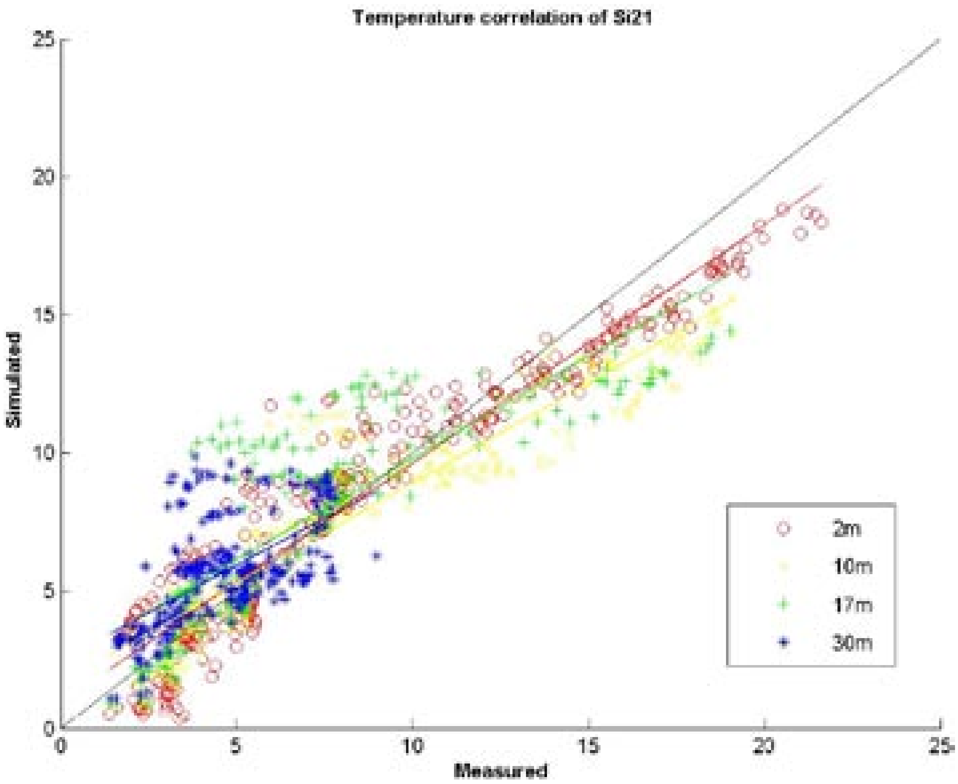


*Figure 3-5.* Scatter diagram for measured and simulated temperature of Si21 with regression lines for the four depths in same colors as is indicated by the legend. The line that indicates a perfect match is depicted in black. The corresponding correlation coefficients are given in Table 2-3 and are 0.95 for the surface layer but diminish to 0.60 at 30 m which is to some extent a consequence of the restricted range of the temperature variation over the year cycle at this depth. The regression lines are quite close to the ideal line in black.

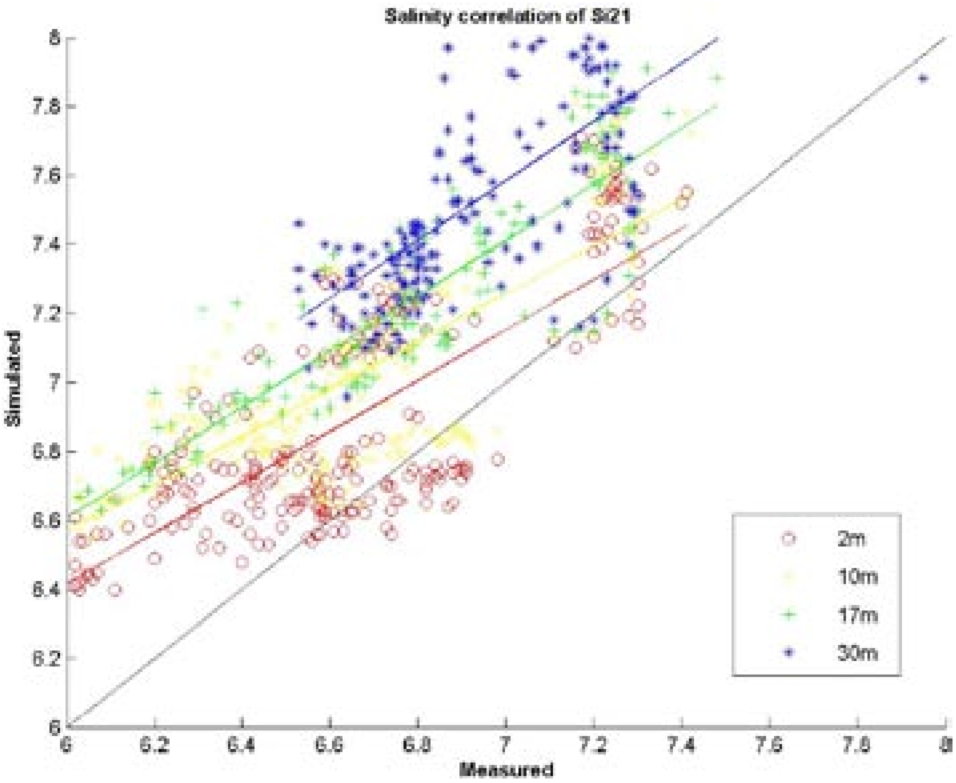


***Figure 3-6.*** *Scatter diagram for measured and simulated salinity of Si21 with regression lines for the four depths in same colors as is indicated by the legend. The line that indicates a perfect match is depicted in black. The corresponding correlation coefficients are given in Table 2-3 and are on the 0.80 level which is a reassuring expression that most of the measured dynamics is captured by the CR-model. The regression lines for the surface measurements are closer to the ideal line, and for all four depths the slope of the regression lines is close to the ideal.*

In Figure 3-7 contour diagrams of measured E/W-velocity (U-) component at station Si21 are depicted with a half-hour sampling rate but processed with a 5 h-running average filter and compared to the correspondingly processed simulated data. The measurements were conducted with an ADCP instrument. There are no striking similarities of the features of these diagrams. The current levels are basically comparable, with only a few notable exceptions. The overall correlation levels are in spite of this comparatively high for the surface and the bottom measurements, see Table 2-3. This figure foremost confirms the apprehended considerable temporal variance in the flow field.

Contour diagrams of measured N/S-velocity (V-) component at station Si21 are shown in Figure 3-8. These diagrams are based on the same sampling rate as in Figure 3-7, i.e. smoothed with a 5 h running average filter and compared to the correspondingly treated simulated data. The current levels are basically comparable with only a few notable exceptions. On JD 350–380 the simulation shows an intensification of current from the surface to the bottom that has no counterpart in the measured data. In spite of this for the two intermediary levels the correlation coefficients are 0.44 (Table 2-3).

In Figure 3-9 a scatter plot between measured and simulated N/S-current velocity (V-component) velocity of Si21 is given. Ocular inspection gives that there is only a faint, if any, tendency of alignment along the ideal diagonal, but the range of the two data sets is the same. The correlation coefficients are given in Table 2-3 for the computed depths that are closest to the measured depths.

Correlation between measured and simulated E/W- current velocity (U-) component velocity of Si21 is shown in Figure 3-10. In comparison to Figure 3-9, ocular inspection shows even less tendency of alignment along the ideal diagonal. The correlation coefficients are given in Table 2-3 and are highest for the top and bottom levels 2 m and 30 m, i.e. complementary to the levels of the maxima found for the N/S-component.

Common to both these velocity correlation diagrams is that the simulated data range is comparable to the measured data range.

In Figure 3-11 a comparison of current speed spectra for six depth levels is presented. The frequency distribution of the variance of the measured and simulated data is similar despite that the found correlation coefficients are quite small and even negative in a few instances. For the surface-most layer there is unevenly distributed variance over the entire frequency range that does not correspond to the simulated data. For the 5 m-layer there is coinciding variance for the frequency around 0.3 day$^{-1}$. For all spectra of the simulated currents, the major variance is found at frequencies lower than about 0.1 day$^{-1}$.

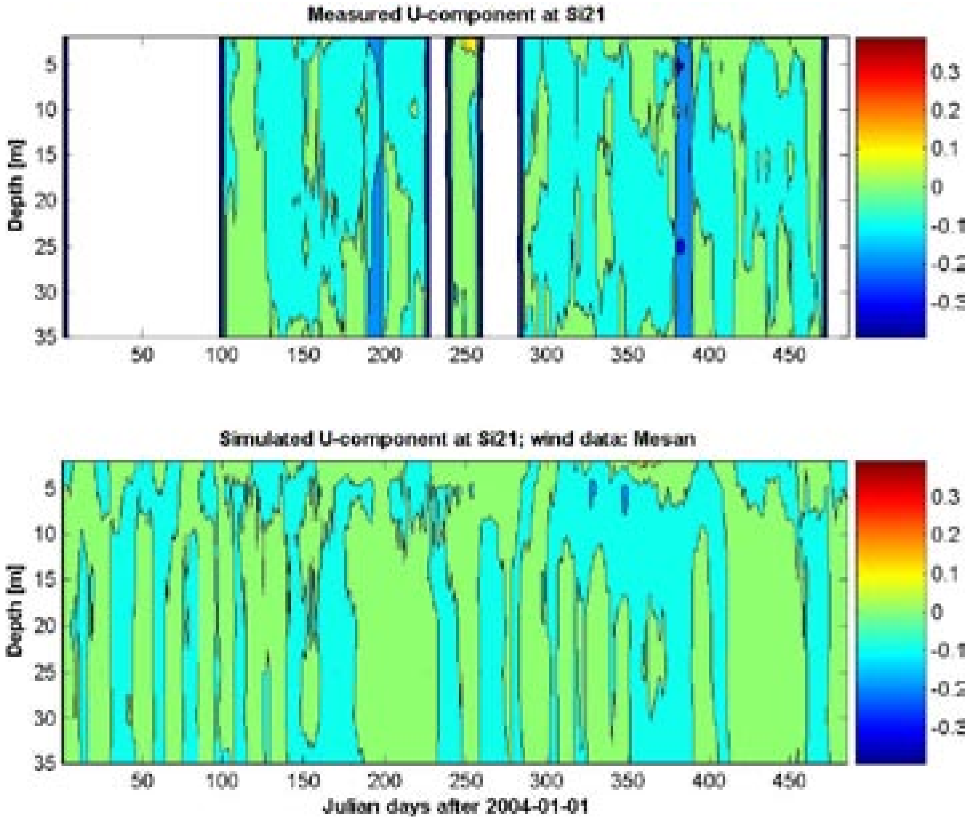


*Figure 3-7. Contour diagram comparison between measured and simulated E/W-velocity (U-) component of Si21. In order to enhance any similar features these data series have been processed with a 5 h-running average filter. The measurements were conducted with an ADCP instrument. Periods with no data are blanked. There are no striking similarities of the features of these diagrams. The current levels are basically comparable with only a few notable exceptions. The overall correlation levels are, in spite of this, comparatively high for the surface and the bottom measurements, see Table 2-3.*

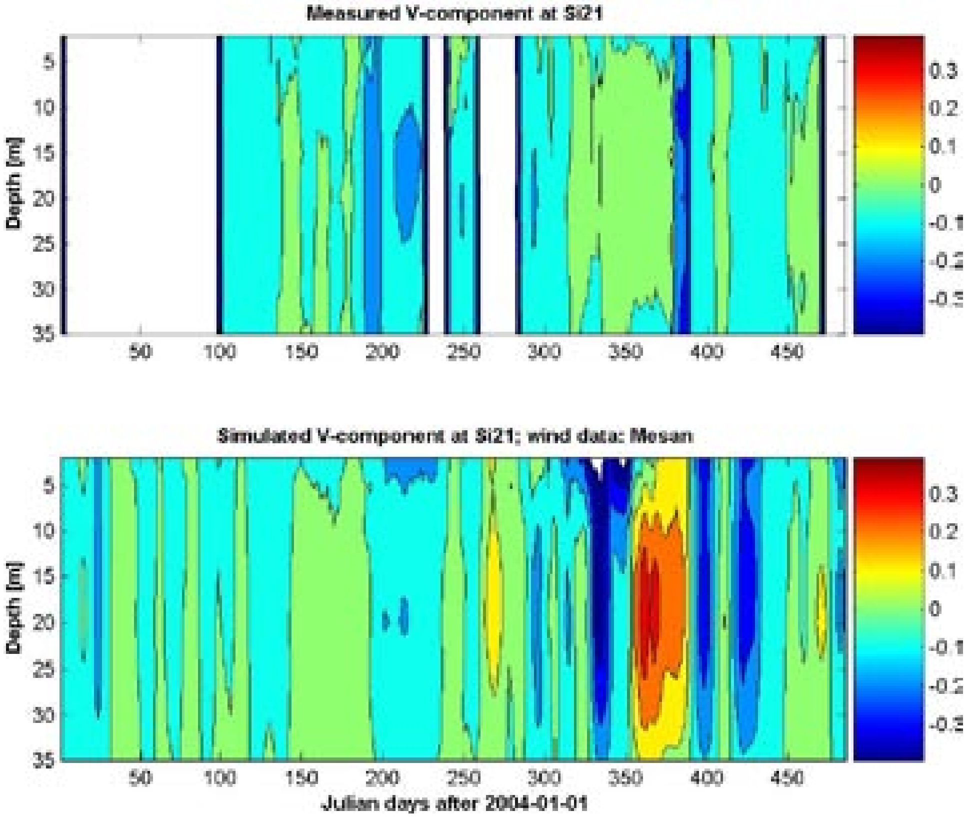


***Figure 3-8.*** *Contour diagram comparison between measured and simulated N/S-velocity (V-) component of Si21. The comparison is based on a 0.5-h sampling rate but processed with a 5 h-running average filter. Periods with no data are blanked. The current levels are basically comparable with only a few notable exceptions. On JD 350–380 the simulation shows an intensification of current from surface to the bottom that has no counterpart in the measured data. For the two intermediary levels the correlation coefficients are 0.44 (Table 2-3).*

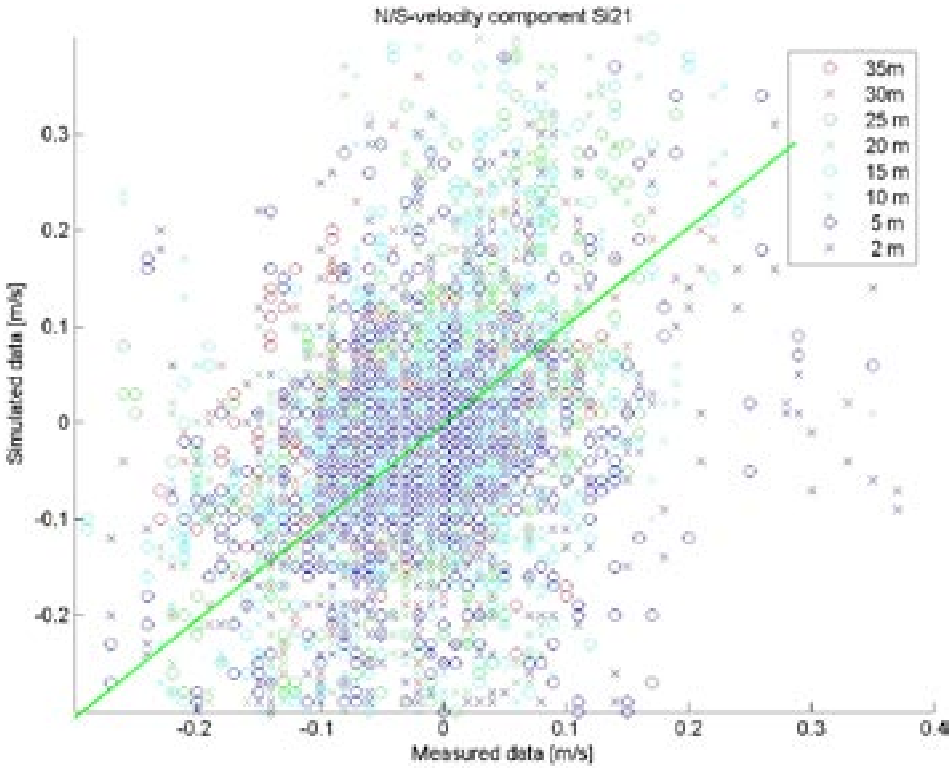


*Figure 3-9.* *Correlation between measured and simulated N/S- current velocity (V)-component velocity of Si21. Ocular inspection may suggest that there is a slight tendency of alignment along the diagonal. The correlation coefficients are given in Table 2-3 and are highest for the intermediary levels 10 m and 17 m.*

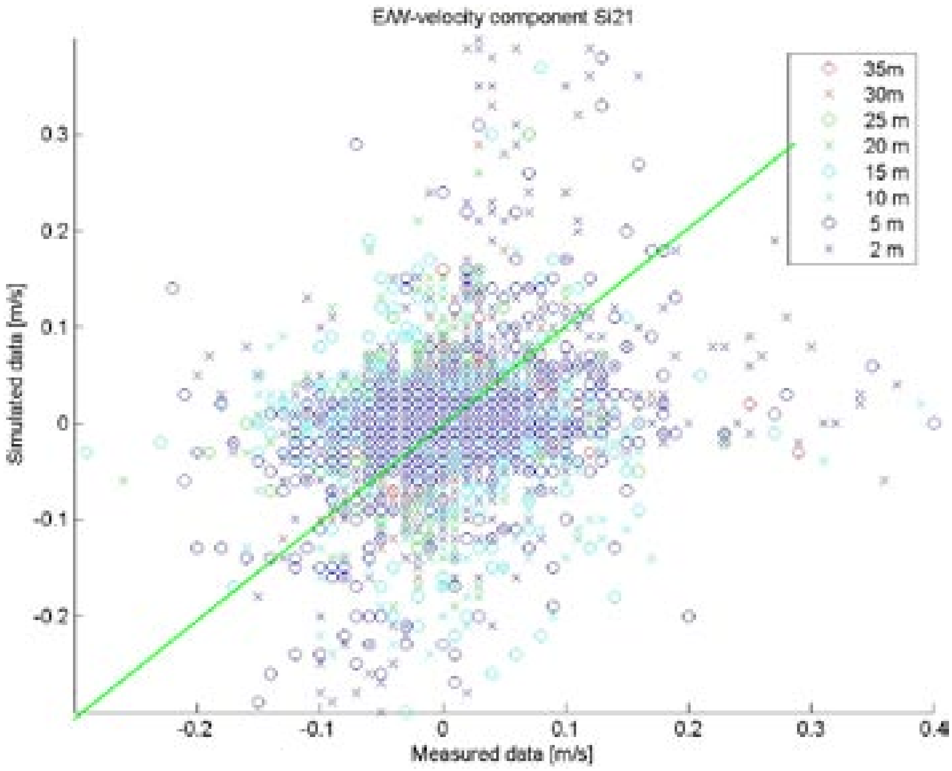


*Figure 3-10.* *Correlation between measured and simulated E/W- current velocity (U)-component velocity of Si21. Ocular inspection does hardly indicate any tendency of alignment along the diagonal. The correlation coefficients are given in Table 2-3 and are highest for the top and bottom levels 2 m and 30 m, i.e. complementary to the levels of the maxima found for the N/S-component.*

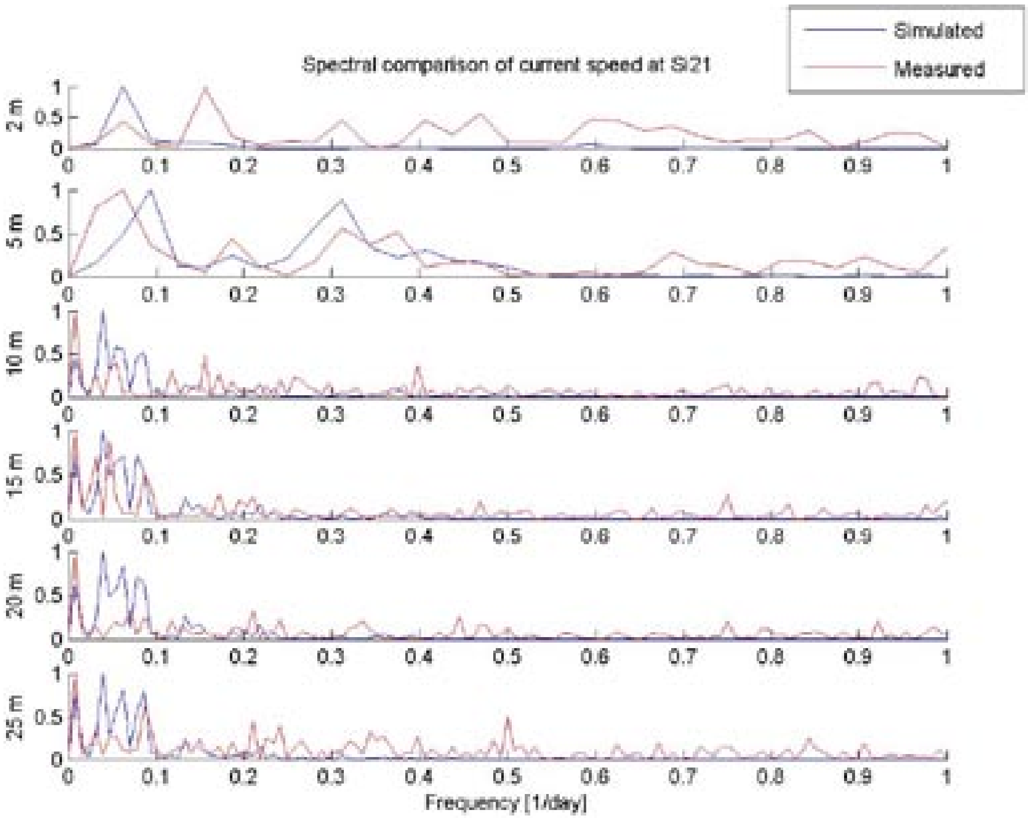


***Figure 3-11.*** *Comparison between measured and simulated velocity spectra of station Si21. For the surface-most layer there is unevenly distributed variance over the entire frequency range that does not correspond to the simulated data. For the 5-m layer there is coinciding variance for the frequency around 0.3 day$^{-1}$. For all spectra of the simulated currents, the major variance is found at frequencies lower than 0.1 day$^{-1}$.*

## 3.3 Station Si22

The measurement data of station Si22 only exist for the third and fourth periods due to instrument failure. During these periods the instrument was dislocated due to interference by ships so that different depths are indicated for the two measurement periods: 58 m (49 m) for the third (fourth) period.

An overview of the salinity and temperature measurements for these two periods is given in Figure 3-12. In spite of the changed measuring depth, both the salinity and the temperature curves are continuous with no obvious jump indicating the transition between the third and the fourth periods. The time when the instrument was inadvertently dislodged has not been possible to establish. To complicate matters further, a second instrument was deployed at Si22 (Table 1-3) but only functioned five days and gave no salinity recordings.

The salinity spiked several times during these two periods but resumed an average interval between 7 and 8 psu. The temperature curve displays an almost monotonous seasonal decline during winter and then rises slightly toward spring which is consistent with the damping of the seasonal surface signal with depths.

A comparison of the measured and simulated temperature at these depths at station Si22 is shown in Figure 3-13. After JD 380 the two curves are obviously quite covariant. Prior to this date there are at least similar levels but the measurements display more rapid transitions that the simulated time series do not capture.

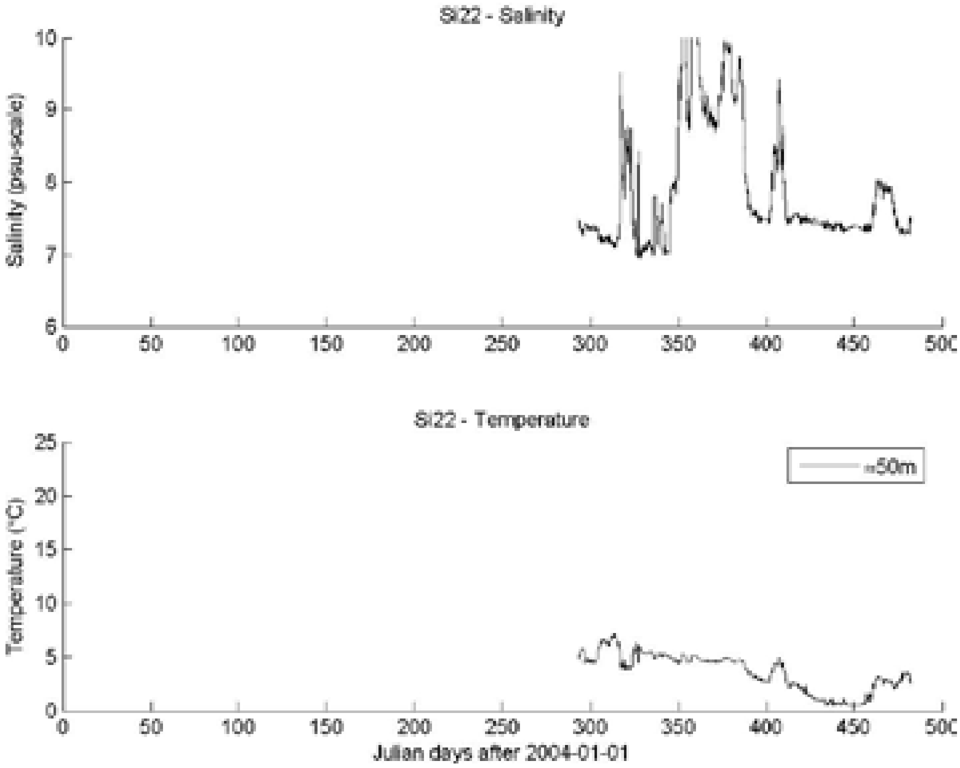


*Figure 3-12.* *Overview of salinity and temperature measurements at station Si22. Only in the third and fourth measurement periods was this instrument in proper operation. It was further accidentally dislodged from its original placement so that different depths are indicated for the two measurement periods: 58 m for the third period and 49 m for the fourth.*

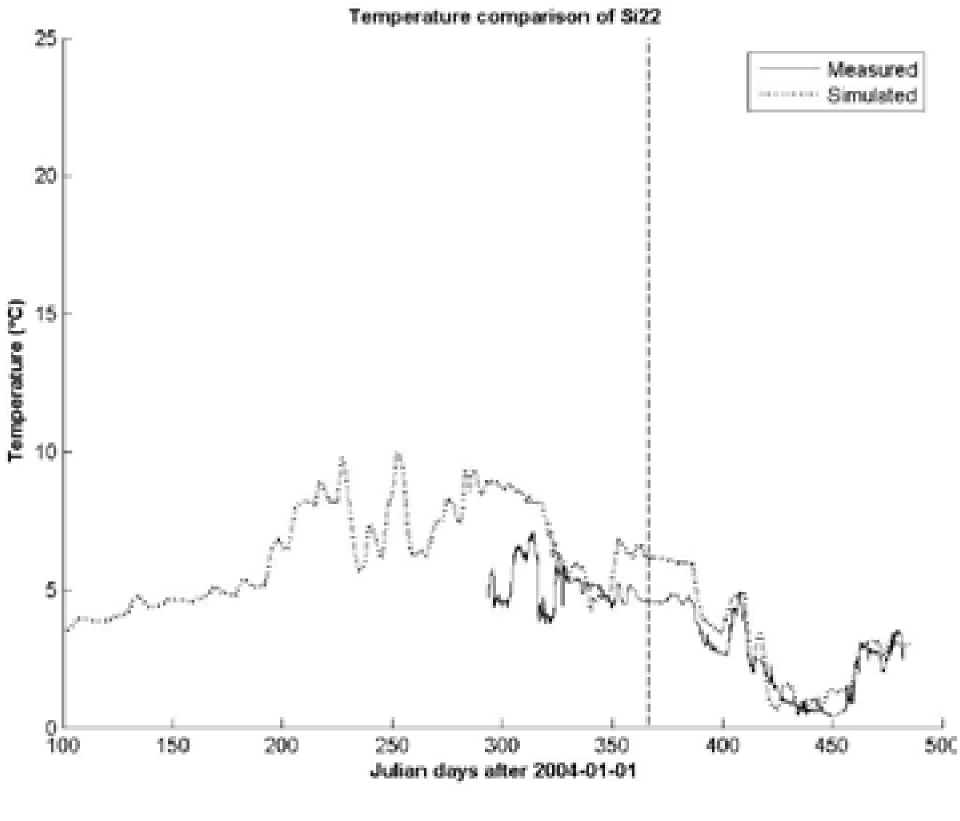


*Figure 3-13.* *Comparison of measured and simulated temperatures at station Si22, with the transition between 2004/2005 indicated by a broken line. At least during 2005, the covariation between the measured and the simulated data is strikingly good which is confirmed by the correlation level given in Table 2-3.*

The corresponding diagram concerning salinity (Figure 3-14) shows that the transition events are almost simultaneous but that the simulated curve does not reach the same amplitudes as does the measured curve, even though the levels are comparable.

In Figure 3-15 a scatter diagram of measured versus simulated temperature at station Si22 is shown. The simulated temperatures are slightly overestimated but the slope of the regression line is acceptably close to the 1:1 slope of the ideal line. The correlation coefficient is 0.90.

The corresponding scatter diagram (Figure 3-16) for salinity displays a regression line that slopes considerably less steeply than an ideal relationship. This could partly be caused by the two different depths that were involved. The correlation coefficient is 0.78.

A comparison of E/W-component of the current at Si22 shows (Figure 3-17) that the measured current component flows steadily to the east while the simulated current reverses direction a number of times. The current intensities are however comparable. The corresponding comparison of the N/S-component (Figure 3-18) shows that there is almost no flow in this direction. The most likely explanation is that the instrument during both periods had been inadvertently deployed in a rift oriented in the E/W-direction.

Scatter diagrams of the east/west(U)- and north/south(V)-velocity components at station Si22 at 12-m depth are given in Figure 3-19 and Figure 3-20 respectively. The corresponding small correlation coefficients (Table 2-3) confirm what an ocular inspection already has made obvious.

In Figure 3-21 a spectral comparison of the simulated and measured current speed at station Si22 is presented. This comparison is independent of the current direction and demonstrates that the spectral appearances are not notably dissimilar in spite of the small correlation coefficients of the U- and V-velocity components, although the measurement data have more variance located towards higher frequencies.

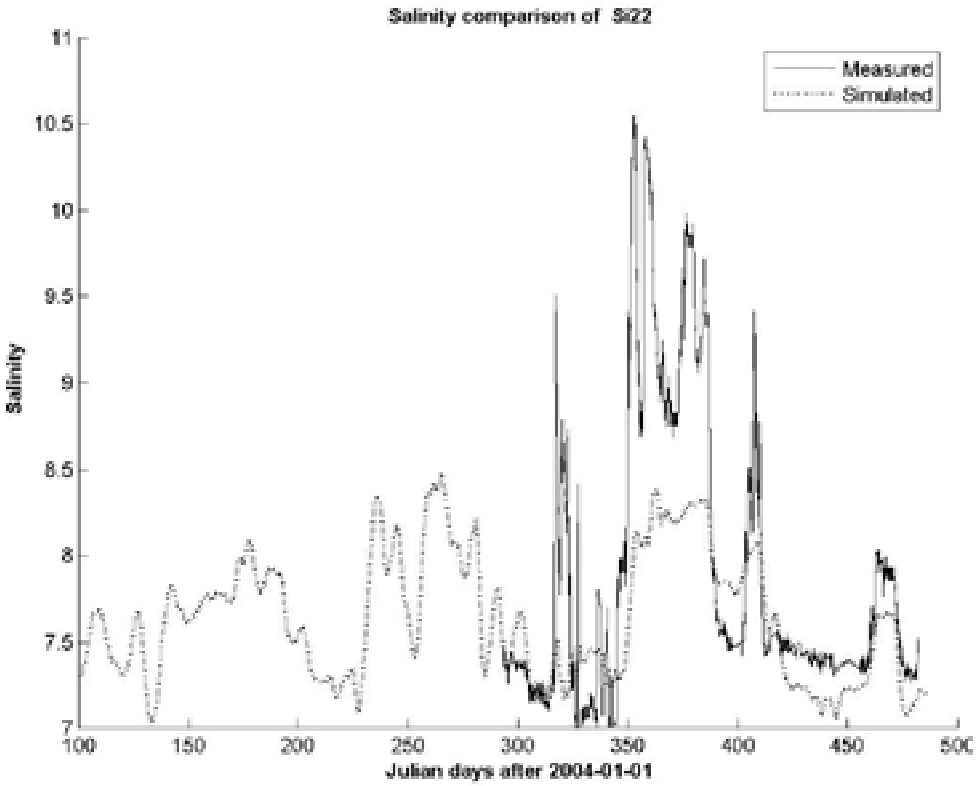


***Figure 3-14.*** *Comparison of the measured and simulated salinity at station Si22. After JD 350 the covariation between the measured and the simulated data is seemingly good which is confirmed by the comparatively high correlation given in Table 2-3. During the period JD 350–390 both the measurement and the simulated data make a simultaneous jump upward even though the measurement time series reaches  higher values than the modeled data.*

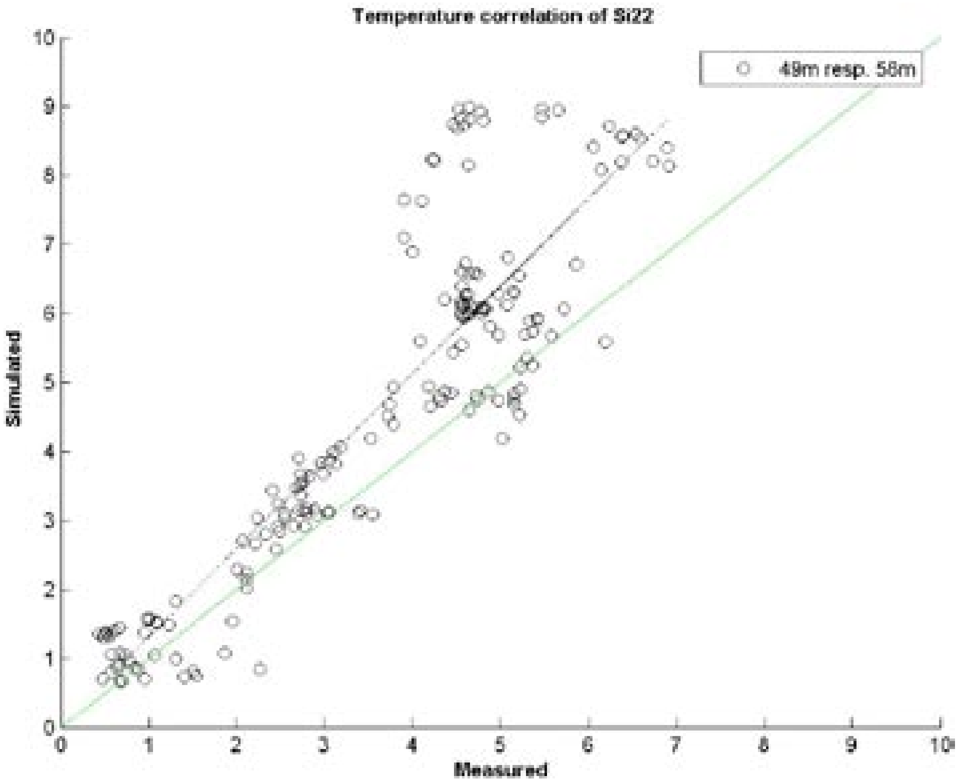


*Figure 3-15.* Scatter diagram for measured and simulated temperature of Si21. The green diagonal line represents the ideal relationship. The black line is a regression line, the slope of which is acceptably close to the green diagonal line.

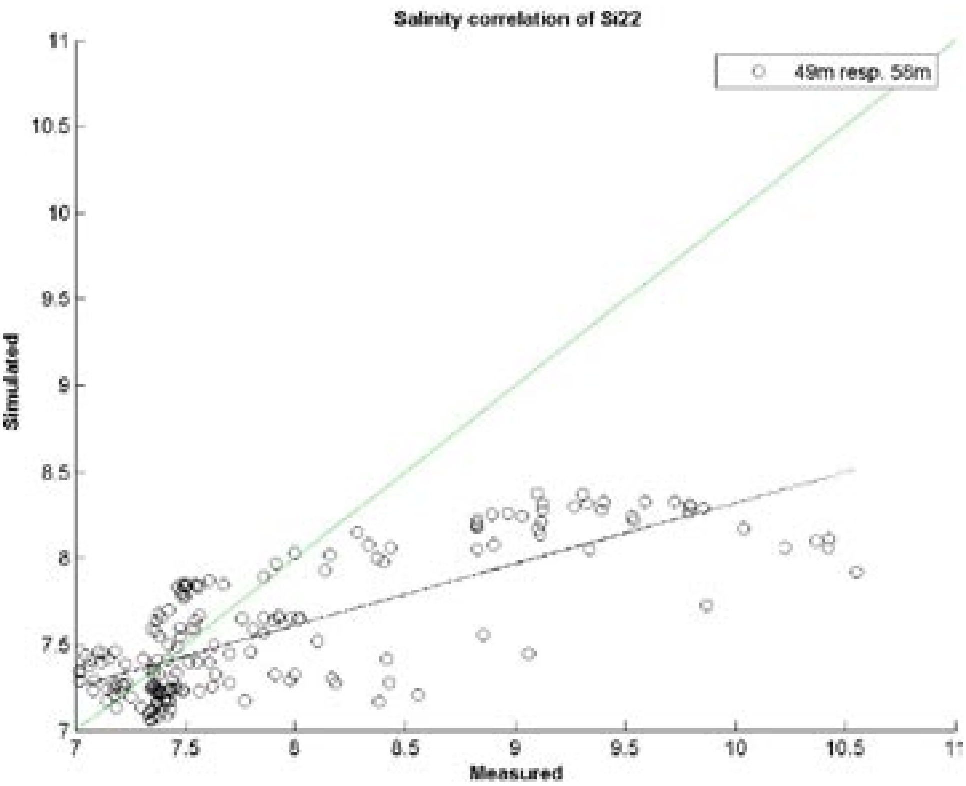


*Figure 3-16.* Scatter diagram for measured and simulated temperature of Si21. The green diagonal line represents the ideal relationship. The black line is a regression line, the slope of which is considerably less steep than the ideal diagonal (green) line. This could at least partly be explained by the two different depths on which the instrument was deployed during the third and fourth periods. The time when the instrument was accidentally dislodged is not possible to establish.

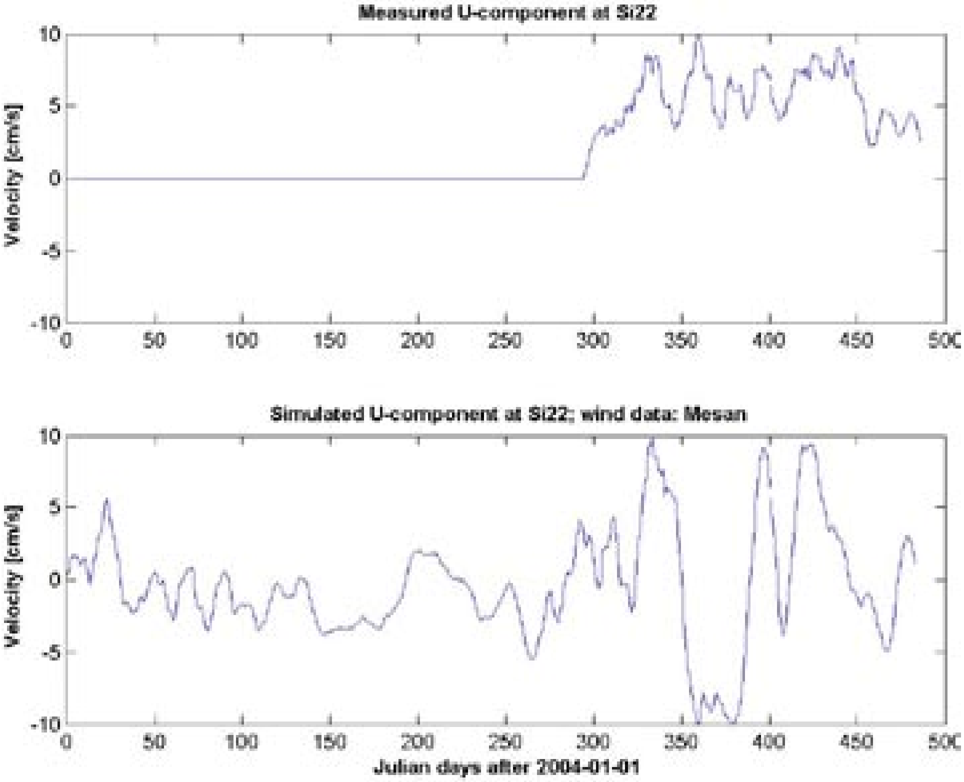


***Figure 3-17.*** *Comparison between measured and simulated E/W-velocity (U-) component of Si22. Data are available only for the two last measurement periods. Virtually no correlation can be visually discerned which is also confirmed in Table 2-3.*

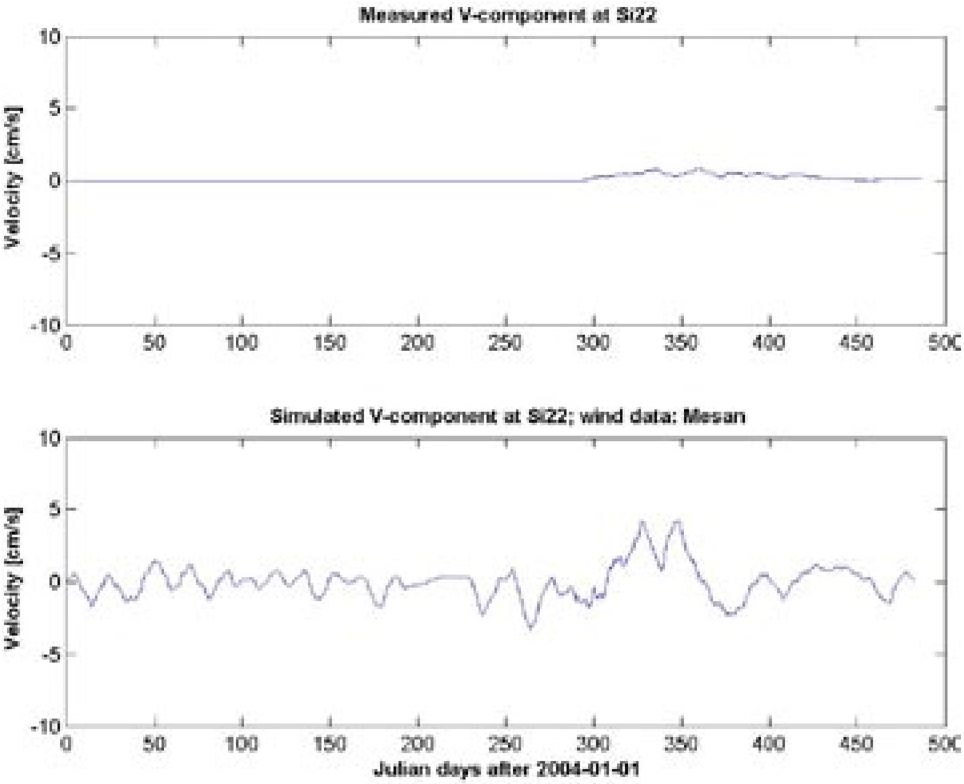


***Figure 3-18.*** *Comparison between measured and simulated N/S-velocity (V-) component at station Si22. Data are available only for the two last measurement periods starting on JD 300. Virtually no correlation can be visually discerned which is also confirmed in Table 2-3.*

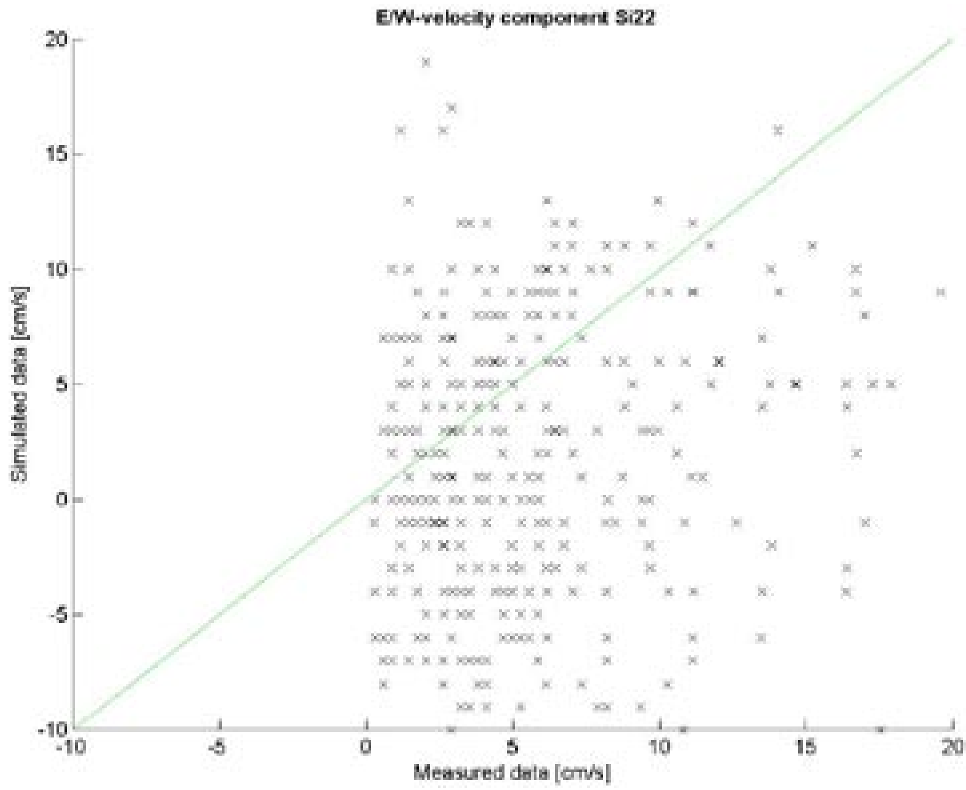


*Figure 3-19.* *Scatter diagram for measured and simulated E/W-velocity (U-) component of Si22. This pattern seems like a rectangular distribution and yields a correlation coefficient of a mere 0.05 according to Table 2-3.*

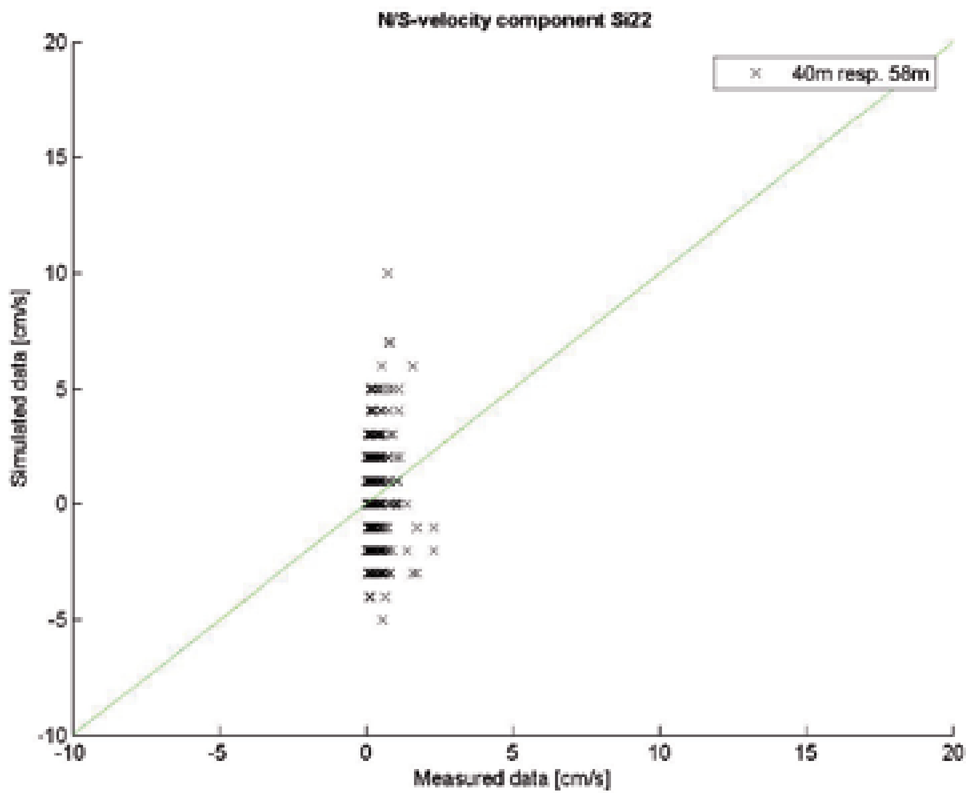


*Figure 3-20.* *Scatter diagram for measured and simulated N/S-velocity (V-) component of Si22. The lack of variation in the measured data is most likely due to an accidental placement of the instrument in a rift that is oriented in the orthogonal (E/W) direction.*

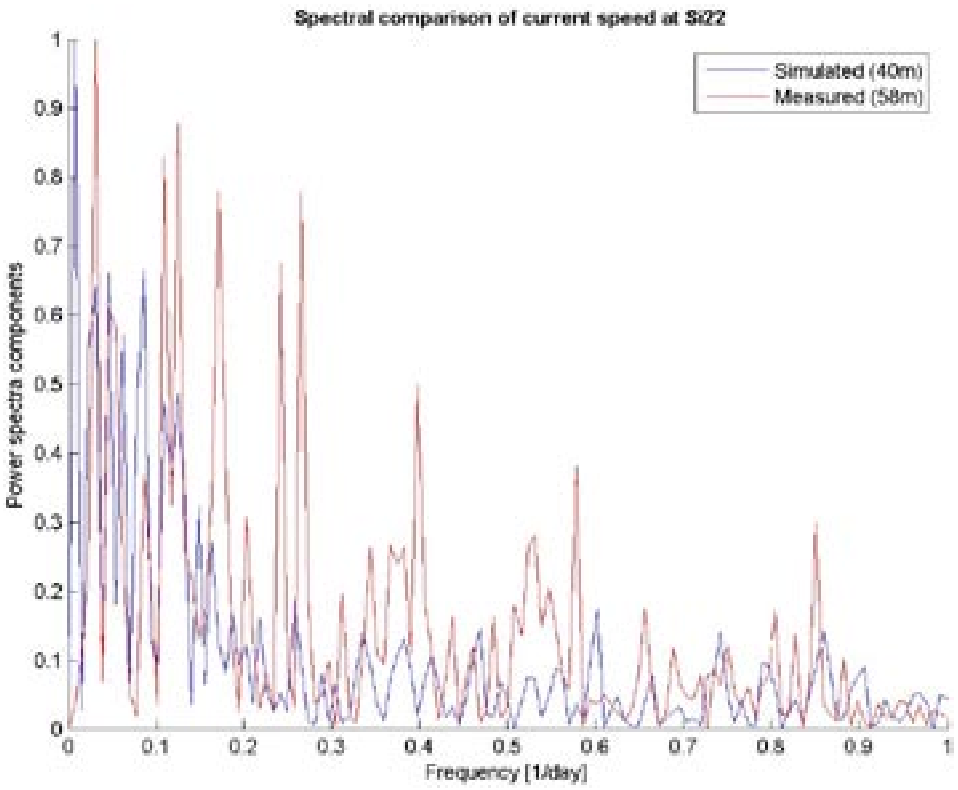


***Figure 3-21.*** *Comparison between measured and simulated velocity spectra of Si22. Both spectra display variance contribution distributed over the entire range down to the Nyquist frequency (once per day) but the measurement data have more variance located towards higher frequencies. The measured data are unknown as to their depth that could be somewhere between 49 m to 58. The compared simulated data are taken from the layer centered about 40 m depth.*

## 3.4 Station Si23

At station Si23 only ADCP-measurements were made. In Figure 3-22 a contour diagram comparison between measured and simulated E/W-velocity components is presented. In order to enhance any similar features, these data series have been processed with a 5 h running average filter. The current levels are basically comparable with only a few notable exceptions, in particular for the surface-most layers.

Corresponding contour diagram comparison of the N/S-velocity component between measured and simulated currents is shown in Figure 3-23. The current levels are again comparable with some exceptions for the surface-most layers.

Scatter diagrams between measured and simulated E/W (N/S)-components of velocity at Si23 are presented in Figure 3-24 (Figure 3-25). No correlation is visually discernible, and the average correlation coefficient over the entire water column amounts to 0.1 (0.01) according to Table 2-3.

In Figure 3-26 a comparison is shown between measured and simulated velocity spectra at Si23. With the exception of the 10-m level, most measured variance is found for frequencies below 0.1 day$^{-1}$. This feature is also regenerated by the simulated data, but with a small contribution to the surface-most layer for daily variations.

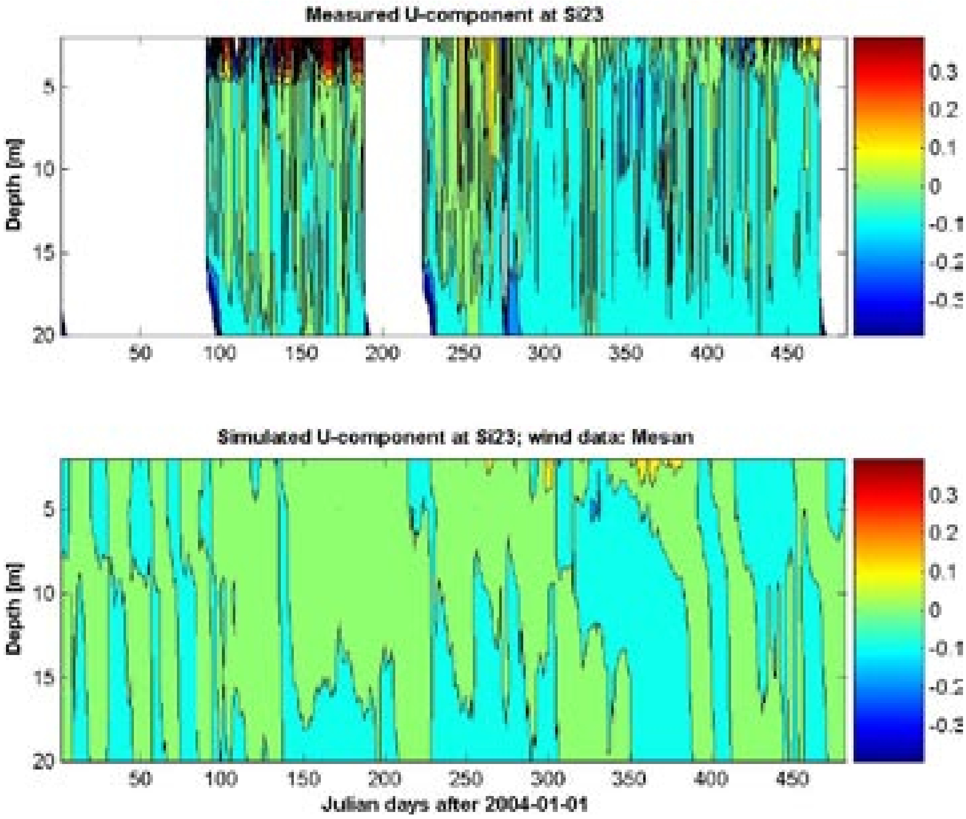


*__Figure 3-22.__ Contour diagram comparison between measured and simulated E/W-velocity (U-) component of Si23. Periods with no data are blanked. In order to enhance any similar features these data series have been processed with a 5 h-running average filter. The measurements were conducted with an ADCP instrument. The current levels are basically comparable with only the notable exception for the surfacemost layers JD 100-180. The overall correlation level averaged over the water column amounts to 0.1, see Table 2-3.*

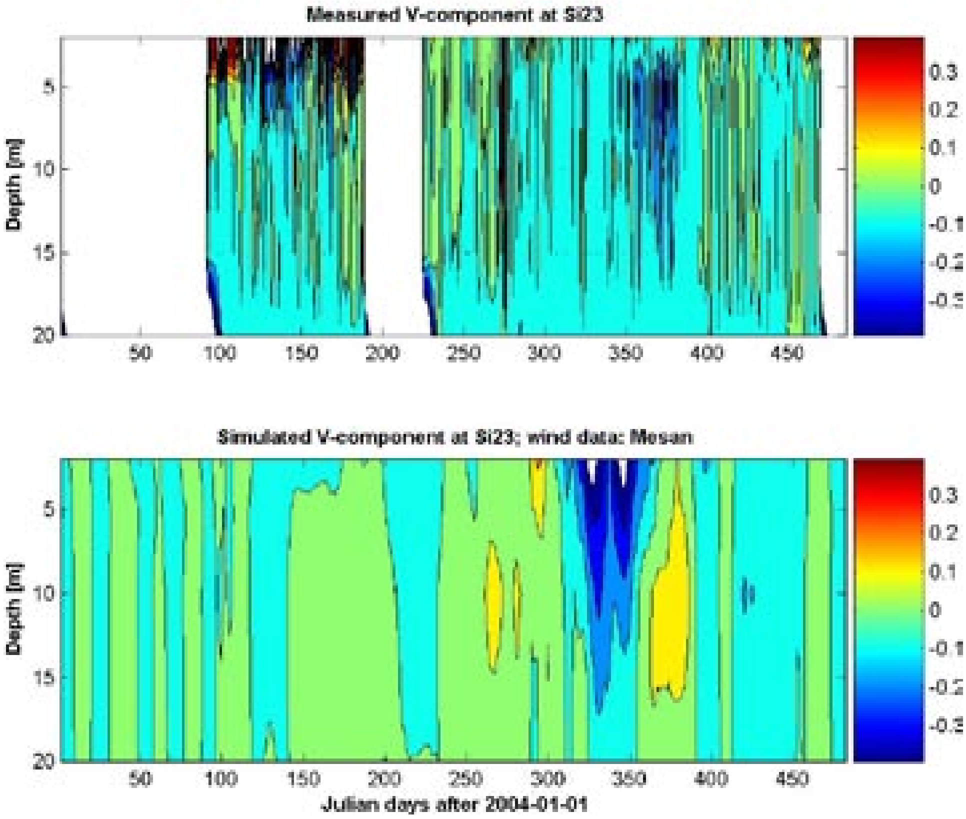


***Figure 3-23.*** *Contour diagram comparison between measured and simulated N/S-velocity (V-) component of Si23. Periods with no data are blanked. In order to enhance any similar features, these data series have been processed with a 5 h-running average filter. The measurements were conducted with an ADCP instrument. The magnitudes of the current levels are basically comparable but otherwise there is virtually no agreement between these two contour plots. The overall correlation level averaged over the water column amounts to a mere 0.01, see Table 2-3.*

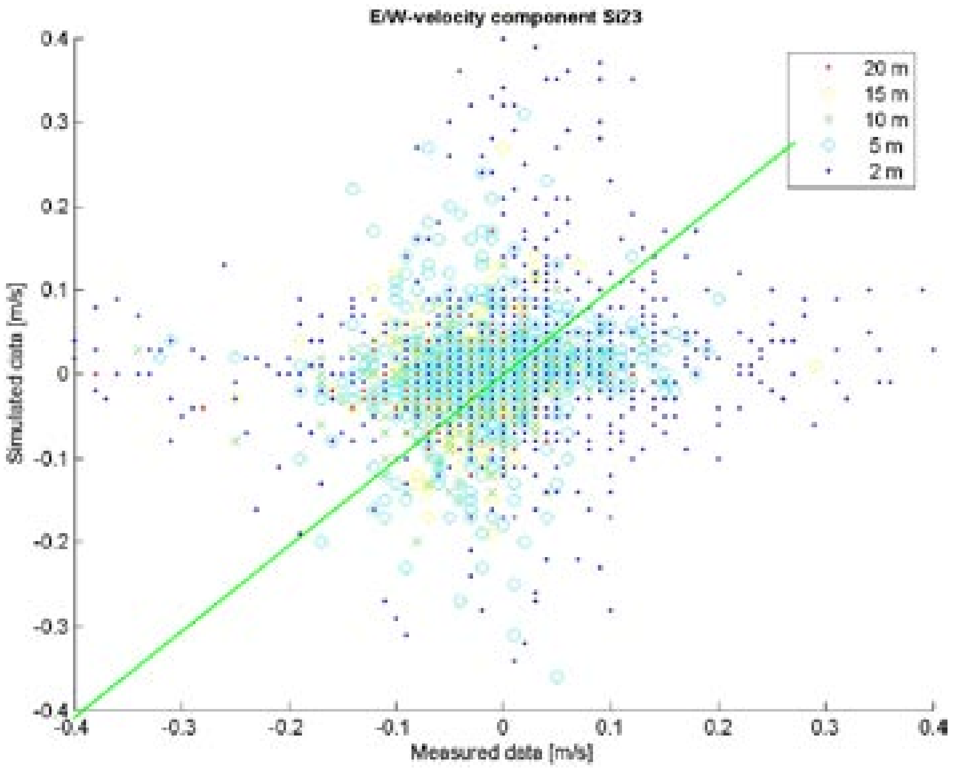


***Figure 3-24.*** *Scatter diagram for measured and simulated velocity (E/W-component) at the station Si23. No correlation pattern is visually discernable, and the average correlation coefficient over the entire water column amounts to 0.1 according to Table 2-3.*

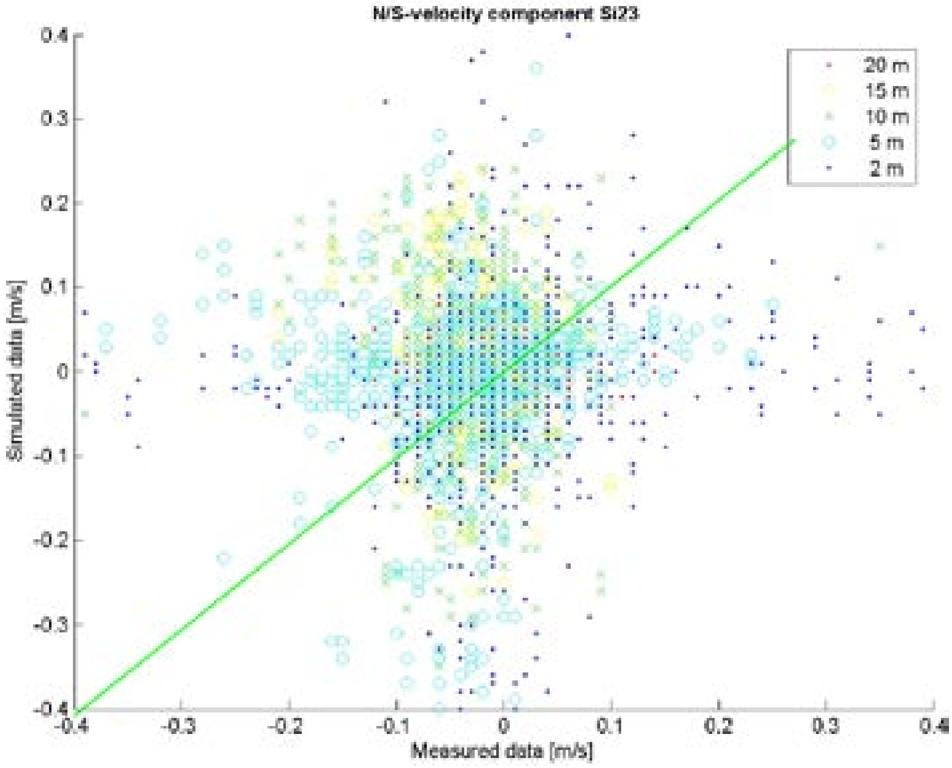


***Figure 3-25.*** *Scatter diagram for measured and simulated velocity (N/S-component) at the station Si23. No correlation pattern is visually discernable, and virtually no correlation exists between these time series. The overall correlation level averaged over the water column amounts to a mere 0.01, see Table 2-3.*

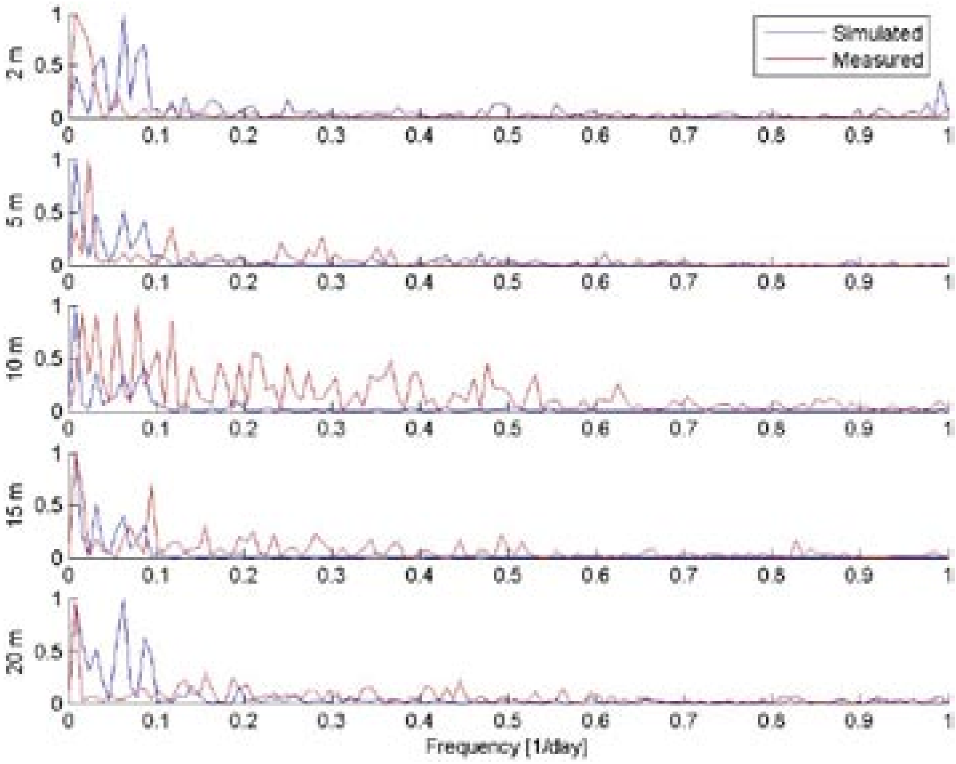


***Figure 3-26.*** *Comparison between measured and simulated velocity spectra of Si23. With the exception of the 10-m level most measured variance is found for frequencies below the 0.1 day$^{-1}$ limit. This feature is also regenerated for the simulated data with a small variance contribution towards the surface-most layer for daily variations.*

## 3.5 Station Si24

The placement of this station (Si24) in the interior of the computational domain of the FR-grid is intended to make it possible to validate to what extent the imposed forcing via the boundaries is propagated and reflected in the interior of the local model grid. All three previous station (Si21 through Si23) have been validated against computed data of the Baltic (CR-) model.

First an overview of the salinity and temperature measurements is given in Figure 3-27. The salinity curves indicate stable stratification during the two first measurement periods, but then the 10-m curve deviates more than what is acceptable according to the stipulated inaccuracy of ± 0.1 units in the psu-scale /Johansson and Morosini 2002/. The temperature curves are consistent with springtime formation of a thermocline, while in autumn penetrative convection makes both the salinity and the temperature curves almost coincidental.

The comparison of measured and simulated temperature curves in Figure 3-28 shows that the events of rapid heating and cooling transitions are strikingly coincidental but not always on the same temperature level. For the 17-m data around JD 250 the levels also coincide in a satisfactory manner. The temperature levels of the rapid heating and cooling instances appear fully consistent which is substantiated by the corresponding correlation coefficients given in Table 2-3.These diminish slightly towards the bottom-most layer (17 m), but as an average still stay over 0.9.

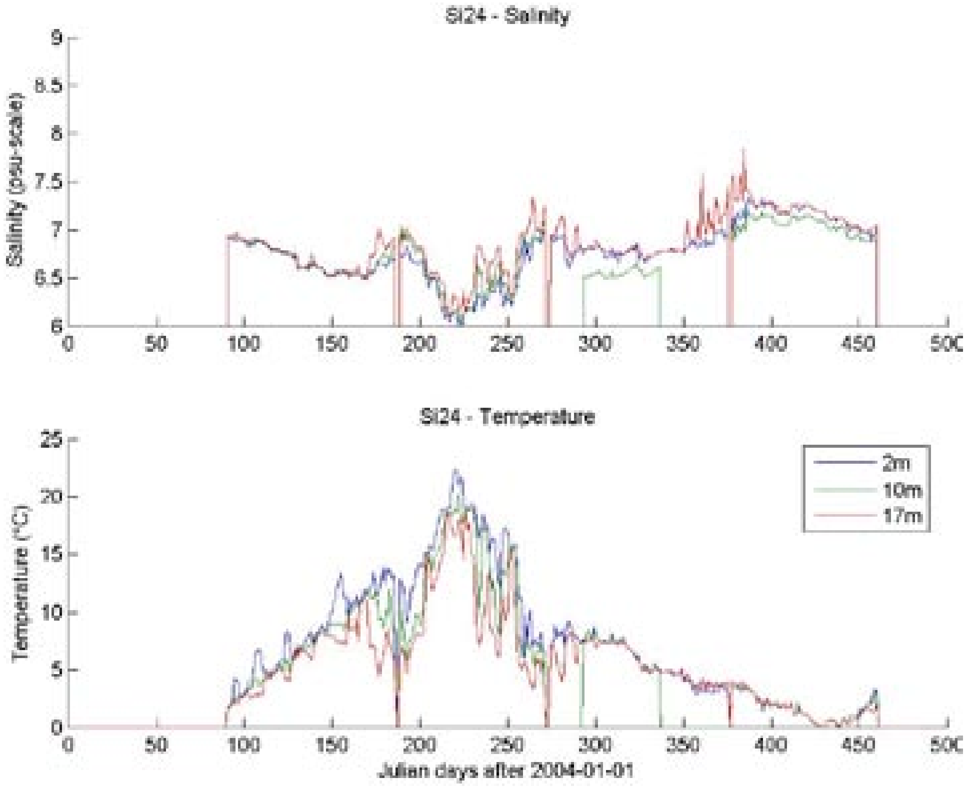


*Figure 3-27. Overview of the salinity and temperature measurements at Si24. The four measurement periods are easily identified by the 17-m curve going down to the x-axis. The salinity stratification is seemingly stable with the exception of the 10-m curve during the third measurement period (JD 290–240) and the entire fourth period. The temperature curves are consistent with springtime formation of a thermocline, while in autumn penetrative convection makes both the salinity and the temperature curves almost coincidental.*

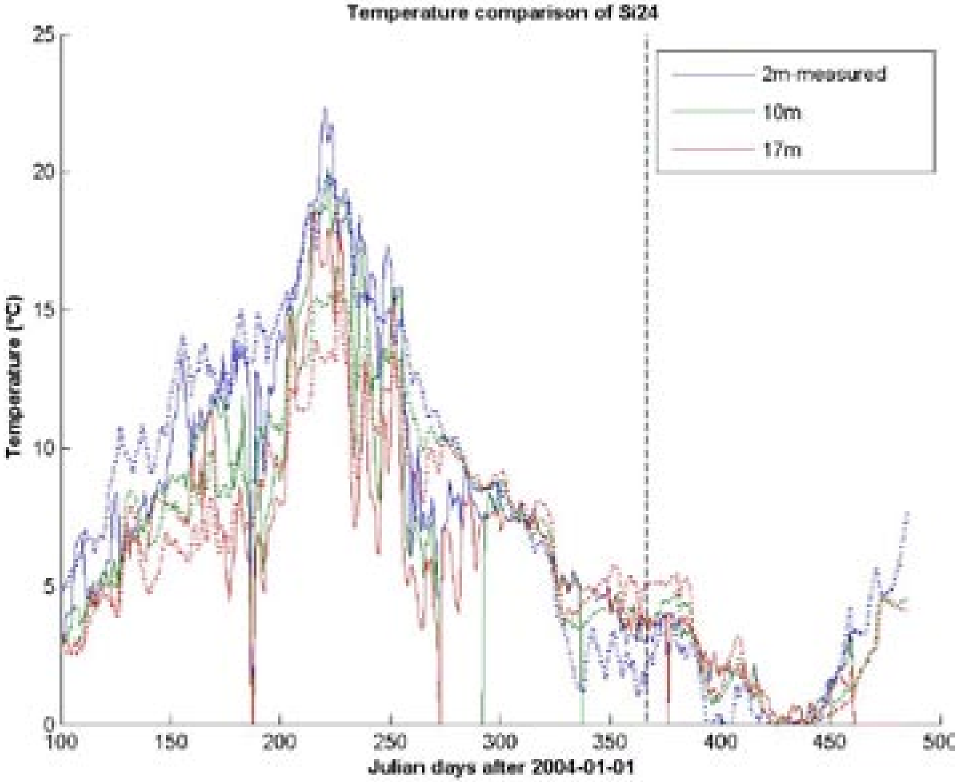


*__Figure 3-28.__ Comparison of measured (solid lines) and simulated (broken lines) temperature at station Si24. The levels and heating and cooling instances appear show a good agreement which is substantiated by the corresponding correlation coefficients given in Table 2-3.*

The comparison of measured and simulated salinities, depicted in Figure 3-29, shows that at the onset of the measurement period on JD 100, the model produces a distinct salinity stratification whereas the measurements show no such stratification. This difference is most likely a consequence of the initialization procedure that in absence of measurement data must resort to reiterated runs with climatologically based forcing. During measurement periods two and three the measured and simulated salinities converge with only a few more instances of elevated values for the bottom-most layer (17 m). The unstable stratification for the measured 10-m data is conspicuous. With these data exempted from the computations, the correlation coefficients fall nevertheless as an average in the range 0.7–0.8, see Table 2-3.

A scatter diagram between measured and simulated temperature data for Si24 is presented in Figure 3-30. The regression line of the surface-most layer coincides well with the ideal line and the corresponding regression lines of the other two depths display that the model slightly under(over)estimates the measured data for temperatures above(below) about 7°C.

The corresponding scatter diagram between measured and simulated salinity data for Si24 in Figure 3-31 also shows satisfactory correlation levels as for the temperature. The regression line of the surface-most layer coincides almost perfectly with the ideal line with only a slight systematic underrepresentation. The corresponding bottom-most layer, on the other hand, systematically over-represents with the same amount. Their slopes are well aligned with an ideal 1:1 slope. The 10-m regression line falls between the regression lines of the two adjacent layers.

The good agreement between measured and simulated temperature and salinity data that are computed for an interior point of the local FR-model evidently vouch for the fully acceptable realism and the precision of this model approach concerning its capacity to simulate the variability of these fields in the interior of the FR-model domain.

At station Si24T the temperature measurement was also complemented by a thermistor chain with eleven sensors that covered the depth range from 1 m to 21 m. According to plan this was deployed during the three first measurement periods. The formation of temporary thermoclines and their resolution by the autumnal penetrative cooling process can be clearly seen in Figure 3-32. The FR-model underestimates the heat penetration but the overall similarity is quite satisfactory.

This is substantiated by the scatter diagram (Figure 3-33) between measured and simulated temperature data for station Si24T. The comparison is made for the measurement levels that coincide closest to the layer partitioning of the numerical model. The regression line of the surface-most layers coincides well with the ideal line in solid black and the corresponding lines of the other three depths are also quite satisfactory, even though their slopes diminish somewhat towards the bottom.

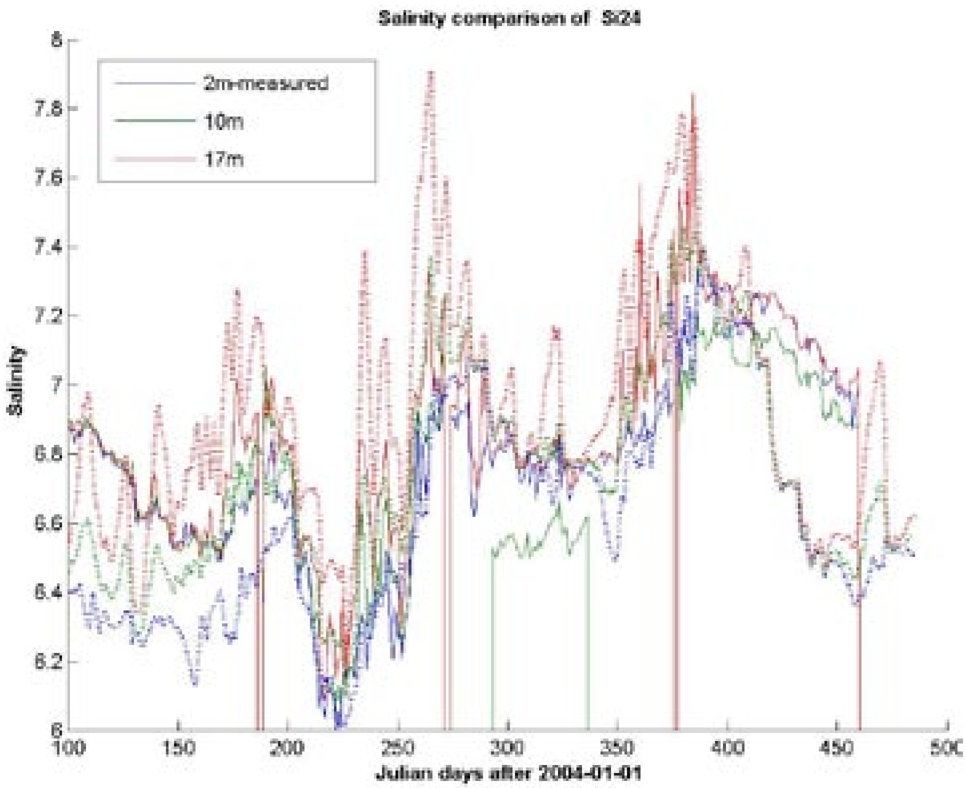


***Figure 3-29.*** *Comparison of measured (solid lines) and simulated (broken lines) salinity at station Si24. At the onset of the measurement period on JD 100 the simulated data show a weak salinity stratification whereas the measurements indicate mainly vertically homogeneous conditions. This difference is probably a consequence of the initialization method. During measurement periods two and three the measured and simulated salinities converge with only a few more instances of elevated values for the bottom-most layer (17 m). The unstable stratification period for the measured 10-m data (JD 290–340) is quite conspicuous and has been exempted from the correlation coefficient computation.*

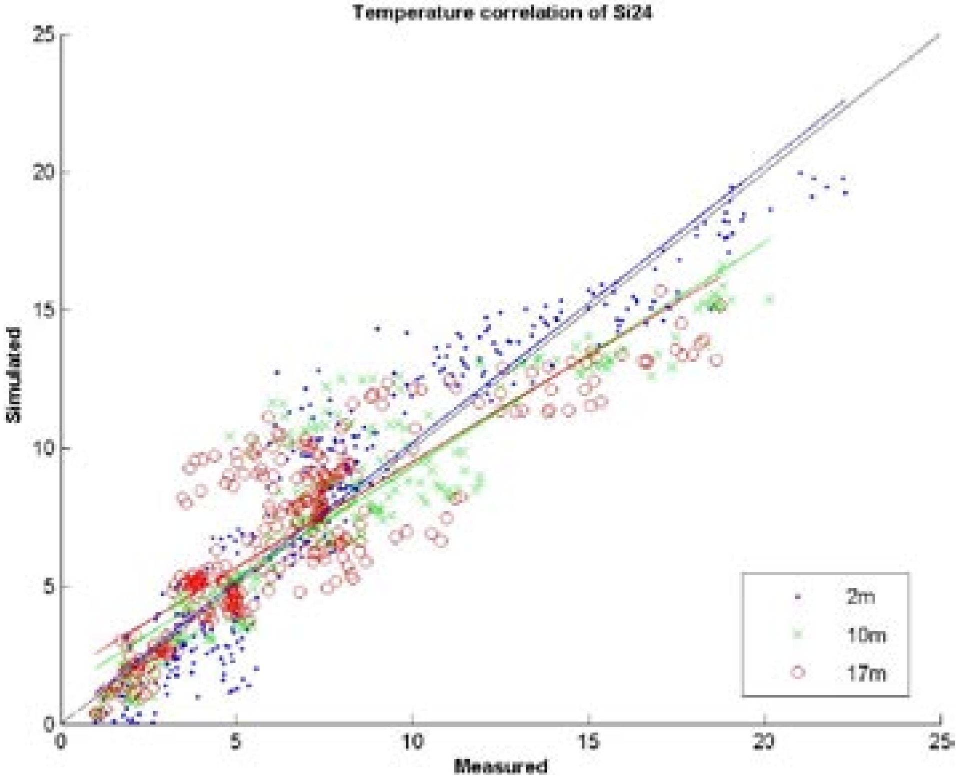


***Figure 3-30.*** *Scatter diagram for measured and simulated temperature data for Si24. The regression line of the surface-most layer coincides almost perfectly with the ideal line in solid black and the corresponding lines of the other two depths are also quite satisfactory. The correlation coefficients diminish slightly towards the bottom-most layer of 17m but their average still stays over 0.9.*

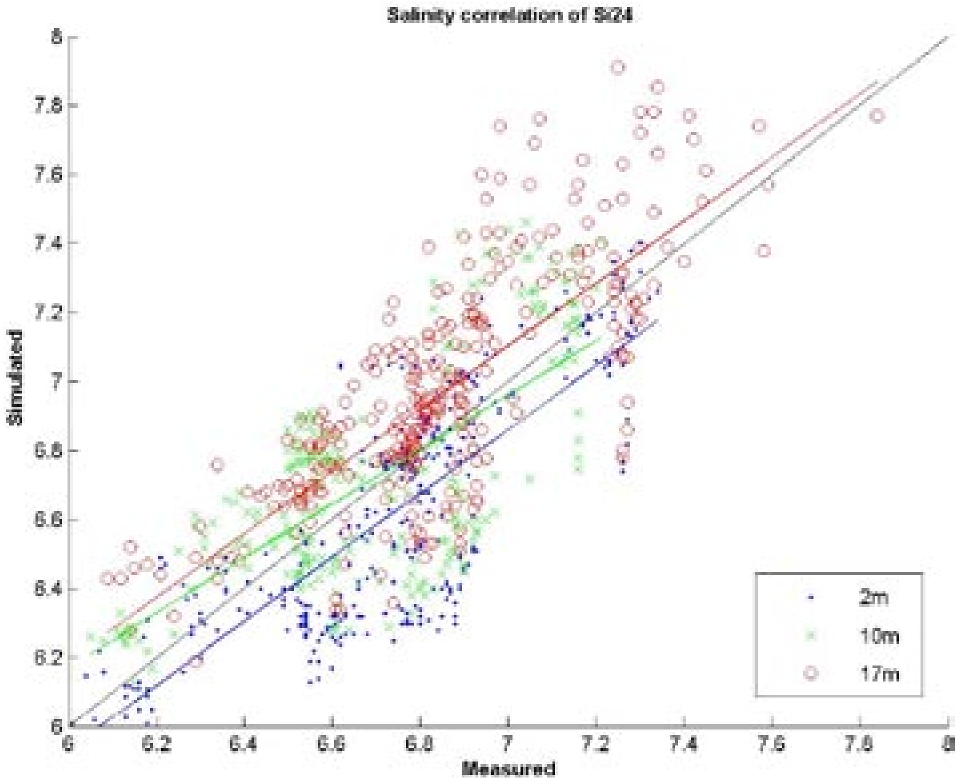


***Figure 3-31.*** *Scatter diagram of measured and simulated salinity data for Si24. The regression line of the surface-most layer coincides well with the ideal line in solid black with only a slight systematic under-representation of about 0.1 psu. The corresponding bottom-most layer on the other hand systematically over-represents with the same amount. All three regression lines have close to an ideal 1:1 slope. The 10-m regression line is only slightly misaligned and falls in between the regression lines of the two adjacent layers. The correlations fall in the range 0.7-0.8 (Table 2-3).*

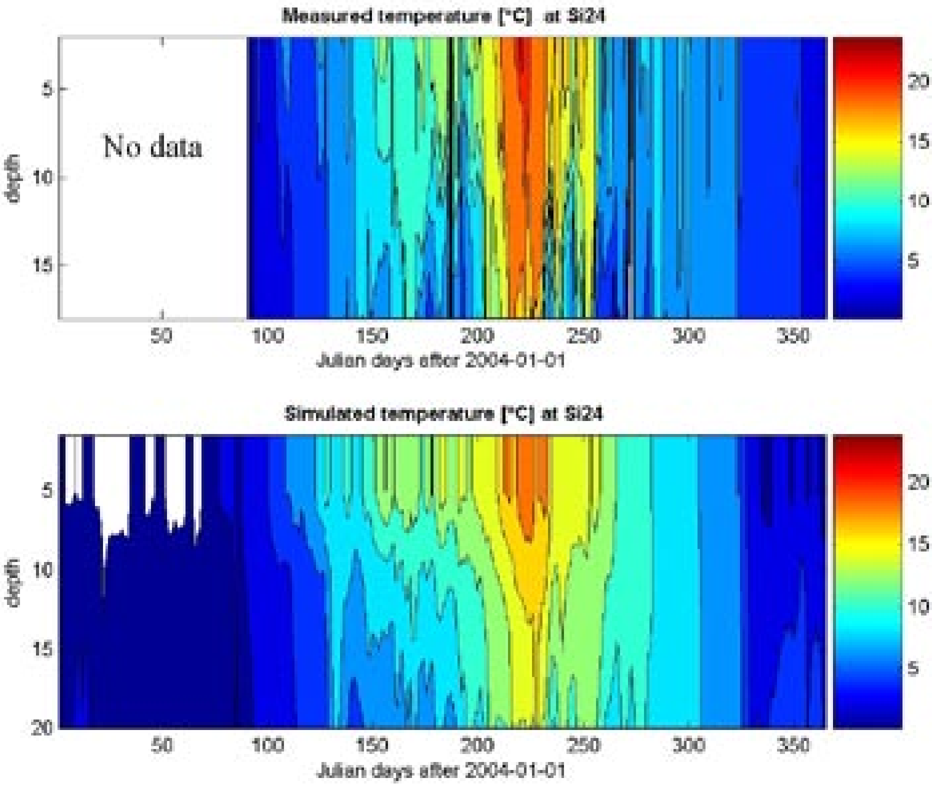


***Figure 3-32.*** *Comparison between measured and simulated temperature of Si24T. The measurements were performed with a thermistor chain and the transition between the three measurement periods can be seen as black/gray vertical stripes. The formation of temporary thermoclines and their resolution by the autumnal penetrative cooling process can be clearly seen. The model evidently underestimates the heat penetration but the overall similarity is satisfactory. The white color for the simulated temperatures denotes temperatures between zero and the freezing point of the local sea water about –0.3°C.*

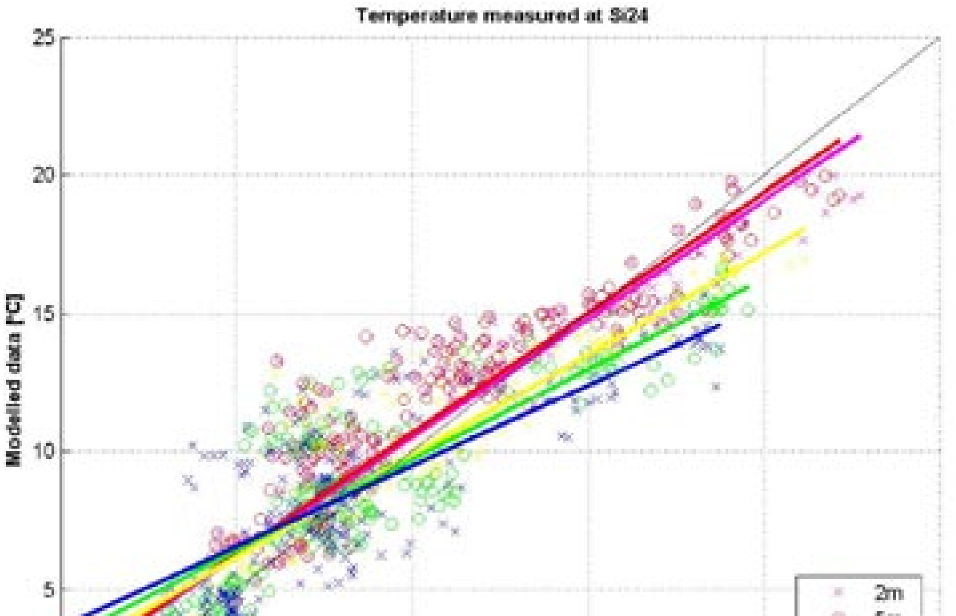


***Figure 3-33.*** *Scatter diagram of measured and simulated temperature data for Si24T, employing a thermistor chain. The comparison is made for the levels that coincide closest with the layer partitioning of the numerical model. The regression line of the surface-most layers coincides well with the ideal line in solid black and the corresponding lines of the other three depths are also quite satisfactory, even though their slopes diminish towards the bottom.*

## 3.6 Station Si25

Figure 3-34 gives an overview of the salinity and temperature measurements at station Si25. At this station these two scalar variables were measured together with the velocity by an instrument deployed near the bottom of the channel-like western part of the elongated major entrance basin Djupesund that connects the interior basins around the Äspö island with the sea (Figure 3-35). For these secluded land-locked basins the local 3D-model must be regarded as inappropriate with regard to realism, foremost because the bathymetrical features cannot be resolved with the resolution set by other considerations. Instead the CDB-model was formulated to this end. This has been developed in stages since it was first applied to the basins adjacent to the Äspö island /Engqvist 1997/. Its present enhanced features have been described in /Engqvist and Stenström 2004/ and it has been successfully validated in the Himmerfjärden area 40 km south of Stockholm /Engqvist and Stenström 2008/. Its adaption to the present task is given in Figure 3-35a. Since Djupesund is considered to be a basin, the corresponding comparison between measured and simulated data is made at the strait S3 connecting the sub-basin Djupesund (SB24) to Kalvholmsfjärden (SB21). For these sub-basins the partitioning is based on strict coastal oceanographic considerations. The accounting of water exchange from an ecological point of view may not need this level of detail. A few basins have thus been conjoined and then given a separate name when passing on the computation results to the ecological modeling group.

The surface heat exchange with the atmosphere for this CDB-model is driven by measurements in the surface layers of Granholmsfjärden and Borholmsfjärden. These measurements compare favorably (Figure 3-36) with modelled surface temperature at the point named R-1 in Figure 3-35a, located about 1 km off the coast. The simulated salinity and temperature profiles at this station are used as boundary forcing for the CDB-model.

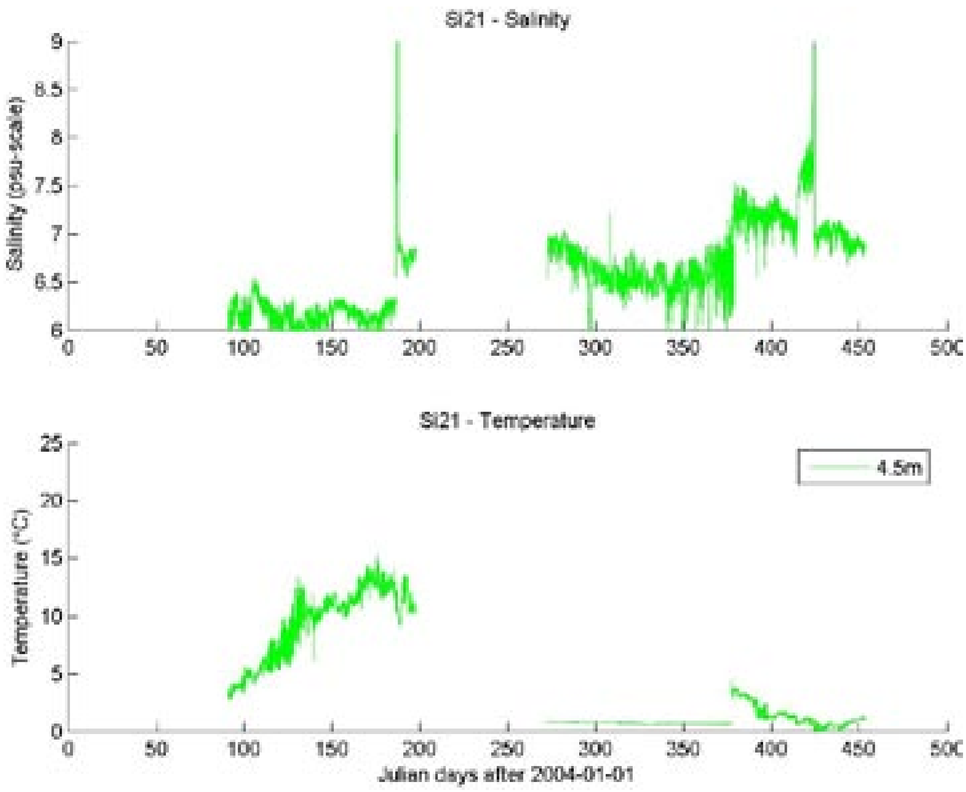


*Figure 3-34. Overview of salinity and temperature measurements at the station Si25. Both salinity and temperature measurements during period two are missing and the temperature data for period three are obviously erroneous.*

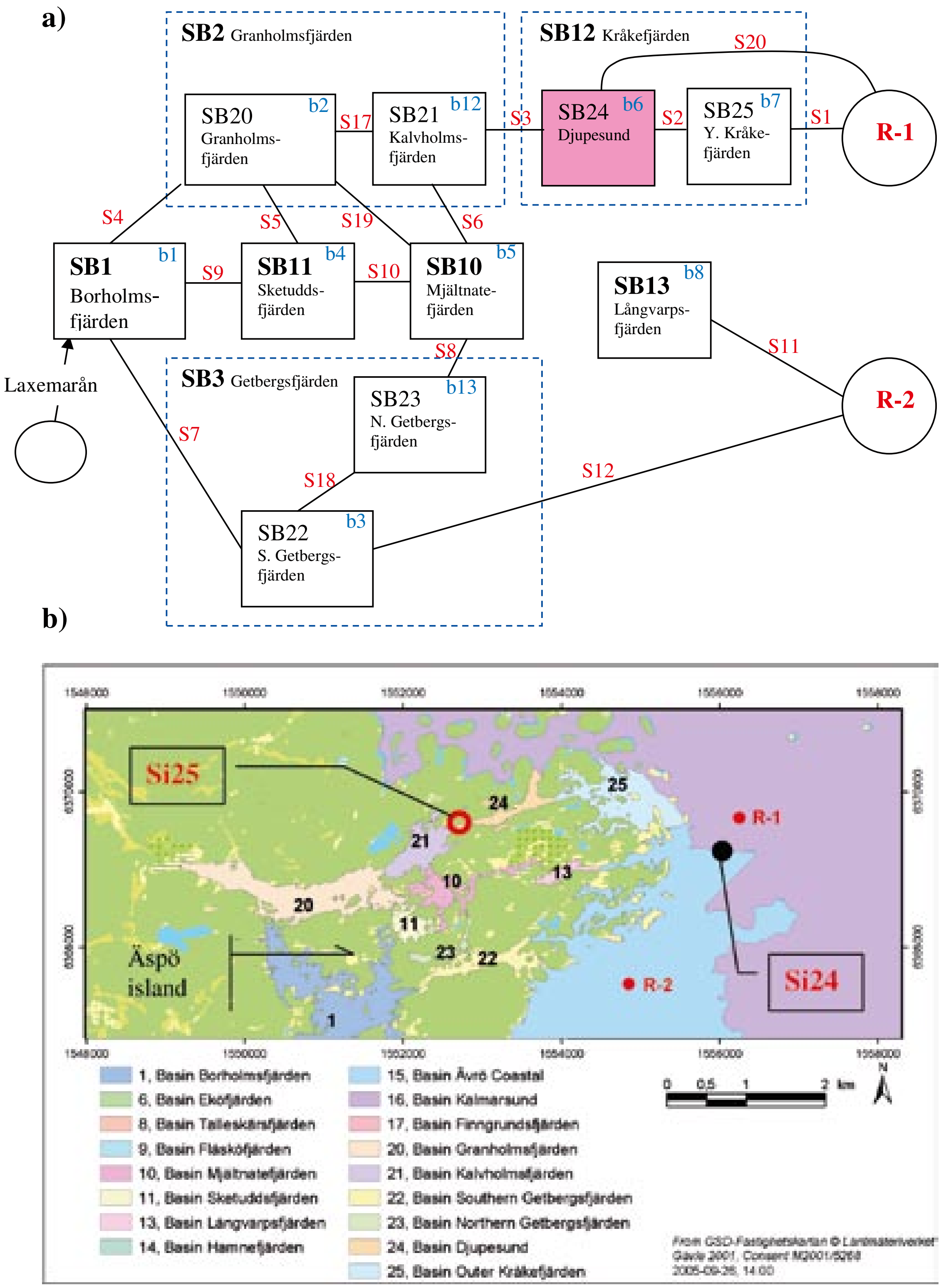


*Figure 3-35. a (upper panel). Stylized block diagram rendering the naming of the sub-basins (SBs) with blue labels (and the straits with red labels) employed in the CDB-model. Basin labels in bold refer to the ones that are accounted for in related ecological analysis. b (lower panel). The partitioning of the Laxemar coastal area into sub-basins. The locations for which the density profiles computed by the 3D-model are used to force the CDB-model have been indicated by R-1 and R-2. The approximate location of stations Si24 and Si25 in Djupesund have been indicated by a black dot and a red circle respectively (excerpt from bassangindelning_20050926_1400.mxd).*

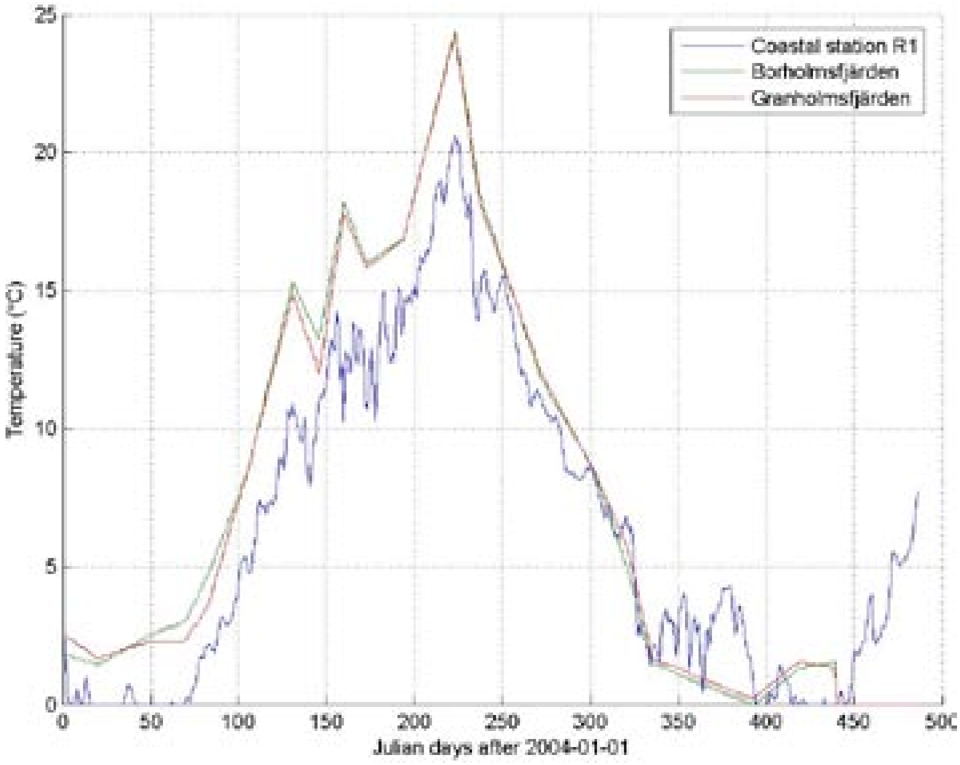


*Figure 3-36. Measured surface temperatures of the inner Laxemar-Simpevarp basins used for forcing of the CDB-model. The average temperature of the Granholms- and Borholmsfjärden are used for all the modeled SBs, while the costal station data apply to R-1 and R-2.*

For the sea-level forcing the simulated sea level at R-1 could have been used, but this would mean that deviations introduced by the FR-model would have added to the inherent uncertainties of the CDB-model. In order to give the CDB-model as fair individual validation as possible, it was decided to use measured sea level data which exist for most of the validation periods at a local station (PSM000371), complemented with about one month (April) of measurements at a more distant gauge station (Oskarshamn), see Figure 3-37. A scatter diagram of the hourly measured sea levels during the overlapping month of May is depicted in Figure 3-38 with a correlation coefficient of 0.93 (N=97), which gives reassuring evidence that this procedure is sound.

Together with the wind data set logged at Ölands Norra Udde (Figure 2-1) and the freshwater discharge of Laxemarsån (Figure 2-2), the CDB-model forcing is accounted for.

A first comparison between modeled and measured salinity and temperature data at station Si25 is shown in Figure 3-39. In addition to the data gap in the second period, there are two shorter periods for which the salinity measurements are obviously erroneous. For the temperature measurements also the third measurement period must be discarded. For the remaining time periods the measurement data generally display a more ragged appearance than the simulated data. This is a consequence of the CDB-model's instantaneous horizontal mixing that precludes the model from upholding the same gradient as the measured differences between the concentrations on the up- and down-estuary sides of the strait.

The correlation between measured and simulated temperatures can be seen from the scatter diagram in Figure 3-40. On average the simulated data underestimate the measured. In spite of the data gaps the correlation coefficient is 0.97.

The corresponding scatter plot between measured and simulated salinity data is shown in Figure 3-41. Since the measured data are split into two periods with differing levels of salinity, this means that the scatter plot shows two isolated clusters. The correlation coefficient of either group is about 0.5 and the one of the conjoined groups encompassing the entire data set amounts to 0.94, which elevated value should be regarded more as a reflection of the bi-modal distribution than as a virtue of the model.

The deployment of the current measurement to a channel reduces to a large extent the degrees of freedom since the current will mainly be constrained to flow in the channel direction. In Figure 3-42 a comparison of the simulated and the measured along-channel current speed at a level near the bottom is presented. It is evident that the current intensities are comparable in spite of possible misrepresentation of the section area at the level of the actual instrument placement. The correlation diagram in Figure 3-43 shows that the intersection point between the regression and the ideal lines is close to the point representing zero velocities for both axes. The difference in slope can thus be attributed to the above-mentioned difference in cross-section area. The correlation coefficient is 0.49 which according to Table 2-3, is in par with the highest correlation levels achieved with the 3D-model.

The corresponding comparison of the spectra of the simulated and measured velocity data can be seen in Figure 3-44. Since the measurements were performed with a temporal resolution of one hour, the Nyquist frequency is 12 day$^{-1}$, though the CDB-model was run with a comparatively shorter time step.

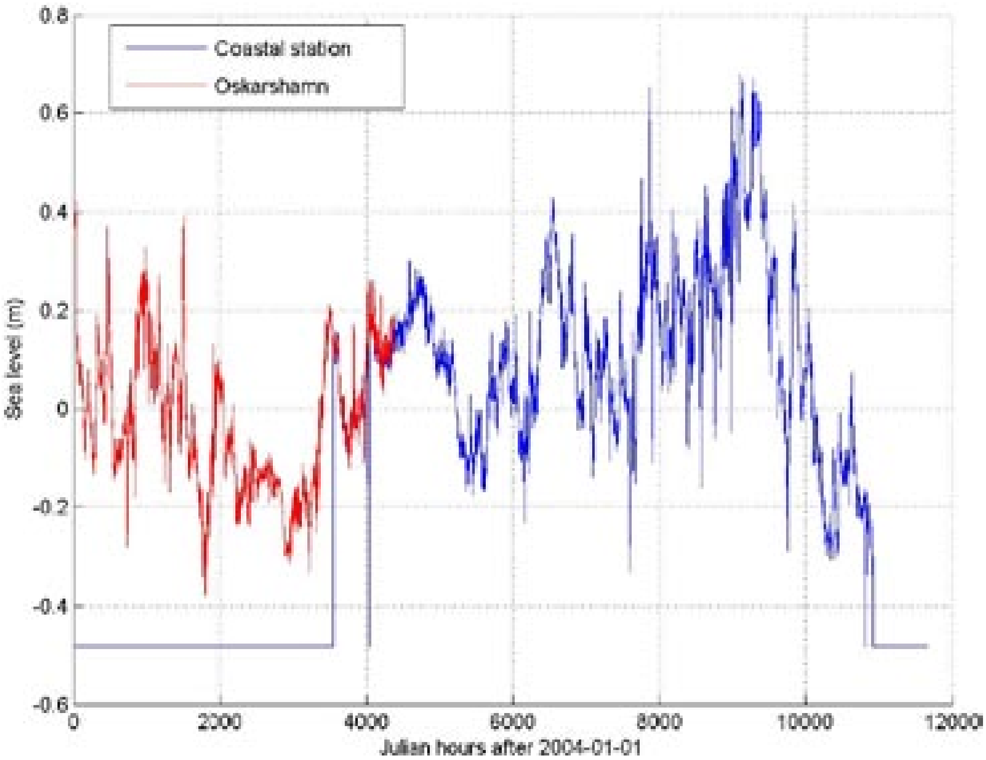


***Figure 3-37.*** *Sea-level forcing of the DB-model. The first part (red line) covers the time period January through May 2004 and is measured by SMHI at their Oskarshamn station. The second part (blue line) is from local measurements at the SKB-site PSM000371 and covers May 2004 through March 2005. Thus there is a one-month overlap of these data sets which makes the scatter diagram in Figure 3-38 possible.*

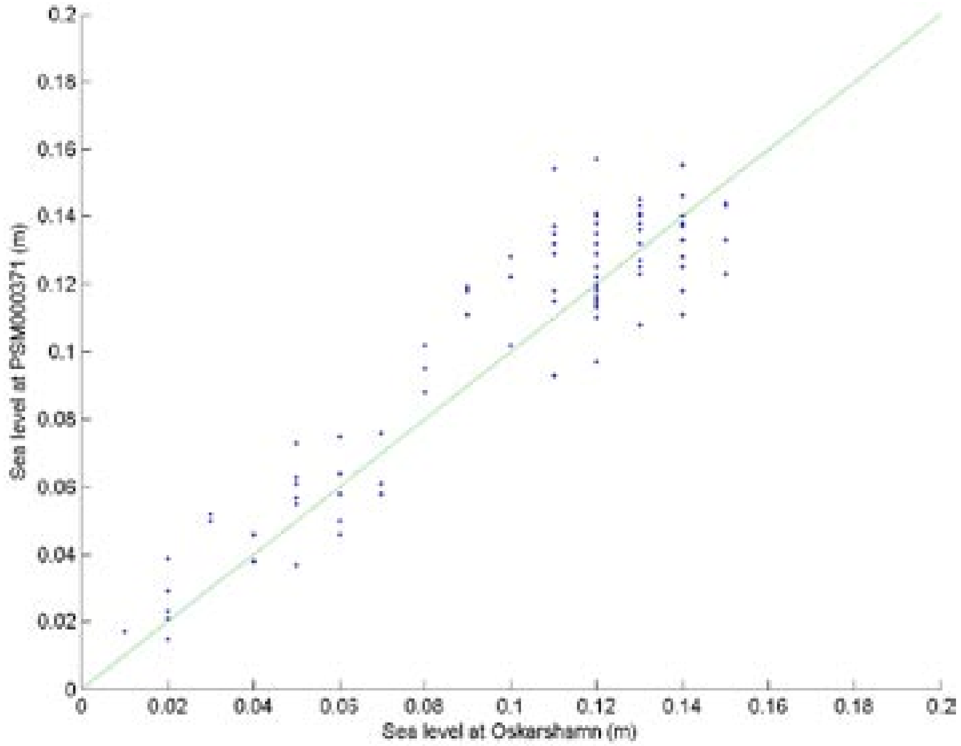


*__Figure 3-38.__ Scatter diagram of the overlap period (May 2004) for the two sea level data sets used. Some points may be coinciding due to the limited numerical resolution. The correlation coefficient is ρ=0.93 (N=97).*

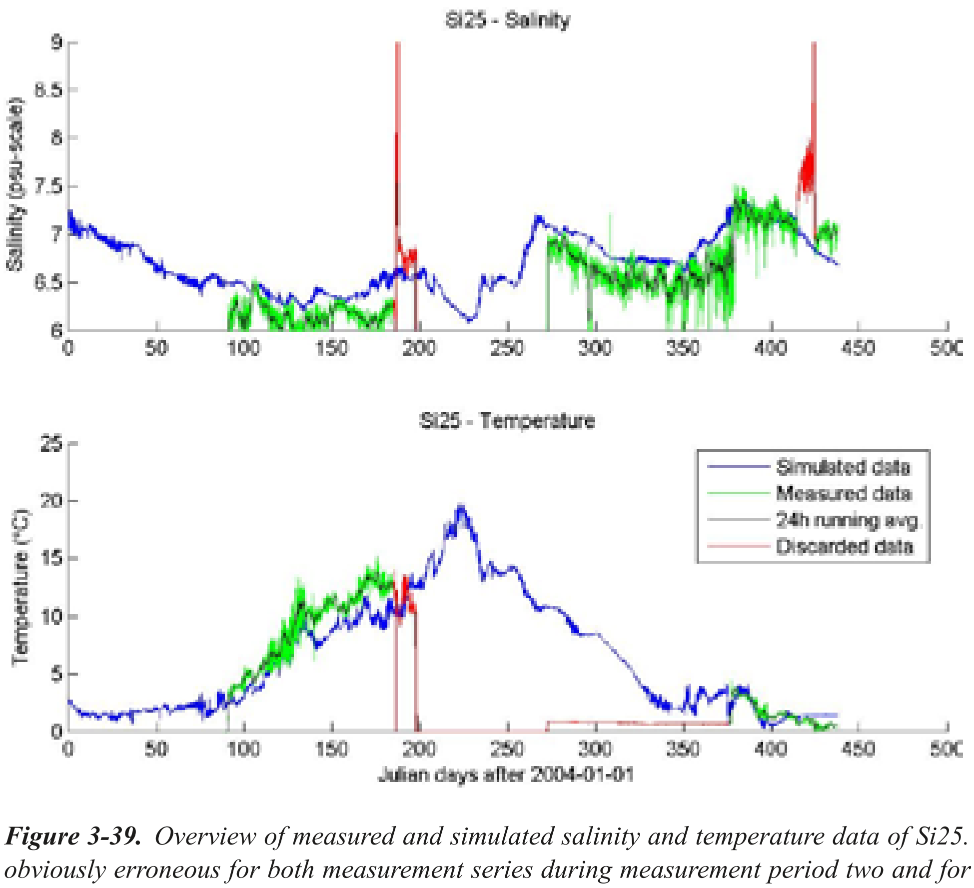


*__Figure 3-39.__ Overview of measured and simulated salinity and temperature data of Si25. The data are obviously erroneous for both measurement series during measurement period two and for the entire period three regarding temperature. The measurement data display generally a more ragged appearance due to the greater differences between the concentrations on the up- and down-estuary side of the strait. A 24-h running average has been superposed on the measured data to facilitate comparison.*

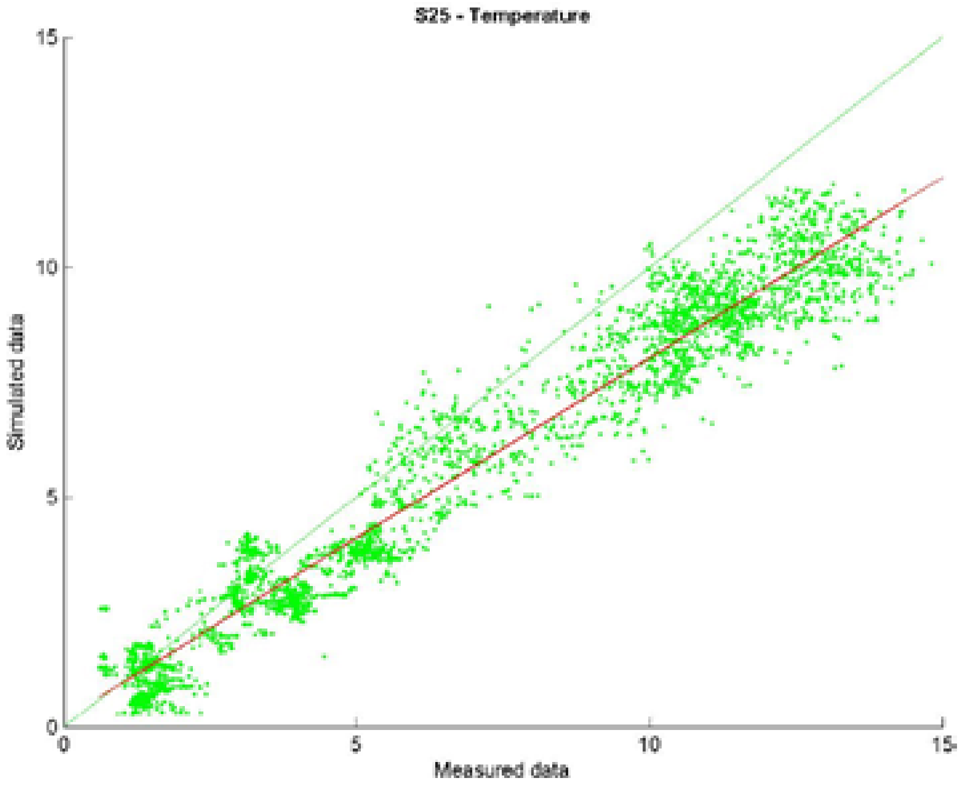


*Figure 3-40.* *Correlation between measured and simulated temperature of Si25. On average the simulated data underestimate the measured. In spite of the data gaps the correlation coefficient is 0.97.*

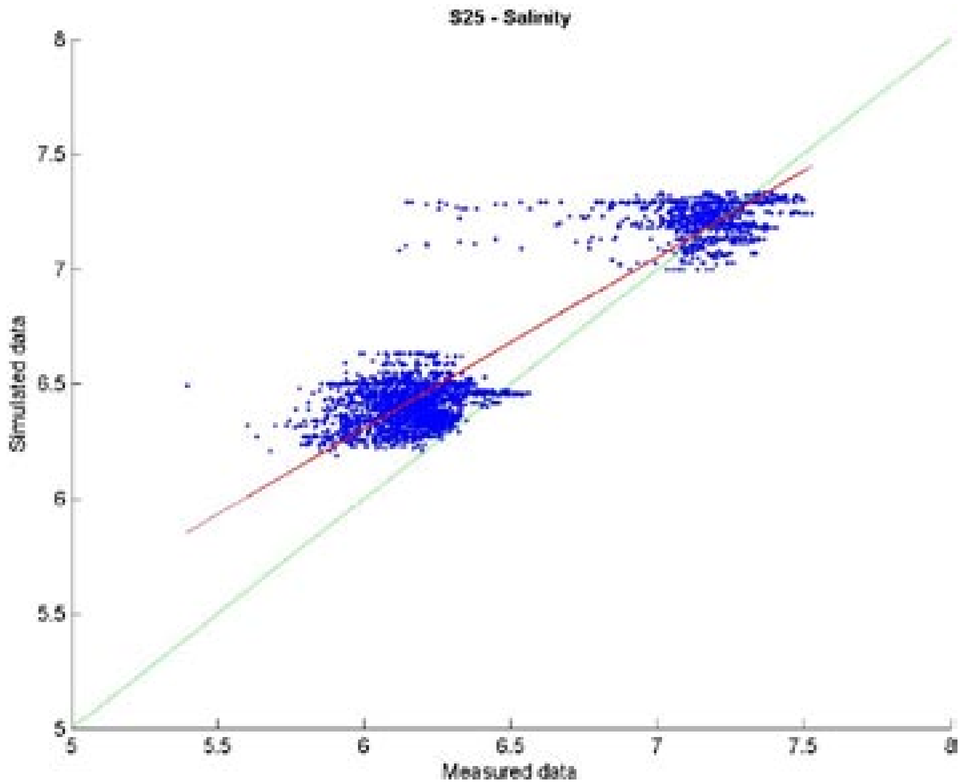


*Figure 3-41.* *Scatter plot for measured and simulated salinity of Si25. Since the measured data are split into two periods with differing levels of salinity, this means that two isolated groups of point cluster occur. The correlation coefficient of the conjoined groups i.e. ρ=0.94, but for each individual group the correlation level is considerably inferior. For the lower of the two groups representing measurement period one, the simulated data overestimates the measurement data, which in turn has the consequence that the slope of the red regression line entailing all data is smaller than the diagonal line in green.*

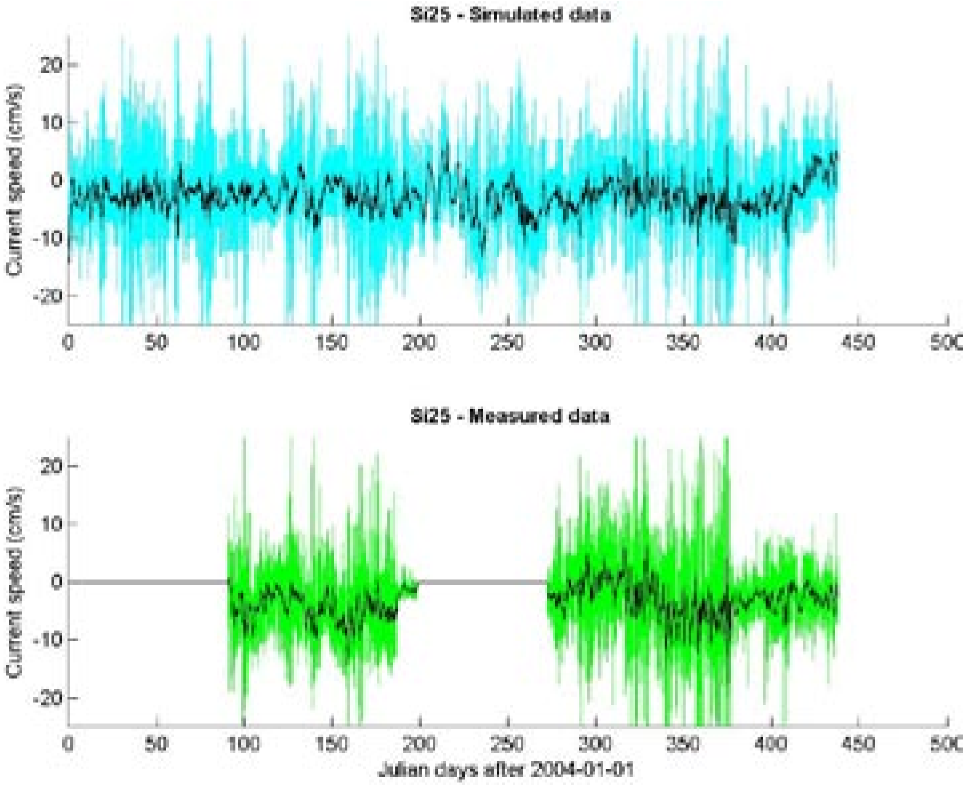


***Figure 3-42.*** *Comparison between measured and simulated current velocity components in the strait direction of Si25. During the fourth measurement period (starting on JD 375) there is a notable change in the current velocity amplitude most likely due to the fact that the instrument was deployed on a deeper location than earlier. Both these data series have been processed with a 24-h running average filter, shown as superposed black curves. Two data items were missing in the measurement file and have been restored by interpolation.*

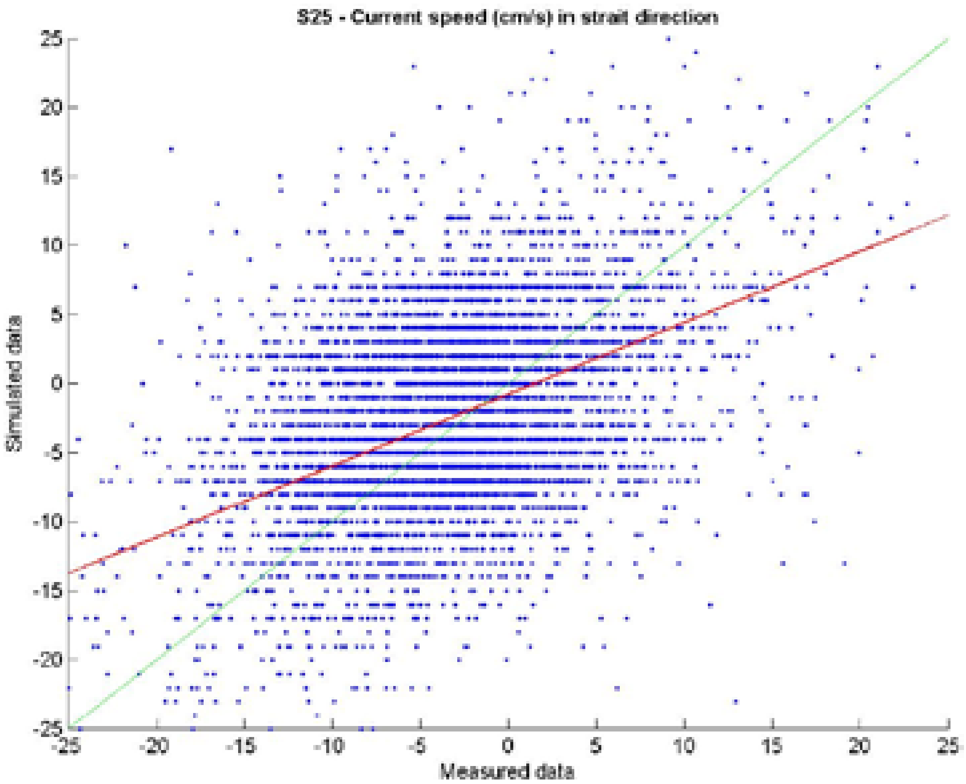


***Figure 3-43.*** *Scatter diagram for measured and simulated current velocity component in the strait direction of Si25 with hourly temporal resolution. The regression line in red underestimates the simulated current but this can be explained by differences in the strait section areas that are represented. In the model a larger area is associated with the computed average flow, while the measured current represents just the strata where the instrument is deployed. The correlation coefficient ρ=0.49, see Table 2-3.*

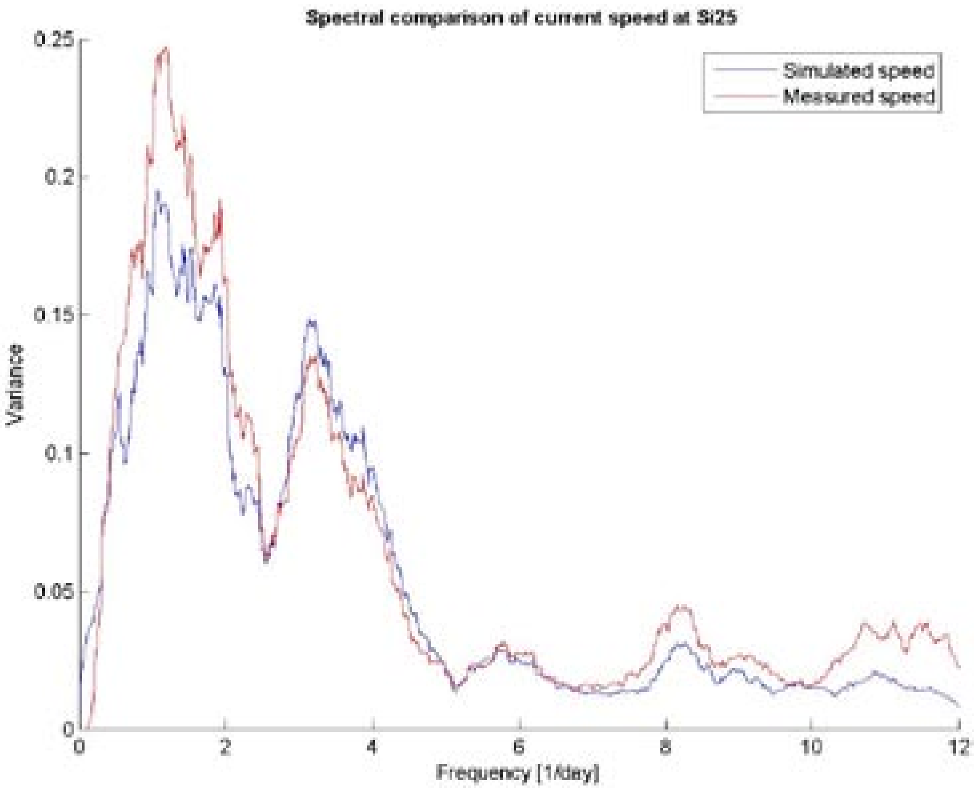


***Figure 3-44.*** *Comparison of spectra of measured and simulated current velocity component in the strait direction of Si25 for the third measurement period with hourly temporal resolution. Current spectral components exist for higher frequencies than the Nyquist frequency, at least for the simulated data. These spectra have been smoothed with a running average filter and the similarity must be deemed as fully acceptable.*

## 3.7 Transects

Five transects with a ship-mounted ADCP instrument have been performed along parts of the southern, northern and eastern boundaries, Figure 3-45. All these transects were done under sufficiently calm weather conditions and can thus not be considered as representative of the average water circulation along these transects. Figure 3-46 shows the transect along part of the southern boundary 2004-04-28 (JD 119 after 2004-01-01) going westward toward station Si23 but not reaching it. Even though station Si23 falls somewhat to the left of the diagrams, the currents measured by the stationary ADCP instrument data (Figure 3-22) are not inconsistent with these vessel-mounted data. The diagrams span close to two nautical miles and give thus an appreciation of the variability within one grid cell of the Baltic CR-model.

The next transect was taken 2004-07-07 (Figure 3-47) with almost identical starting and ending points as for Figure 3-46, but the surface current direction is reversed and the feeble current of the bottom layer is flowing southward. The horizontal homogeneity of the flow pattern representing one grid cell of the Baltic CR-model is again convincingly apparent. Comparison to the measurements with the stationary ADCP deployed at station Si23 is not easy due to the weak current intensities but no obvious inconsistencies between these measurements can be detected.

The transect along part of the northern boundary 2004-10-20 going westward toward station Si21b (see Figure 3-45) – but not reaching it – is shown in Figure 3-48. The homogeneity of the diagrams that span one grid cell of the Baltic CR-model is fully acceptable even though there is a slight deepening of the surface layer to the east. The date of this transect corresponds to JD 294 in Figures 3-22 and 3-23 and a comparison to these stationary ADCP-measurements is again hampered by the weak current intensities.

In Figure 3-49 is depicted the transect along part of the northern boundary 2005-04-13 going eastward from station Si21b. This date represents the last measurement day. In fact this transect was taken a couple of hours after the stationary ADCP instrument was lifted out of water.
In spite of the differing current scale compared to the previous transects, the current magnitude was very weak. Because of this, the heterogeneity displayed for the horizontal layers, shifting from currents setting northward in the right half of the diagram to currents setting west in the left half, can hardly be interpreted as an indication of current features appearing on a sub-grid cell level.

Finally, the transect along part of the eastern boundary on the same date (2005-04-13) as the previous transect going southward passing near station Si22, see Figure 3-50. The vessel-mounted ADCP instrument gives current readings down to about 40 m. Beyond this range, however, only occasional data are given. At the date of this transect, the current meter at Si22 was deployed at a depth of 49 m. This completely dismisses any possibility to compare with the stationary current meter at this station. The current pattern within the two nautical miles covered does not give rise to concern about the horizontal current homogeneity of the Baltic CR-model.

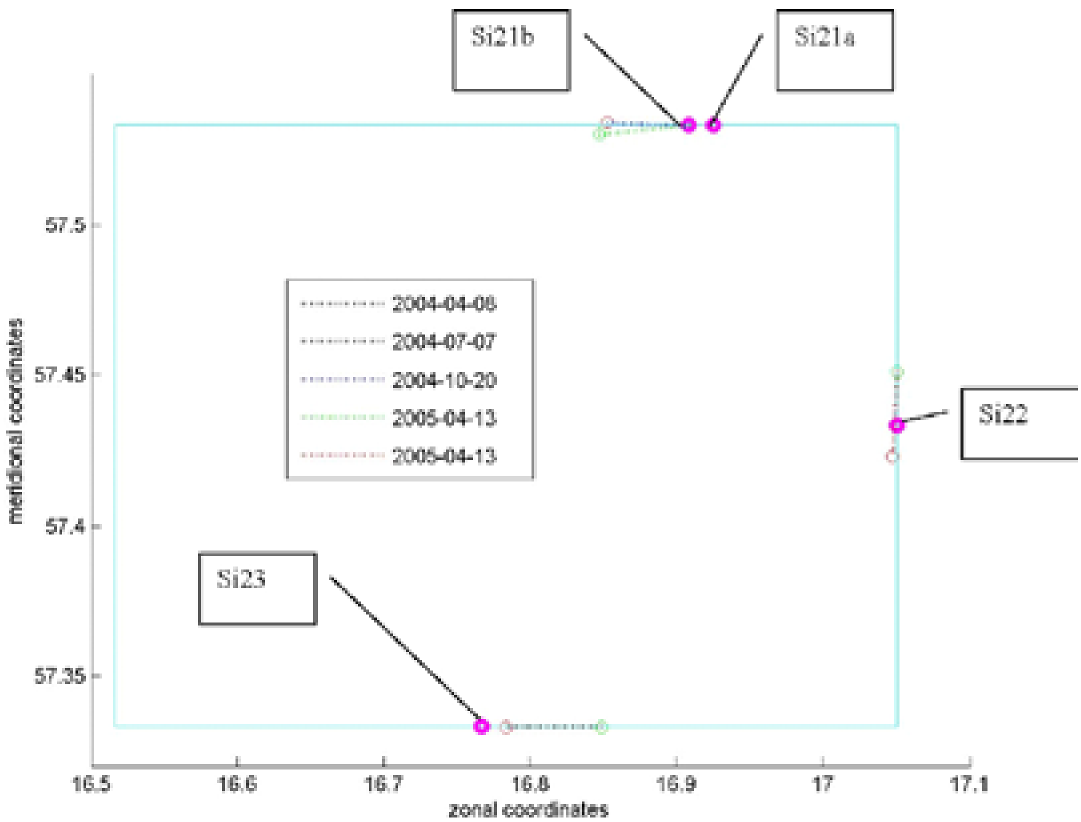


***Figure 3-45.*** *Transects along parts of the southern, northern and eastern FR-model boundaries. The starting points are marked as green circles and the end points with a red circle. The FR-model domain is outlined as a light blue rectangle with measurement stations marked as bold magenta circles. Only at the eastern boundary does the transect pass through the measurement point. The other transects have the other stations at or near their endpoints.*

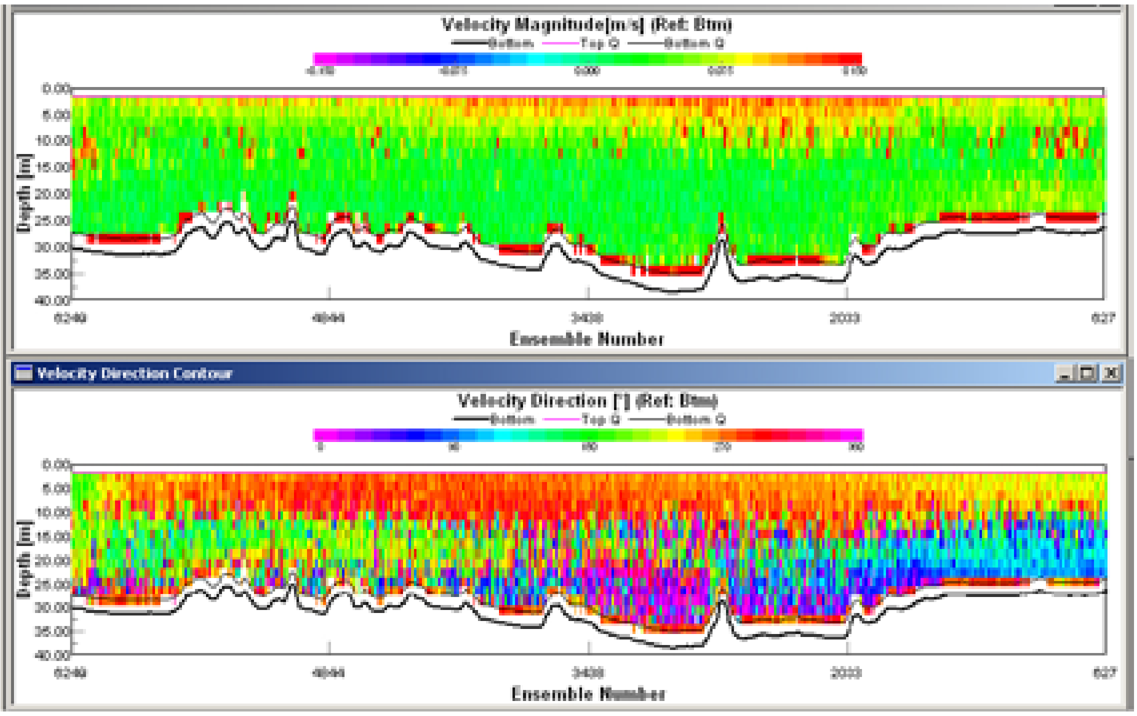


***Figure 3-46.*** *Transect along part of the southern boundary 2004-04-28 (corresponding to JD 119 after 2004-01-01) going westward toward station Si23, but not reaching it. The surface current sets to the west while at about 15 m depth the lower layers are mostly going in the other direction. Even though station Si23 is somewhat to the left of the diagrams the currents measured by the stationary ADCP instrument data (Figures 3-22 and 3-23) are not inconsistent with these vessel-mounted data. The diagrams span close to two nautical miles and give thus an appreciation of the variability within one grid cell of the of the Baltic CR-model.*

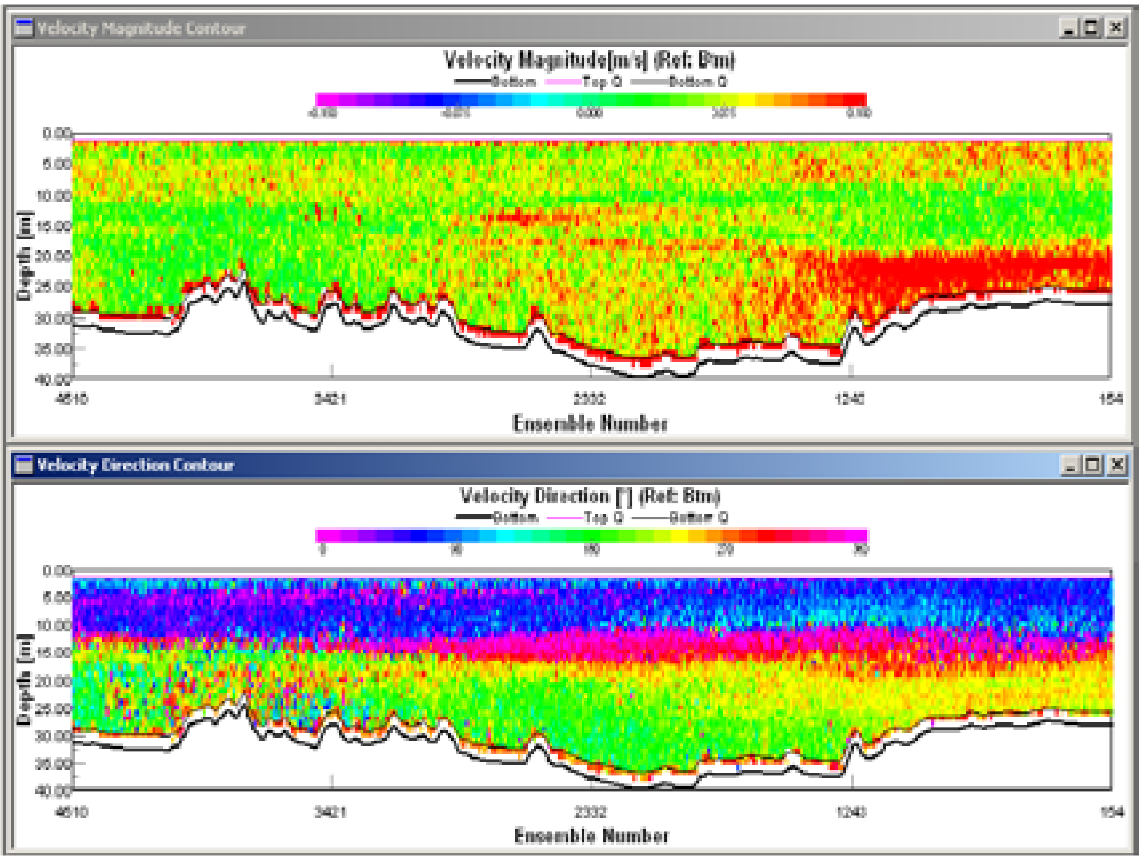


***Figure 3-47.*** *Transect along part of the southern boundary 2004-07-07 (corresponding to JD 189 in Figures 3-22 and 3-23) going westward. The route is very similar to the one in Figure 3-46 which is reflected by the bottom contours (coarse black line), but the surface current direction is reversed and the feeble current of the bottom layer is flowing southward. The homogeneity of the flow pattern representing one grid cell of the Baltic CR-model is convincingly apparent. Comparison to the measurements with the stationary ADCP deployed at the station Si23 is not easy due to the weak current intensities but at least there are no obvious inconsistencies between these measurements.*

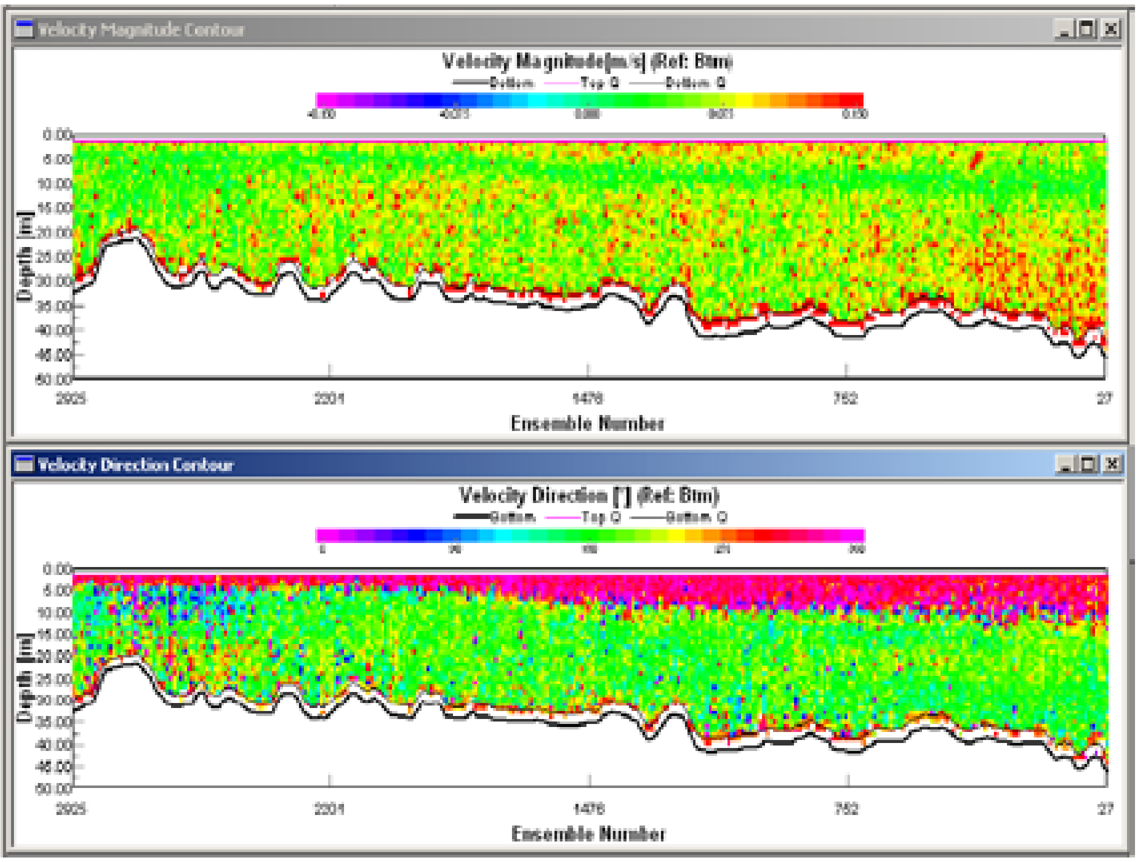


***Figure 3-48.*** *Transect along part of the northern boundary 2004-10-20 going westward toward station Si21b but not reaching it. The homogeneity of the diagrams that span one grid cell of the Baltic CR-model is fully acceptable even though there is a slight deepening of the surface layer to the east. The date of this transect corresponds to JD 294 in Figures 3-22 and 3-23 and a comparison to these stationary ADCP measurements is again hampered by the weak currents.*

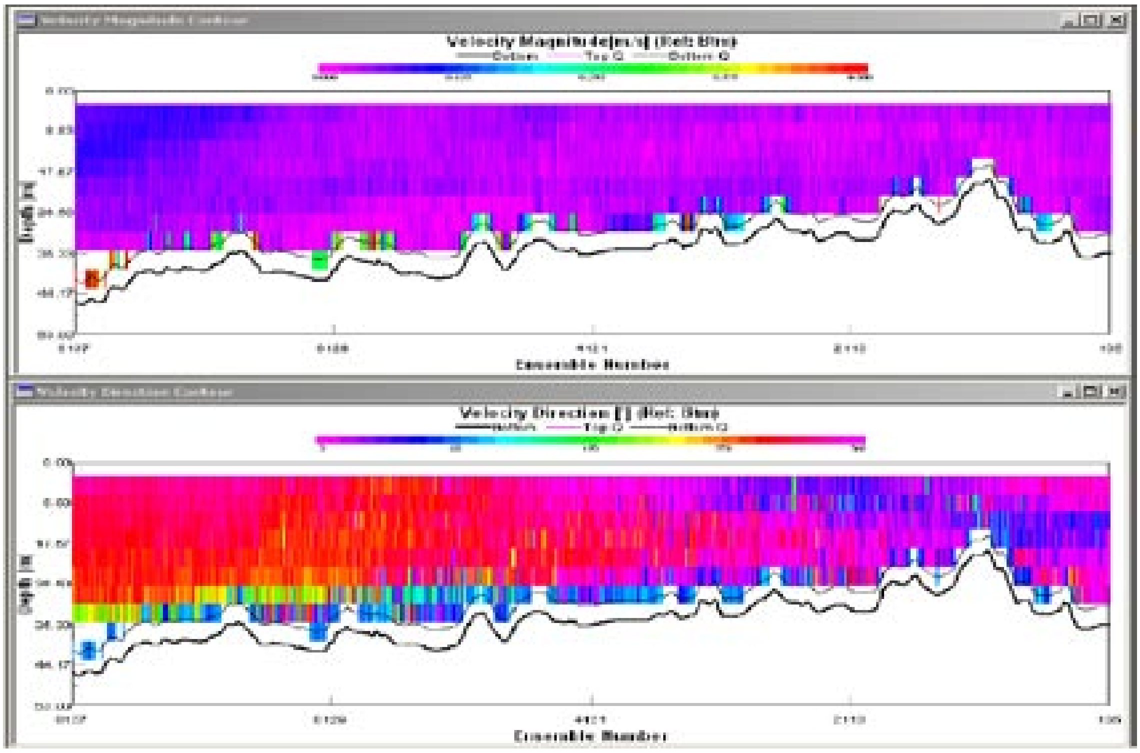


***Figure 3-49.*** *Transect along part of the northern boundary 2005-04-13 going eastward from station Si21b. This date corresponds to JD 469 in Figures 3-22 and 3-23 representing the very last measurement data. In fact this transect was taken a couple of hours after the stationary ADCP instrument was lifted out of water. In addition, the current magnitude diagram (upper panel) indicates very weak currents. Because of this, the heterogeneity displayed for the horizontal layers, shifting from currents setting northward in the right half of the diagram to currents setting westward in the left half, cannot be interpreted as an indication of current features appearing on a sub-grid cell level.*

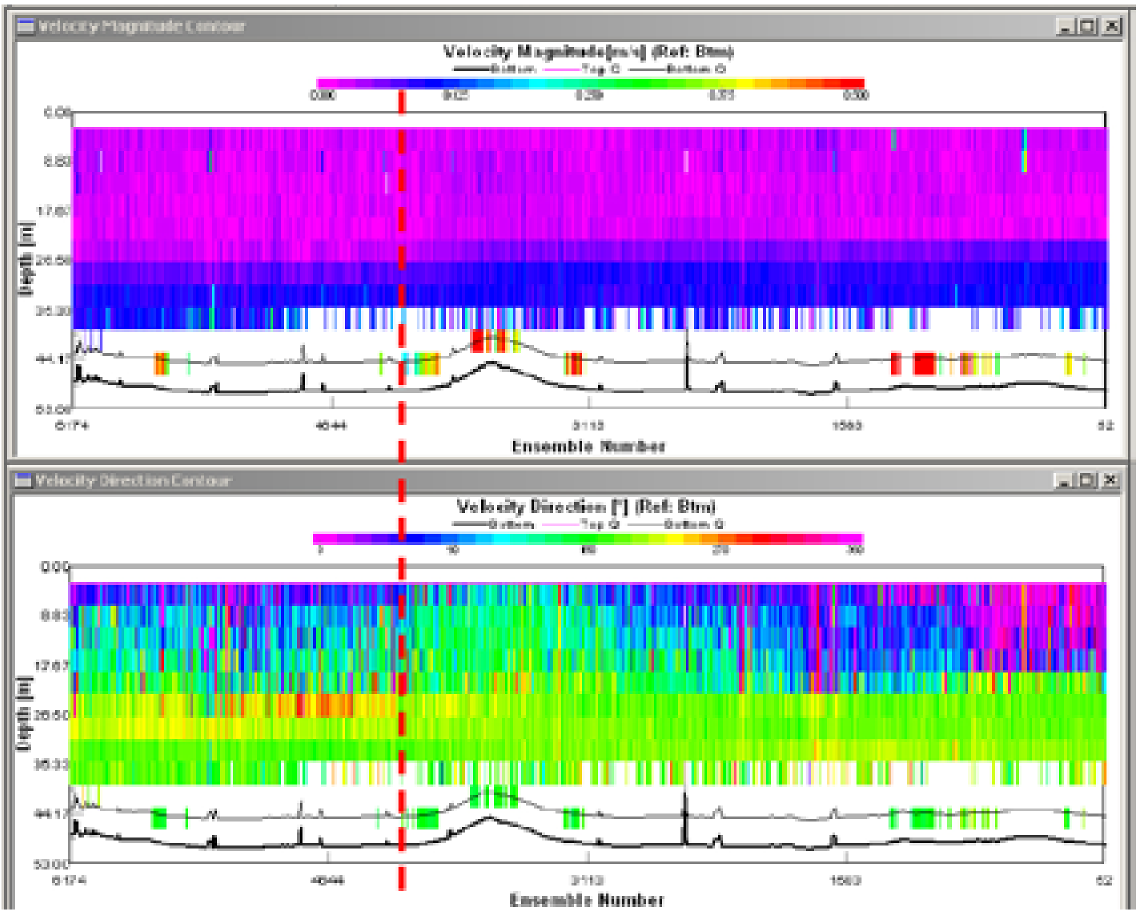


***Figure 3-50.*** *Transect along part of the eastern boundary 2005-04-13 going southward. The approximate position of the station Si22 is indicated by a broken red line. The vessel-mounted ADCP instrument gives current readings down to about 40 m. Beyond this range only scattered data are occasionally given. At the date of this transevct, the current meter at Si22 was at a depth of 49 m. This fact completely dismisses any possibility for making comparisons. The upper velocity magnitude diagram shows an almost ideal homogenous current pattern with weak current down to the 30-m level. From this level and downward a south-going current intensifies across the two nautical mile range.*

# 4 Discussion

## 4.1 Comparison of currents

As for the parallel study of the Forsmark coastal area /Engqvist and Andrejev 2008/ the argument presented by Andrejev and Sokolov /Andrejev and Sokolov 1989/ still applies to the present study, namely that spectral comparison possibly would be the most adequate way of evaluating modelled current results against measurements. Moreover, if the current direction information is neglected by comparing only the speed of the current, then the overall spectral appearances can be compared irrespective of possible bathymetrical forming and deflection of the flow field. A spectral agreement with regard to the distribution of the variance (Figures 3-11, 3-21, 3-26 and 3-44 then should be a reflection of a set of forcing (Table 2-1) that is balanced both to its relative magnitude and temporal resolution. If so, the statistical distribution of velocities should also be mainly congruent with regard to the frequency.

In contrast to the earlier performed validation of the Forsmark coastal area, the present current comparison is considerably more favorable. The results in Table 2-3 can be summarized in that at least one of the principal U- or V- components is acceptable, spanning the range from 5% to almost 50% with an average of 30%. The low end of this range is represented by the problematic station Si22 which instrument was inadvertently dislocated to at least two different depths. The high end of the same range consists of the instrument placed in the narrows of Djupesund (Si25). The spectral comparison of measured and simulated data at Si25 shows a close similarity (Figure 3-44) which can be attributed to similarities not only to realistic forcing, but also to the model's capacity to capture the dynamic response of this forcing. In this diagram there is also low-frequency (about 1.5 per day) variance in the measured spectrum that is not matched by the simulated spectrum. The latter, on the other hand has variance on the high-frequency end of the axis that is cut off by the Nyquist limit of the measured one. This provides a plausible explanation of the found aberration between the fluctuations of the salinity and temperature measurements in Figure 3-39. The graphical resolution of this figure may not show this but in fact, the model performs the exchange more frequently and in smaller transactions so that the total exchange over longer time periods is mainly equal to the measured rate. This is substantiated by the curves being closely aligned.

The transects (Figures 3-46 through 3-50), though taken in calm weather conditions, indicate a fairly homogeneous flow field on the scale of the chosen horizontal resolution of the Baltic model. This resolution thus is likely sufficient to resolve the flow structure in this area. In rougher weather conditions – with more elevated winds – local eddies may occur. The discrepancies between measured and simulated current components in Figures 3-7, 3-8, 3-22 and 3-23 can then possibly be explained by formation of eddies that may be simultaneous but separated by distances exceeding the length of a couple of CR-grid cells.

## 4.2 Temperature evaluation

The temperature dynamics displays a distinct seasonal curve that invariably peaks in summer and has a minimum during winter. This is the basic explanation for why most models are capable of producing temperature data for which the correlations are good. The presently simulated temperature data are no exception, with correlations averaging above 0.9 (Table 2-3). However the correlations decrease with depth. The rather crude formulation of the heat exchange through the air/water interface ignores the radiation portions of heating and cooling /e.g. COHERENS 2004/. Temperatures are routinely measured with thermistor sensors that are mainly unaffected by getting clogged by biological growth of epiphytes and can thus be regarded as an example of a fully reliable metrological device.

## 4.3 Salinity validation

It seems that the most pertinent validation entity is the salinity, because salt is an almost ideal tracer of water exchange. It lacks state transitions (at least at the salinity levels occurring in normal coastal waters) and is from a chemical point of view basically inert. The good correlations obtained at all stations with an average of explaining more than two thirds of all measured salinity variance thus bears a very favorable testimony to the model's capacity to simulate the bulk of water exchange of the entire Laxemar-Simpevarp coastal area. From other studies of coastal embayments around the Baltic coast /e.g. Engqvist 1996/ and the same experience from other Scandinavian sites of investigation /Stigebrandt 1990, Stigebrandt and Aure 1990/, it is well established that the most effective mode of water exchange is the so-called intermediary exchange that is driven by relative density differences between the inside and the outside of an embayment. Since the salinity is the dominant factor in determining the varying horizontal density gradients, it follows that good salinity correlations mean that the water exchange is adequately modeled.

The malfunction of the salinity sensors for instruments in the photic zone near the surface, in particular during the production season in summer, is a known hazard (Björn Kjerfve pers comm) impeding all salinity measurements based on conductivity measurement as a proxy for salinity. In this study there have been several occasions when this ailment has occurred also while the salinity seems to be decreasing for regular oceanographic reasons. This makes it even more difficult to discriminate between which salinity data should be retained for the statistical analysis and which should be discarded.

As a bonus, the executioner of the field program (SMHI) undertook a series of complementary salinity and temperature measurements so as to produce profiles of these entities with enhanced vertical resolution /Lindow 2005/. This was achieved by casting an assumingly well-calibrated CTD instrument at the stations while the deployed meters were still in operation before lifting and after redeploying the instruments for data retrieval. These comparisons mostly confirmed that the deployed instrument complied within the specified inaccuracies with only a few notable exceptions. One concerns station Si21 2004-06-09 for which there was a 2-unit discrepancy in the psu scale. The probable explanation for this difference is the growth of epiphytes that seemingly had not sufficiently been removed during servicing.

The good salinity correlations found in the present study for the peripheral instruments deployed at the interface between the two 3D-models are in stark contrast to what was found for the parallel study of the Forsmark area and thus begs an explanation. The interior station of the Forsmark study (Fo13) gave comparable results to the interior station of the present study (Si24) with only somewhat lower correlation coefficients.

In the present study the Baltic model data have been indiscriminately used for comparison of the stations located on the boundary between the CR- and the FR-models, while for the Forsmark area the comparison was made to the local model. This cannot provide an explanation for the differing correlation levels since the boundary data from the Baltic model are imposed on local model in such a way that only minor deviations should arise.

Instead, the most plausible explanation must be found in the long-term behavior of the Baltic model. For the Forsmark coastal area the induced residual south-flowing current is occasionally interrupted by wind-induced reverse currents and the fronts of freshwater (from the collective discharge of all rivers in Gulf of Bothnia, in particular the nearby Dalälven) meeting with more saline Baltic Proper water, causing a delicate balance of advection and mixing that the model cannot uphold for extended time periods. This problem does not to the same extent affect the more open Laxemar-Simpevarp coast with a much larger adjacent water body with radically reduced formation of fronts. This hypothesis has been considerably strengthened by a control run with the lately provided Mueller data replacing the previously used Mesan data set. This data set yields for the Forsmark area a noticeably different boundary forcing, which is an indication of how sensitive the local results may be to the large-scale CR-model meteorological forcing.

# 5 Conclusions

The overall good salinity and temperature (but only comparatively good current speed component) correlations found in this study give reassuring credibility to the combined model effort to simulate the water exchange of the coastal section off the Laxemar-Simpevarp area. This in turn ascertains that the overall wind-moderated and density-driven coastal water exchange is realistically modeled, indicating that both the modeling and the validating approaches are adequately designed.

# 6 Acknowledgements

We thank in the first place Tobias Lindborg and Ulrik Kautsky, both affiliated with SKB, for the confidence of giving us the opportunity to design and analyze this validation program. A nonymous external reviewer has improved the readability of this report considerably and deserves due gratitude. We also thank Erik Wijnbladh, local ecologist at Laxmar-Simpevarp area at the time of the study for lending us a helping hand on several occasions.

# 7 References

**Andrejev O, Sokolov A, 1989.** Numerical modelling of the water dynamics and passive pollutant transport in the Neva inlet. Meteorologia i Hydrologia, 12, 78–85, (in Russian)

**Andrejev O, Sokolov A, 1990.** 3D baroclinic hydrodynamic model and its applications to Skagerrak circulation modelling. 17th Conf. of the Baltic Oceanographers, Proc. 38–46, 23, 280–287.

**Andrejev O, Sokolov A, 1997.** The data assimilation system for data analysis in the Baltic Sea. System Ecology contributions No. 3. 66 pp.

**Andrejev O, Myrberg K, Lundberg P, 2004a.** Age and renewal time of water masses in a semi-enclosed basin – application to the Gulf of Finland, Tellus, 56A, 548–558.

**Andrejev O, Myrberg K, Alenius P, Lundberg P, 2004b.** Mean circulation and water exchange in the Gulf of Finland – a study based on three-dimensional modelling. Boreal Env. Res. 9, 1–16.

**Arakawa A, 1966.** Computational design for long-term numerical integration of the equations of fluid motion: Two-dimensional incompressible flow. Part I. J. Comput. Phys, 12, 12–35

**COHERENS, 2004.** EU Marine Science and Technology Programme, Contract No MAS3-CT97-0088.

**Engqvist A, 1996.** Long-term nutrient budgets in the eutrophication of Himmerfjärden estuary. Estuarine, Coastal & Shelf Science, 42, 483–507.

**Engqvist A, 1997.** Water exchange estimates derived from forcing for the hydraulically coupled basins surrounding Äspö island and adjacent coastal water. SKB TR-97-14, Svensk Kärnbränslehantering AB. ISSN 0284-3757. 44 pp.

**Engqvist A, Andrejev O, 1999.** Water exchange in Öregrundsgrepen – A baroclinic 3D-model study. SKB TR-99-11, Svensk Kärnbränslehantering AB.

**Engqvist A, Andrejev O, 2000.** Sensitivity analysis with regard to variations of physical forcing including two possible future hydrographic regimes for the Öregrundsgrepen. A follow-up baroclinic 3D-model study. SKB TR-00-01, Svensk Kärnbränslehantering AB. 44 pp.

**Engqvist A, Andrejev O, 2003.** Water exchange of the Stockholm archipelago – A cascade framework modeling approach. J. Sea Res. 49, 275–294.

**Engqvist A, Stenström P, 2004.** Archipelago Strait Exchange Processes – An overview. Deep Sea Research II, 51, 371–392.

**Engqvist A, Andrejev O, Döös K, 2006.** Modelling water exchange and contaminant transport through a Baltic coastal region. Ambio, XXXV, 435–447.

**Engqvist A, Andrejev O, 2008.** Validation of coastal oceanographic models at Forsmark. SKB TR-08-01, Svensk Kärnbränslehantering AB.

**Engqvist A, Stenström P, 2008.** Flow regimes and long-term water exchange of the Himmerfjärden estuary. Estuarine, Coastal & Shelf Science. In press.

**Johansson L, Morosini M, 2002.** Metodbeskrivning för Oceanografiska mätningar. SKB MD 364.009 (in Swedish).

**Lindborg T, Lindborg R, Löfgren A, Söderbäck B, Bradshaw C, Kautsky U, 2006.** A strategy for describing the biosphere at candidate sites for repositories of nuclear wase: linking ecosystems and landscape modeling. Ambio, XXXV, 418–424.

**Lindow H, 2005.** Oskarshamn site investigation Oceanographic measurements. SKB P-05-191, Svensk Kärnbränslehantering AB.

**Omstedt A, 1999.** Forecasting ice on lakes, estuaries and shelf seas. In: J S Wettlaufer, J G Dash and N Untersteiner (Eds.) Ice physics and the natural environment, NATO ASI Ser. Vol. I 56. Springer-Verlag, Berlin. pp. 185–207.

**SKB, 2001.** Site investigations. Investigation methods and general execution programme. SKB TR-01-29, Svensk Kärnbränslehantering AB.

**Stigebrandt A, 1990.** On the response of the horizontal mean vertical density distribution in a fjord to low-frequency density fluctuations in the coastal water. Tellus, 42A, 605–614.

**Stigebrandt A, Aure J, 1990.** De ytre drivkrefternas betydning for vannutskiftningen i fjorderne fra Skagerrak til Finnmark. Rapport FO 9003, Havforskningsinstituttet, Nordnes (N). 24 pp.

ISSN 1404-0344
CM Gruppen AB, Bromma, 2009